THE UNIVERSITY OF ADELAIDE

DEPARTMENT OF MECHANICAL ENGINEERING

HYDROJET
DUCTED PROPULSION SYSTEM

IMPELLER INDUCED VIBRATORY PRESSURES

and

PERFORMANCE CHARACTERISTICS

by

M. R. HALE and D. H. NORRIE

NOVEMBER 1966

THE UNIVERSITY OF ADELAIDE

DEPARTMENT OF MECHANICAL ENGINEERING

HYDROJET

DUCTED PROPULSION SYSTEM

IMPELLER INDUCED VIBRATORY PRESSURES

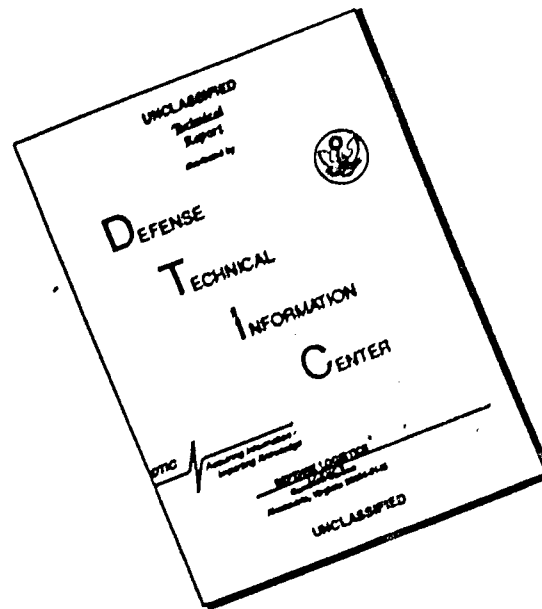## and

PERFORMANCE CHARACTERISTICS

by

M. R. HALE and D. H. NORRIE

NOVEMBER 1966

DISCLAIMER NOTICE

THIS DOCUMENT IS BEST QUALITY AVAILABLE. THE COPY FURNISHED TO DTIC CONTAINED A SIGNIFICANT NUMBER OF PAGES WHICH DO NOT REPRODUCE LEGIBLY.

TABLE OF CONTENTS

-- ooOoo --

LIST OF FIGURES

LIST OF FIGURES (continued)

NOMENCLATURE

A_o Impeller annulus area $= \frac{\pi}{4}(D^2 - D_h{}^2)$

A_i Modulus of pressure component (i'th harmonic)

A_J Nozzle exit area

c Blade chord

C_D Drag coefficient

C_F Frictional drag coefficient

C_L Lift coefficient

C_{ph}, C_{Ph} Pressure coefficients

C_{TL} Thrust load coefficient

D Impeller outer diameter

D_d Duct internal diameter

D_h Impeller hub diameter

e Saturated vapour pressure

J_I Advance coefficient

K_A Ratio of impeller annulus area A_o to area of duct at intake

K_{Pi} Pressure coefficient (i'th harmonic)

K_{Pt} Pressure coefficient (total)

K_Q Torque coefficient

K_T Thrust coefficient

L Duct length

m_x Blade camber

n Propeller rotational speed

P, p Pressure

P_o Free stream pressure

Q Torque

r Radius

R Blade tip radius

R_n	Reynold's number
T	Thrust
t_x	Blade thickness
V_a	Fluid axial velocity at impeller
V_I	Intake velocity
V_J	Jet velocity
V_R	Velocity relative to blade
X	Axial distance along duct
Z	Number of blades
α, β	Angle
γ	Angular position of point (x,y,z)
ϵ	Drag to lift ratio
ϵ_i	Phase-lead angle of i'th harmonic
n_E	Impeller efficiency
n_H	Hull efficiency
n_i	Blade element efficiency (ideal)
n_o	Impeller overall efficiency
n_P	Propulsive efficiency
n_{Popt}	Maximum impeller efficiency
θ	Blade angle with respect to axis
μ	Velocity ratio $= \dfrac{V_I}{V_J}$
μ_m	Viscosity factor
ξ	Energy loss factor
ρ	Mass density
σ_p	Pressure minima cavitation number
σ_s	Sectional cavitation number
ω	Angular velocity

ABSTRACT

Theoretical and experimental studies were conducted on a Hydrojet
ducted impeller system with the aim of developing an efficient and vibration-
free propulsion unit for ships. Initial estimates of the propulsive effi-
ciency of the Hydrojet showed this to be a practical means of propulsion
and further detailed investigations were undertaken.

A theoretical analysis of an impeller operating in an infinitely long
duct was developed by assuming the impeller to be replaced by bound vortex-
lines. The optimum geometry for an impeller was taken to be that design
for which the induced and profile drags had minimum values, the maximum
blade stress was equal to the design stress, and the blade sections operated
free from cavitation at the design conditions. Experimental and theoretical
values of impeller efficiency indicated that values of the order of 0.85
to 0.90 may be possible.

Impeller-induced vibratory pressures on the inner duct surface were
measured under various impeller loading conditions, and different inflow
velocity patterns to the impeller. An intense pressure field existed near
the impeller plane, but its magnitude rapidly attenuated with distance
from the impeller. Pressure coefficients $\frac{P}{\rho n^2 D^2}$ in the order of 0.5 were
measured at the impeller plane, but values of less than 0.01 existed at distances
greater than 0.4 of the impeller diameter (D). The blade frequency harmonic
content of the total pressure was extremely large, with the 2nd and 3rd har-
monics being approximately 60% and 25% respectively of the 1st harmonic.
The phase angle of all harmonics of the induced pressure were constant forward
of the impeller and varied linearly with distance behind the impeller. The
trailing vortices of the impeller blades appeared to originate near the
mid-point of the blade chord and had a tendency to move forward as the

harmonic number increased. The helical vortex line at the duct surface had a constant pitch.

It is concluded that the duct need only extend forward a distance of 0.3 of the impeller diameter and aft a distance of 0.2 for the most intense portion of the fluctuating pressure field to be contained within the duct, for a ducted impeller of similar configuration to that used in this investigation.

INTRODUCTION

Naval architects and marine engineers are continually endeavouring to improve the propulsive efficiency and power of ships to obtain higher speeds. Unfortunately, the increase in power and speed is accompanied by an increase in the unsteady forces which are created by the propeller and which act on the hull of a ship. The vibrations produced by these forces may reach magnitudes which will have a detrimental effect on the machinery as well as producing considerable discomfort to passengers and crew. Thus designers are faced with the problem of reducing these unwanted forces to more acceptable levels.

Two types of forces are generated:--

(a)   bearing forces

(b)   surface forces

The former forces are transmitted to the hull through the propeller shaft and bearings. They arise from the propeller operating in a ship's wake which has a non-uniform velocity field. This field is primarily caused by the viscous boundary layer of the hull and to lesser extent by the potential flow field.

The latter forces are created through the interaction of the pressure field with the hull surface. The pressure field surrounding the propeller is dependant on the instantaneous loading on the propeller, on the blade geometry and, in particular, on the blade thickness. The resultant surface force on the hull is governed by the geometrical relationship between the propeller and the surface.

A considerable number of experimental investigations have been carried out to determine comfortable enviromental levels of vibration, the levels existing in ships, the magnitude of the forces present, and

the effect the geometry of the afterbody has on these forces. (Ref. 0.1 and 0.2).

The results of these investigations lead to the conclusion that, with conventional hull form and propeller design, it is difficult to reduce the vibration to acceptable levels. It also suggests that it will be necessary to examine other forms of marine propulsion where the propeller-excited vibrations may be reduced and the propulsive efficiency increased. One such system is a ducted propulsion unit.

This report deals with a theoretical and experimental investigation into the feasibility of a ducted propulsion system, herein called a "Hydrojet". The Hydrojet consists of an impeller operating in a cylindrical duct of several impeller diameters in length. The following were carried out during the project period: -

(a)   An estimate of the propulsive efficiency of the Hydrojet.

(b)   A theoretical analysis of the impeller.

(c)   A model impeller based on the above theory was constructed to a high dimensional accuracy by a new machining technique.

(d)   The fluctuating pressure induced by the impeller was measured at the inner duct surface.

(e)   Experimental values of the impeller characteristics were measured and compared with those obtained by theory.

(f)   A theoretical solution to the impeller near-field was attempted.

1.1   <u>ROTODYNAMIC PROPULSION UNITS</u>

Many investigators have studied the screw propeller with a view to reducing the vibration levels due to the bearing and surface forces (Ref. 1.1). The factors governing the efficient operation of such a propeller are well known and can easily be adjusted when selecting a propeller for a given duty. The vibratory forces however, are not easily controlled, and in many instances, it is difficult to obtain acceptable levels. A stage has been reached in the evolution of the displacement vessel at which propeller-excited vibrations are beginning to exceed the acceptable level. Since the problem will become more serious, research directed towards low-vibration propulsion was considered worthwhile. Accordingly, in 1962, an investigation was begun at the University of Adelaide on possible configurations of propulsion systems for large displacement vessels, which would have inherently lower vibration characteristics than the conventional propeller.

If the propulsion system is to be theoretically vibrationless, there must be no fluctuating forces generated. If the energy transfer in the propulsive unit is to be by a rotor then physical reasoning indicates that two requirements must be satisfied if there are to be no unsteady forces generated. The first requirement is that the velocity field relative to each blade should not change in magnitude or direction (i.e. the velocity field should be symmetric about the axis). This will mean that the blade forces will be steady with time. The second requirement, which is in some degree inter-related with the first is that the net forces due to the blade pressure fields on the boundaries be invariant with time. This can only be achieved with a finite number of rotor blades if the solid boundaries in the proximity of the rotor are symmetrical around the axis.

These two requirements can be summarized as: symmetry of flow and boundaries about the axis. Although this ideal may be impossible to achieve in practice,

it can be shown that the closer it is approached, the smaller will be the unsteady forces. This applies to both requirements. Enclosing the rotor in a rigid duct, for example, since it satisfies the boundary, symmetry condition will reduce the unsteady surface forces even though the rotor may remain operating in a non-symmetric flow and be generating considerable unsteady rotor forces.

A number of configurations which wholly or partly satisfy the above requirements have been considered. These fall basically into two groups: -

(a) "Open" configurations in which the rotor is relatively distant from solid boundaries, and in which the rotor operates in either a uniform or axially symmetric fluid stream.

(b) "Enclosed" systems in which the rotor is enclosed by axially symmetric boundaries, and operates in an axially symmetric fluid stream. A variant of this type is the rigid-duct system mentioned above, in which the requirement on axial flow symmetry is relaxed.

For any new propulsion system to be suitable for large displacement vessels there are a number of requirements, in addition to those mentioned above, which must be satisfied, viz: -

(a) Propulsive efficiency must be comparable with the screw propeller.

(b) Steering power must be adequate.

(c) The ability to maintain satisfactory performance in varying conditions of seaway must be maintained.

(d) The ability to withstand damage in exceptional conditions must be comparable with screw propellers.

The following configurations considered would have inherently low vibration characteristics: -

(a)   A conventional screw propeller behind a hull with modified
after-body.

(b)   Various configurations with the propeller mounted at or forward
of the bow.

(c)   Various multi-hull configurations in which the propeller or
propellers would operate in more uniform wakes than with the
conventional screw system.

(d)   A submersible hull consisting of a cigar-shaped main body
completely submerged with a narrow stream-lined superstructure
protruding above the water line.

(e)   A hull with propulsive units in pods on outriggers.

(f)   Various forms of internal duct system (hydraulic jet propulsion
or Hydrojet).

Preliminary studies of the above configurations indicated that the
type mentioned in (f) was most suited as a replacement for the screw
propeller on large displacement vessels. For this reason it was
considered profitable to carry out a more detailed analysis of this type
of propulsion system.

1.2   PERFORMANCE OF A HYDROJET.

A Hydrojet or ducted impeller system is one in which the impeller
operates in a duct or tunnel of dimensions comparable with the impeller
diameter. The duct diameter (D_d) would be very nearly that of the
impeller (D). The length would be of the order of several impeller
diameters depending on its application.

$$L \approx 3D \text{ to } 5D$$
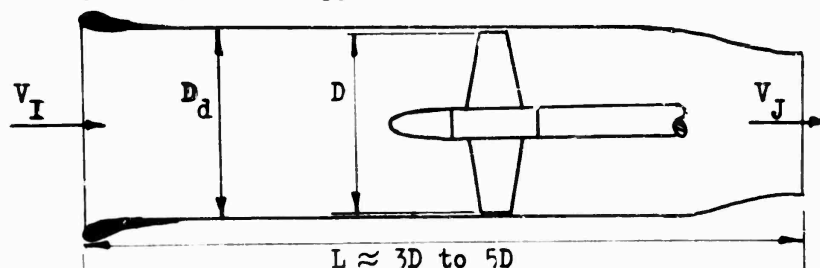
In order to develop the desired thrust by increasing the axial momentum of the fluid, there is a contraction at the exit of the duct so that the exit or jet velocity (V_J) exceeds that of the intake (V_I).

1.2.1 Propulsive Efficiency.

The fundamental nature of the energy losses in a Hydrojet is extremely complicated. To obtain an estimate of this, the hydrodynamic energy losses are divided into:-

(a)   Impeller losses.

(b)   The losses due to the intake, duct and nozzle.

(c)   Loss due to the interaction of hull and duct.

The losses associated with the impeller are accounted for in the impeller efficiency η_E. The intake, duct and nozzle losses, termed the duct loss, may be expressed as a fraction of the intake kinetic energy.

ie. Ductwork losses per unit mass flow $= \zeta \dfrac{V_I^2}{2}$ ... 1.1

where ζ = the loss factor

V_I = intake velocity

The hull efficiency η_H takes into account the effect of operating the Hydrojet in the vicinity of a hull (Appendix A4). Hence the propulsive efficiency η_P can be expressed as follows:-
(See Appendix A4 for the derivation).

$$\eta_P = \eta_E \, \eta_H \, \frac{2\mu(1-\mu)}{[1 - \mu^2(1 - \zeta)]} \qquad \ldots 1.2$$

where $\mu = \dfrac{V_I}{V_J}$ = velocity ratio

and

V_J = velocity at exit of duct

A more useful relationship of η_P can be given in terms of the thrust load coefficient (C_{TL}) based on the area (A_o) and the relative axial velocity (V_a) of the fluid at the impeller.

Thus

$$\eta_P = \eta_E \, \eta_H \, \frac{4(C_{TL} K_A)}{[\,(C_{TL} K_A)^2 + 4(C_{TL} K_A) + 4\xi\,]} \qquad \ldots 1.3$$

where $C_{TL} = \dfrac{T}{\frac{1}{2}\rho V_a^2 A_o}$

and T = thrust of the Hydrojet

K_A = ratio of area of impeller annulus to area of duct

Fig. 1.1 shows curves of propulsive efficiency (η_P) against thrust load coefficient (C_{TL}) for different duct loss factor (ξ) as expressed by equation 1.3. It will be observed that for a fixed value of ξ, the efficiency η_P will increase with increasing C_{TL} and reach a maximum; further increasing the C_{TL} results in a decrease of propulsive efficiency (η_P).

The maximum impeller efficiency (η_{Popt}) of a ducted propulsion system for a given duct geometry and hence loss factor is:-

$$\eta_{Popt} = \eta_E \, \eta_H \, \frac{1}{1 + \sqrt{\xi}}$$

$$= \eta_E \, \eta_H \, \frac{2}{(C_{TLopt} K_A) + 2} \qquad \ldots 1.4$$

This maximum efficiency occurs when

$$\mu_{opt} = \frac{1}{1 + \sqrt{\xi}}$$

and

$$C_{TLopt} = \frac{2\sqrt{\xi}}{K_A} \qquad \ldots 1.5$$

Drawing a line passing through the maximum efficiency (η_{Popt}) of each individual curve of ζ shows that the η_{Popt} will increase with decreasing thrust load coefficient and approach unity. Hence for high efficiency the duct loss factor and the thrust load coefficient must be kept as low as possible (Ref. 1.3 and 1.4).

It might be mentioned that below the maximum efficiency (η_{Popt}) line the propulsive efficiency is greatly dependant on the thrust load coefficient (C_{TL}) and hence the velocity ratio (μ) for a given ζ ; above this line, however, η_P is not significantly affected by a change in C_{TL}.

In order to apply the theoretical results shown in Fig. 1.1 it is necessary to estimate the duct loss factor (ζ) and the impeller efficiency (η_E).

1.2.2 Estimation of Duct Losses.

An initial estimate of the hydrodynamic loss can be made by first assuming the impeller does not effect the growth of the boundary layer in the duct. Therefore it is possible to replace the duct by a flat plate, having the same length and area as the inner surface of the duct. It is also assumed that the plate is in a uniform fluid stream having a velocity equal to the intake velocity of the propulsion unit. The loss factor (ζ), which is the ratio of energy loss to the kinetic energy of fluid at the leading edge, is expressed by the following equation:--

$$\zeta = \frac{\text{energy loss}}{\text{K.E. at inlet}}$$

$$= \frac{[\frac{1}{2} C_D \, \rho \, V_I^{\,2} \, (\pi \, D_d \, L \,) \,] \, V_I}{\frac{1}{2} [\, \rho \, (\frac{\pi \, D_d^{\,2}}{4}) \, V_I \,] \, V_I^2}$$

$$= \frac{4 \, C_D \, L}{D_d}$$

... 1.6

where C_D = drag coefficient of the plate

and D_d = diameter of duct

and assuming $C_D = C_F + \Delta C_D$ ... 1.7

where C_F is given by the ATTC (1947) mean friction line as
expressed in the relationship

$$(C_F)^{-0.5} = 4.132 \log_{10} (R_n C_F) \qquad \ldots 1.8$$

and R_n is Reynolds number of the plate based on
its length.

also $\Delta C_D = 0.001$ is an allowance for the surface and its
coating.

The magnitude of ξ for varying duct geometry and operating conditions
is given in Fig. 1.2. The values are based on the assumption that the
density of fluid is 1.99 slugs/cub.ft.

The value of the duct loss factor (ξ) for a practical arrangement
of ducting which has a length-to-diameter ratio of about 5 is, from
Fig. 1.2, between 0.04 and 0.06. The corresponding value of the
optimum performance ratio $\dfrac{n_P}{n_E \, n_H}$ from Fig. 1.1 is between 0.81 and 0.84.

The propulsive efficiency of the hydrojet can be determined, if the
impeller efficiency n_E and the hull efficiency n_H are known. An
estimate for the impeller efficiency is of the order of 0.90, based on
high specific-speed axial-pump data (Ref. 1.5). Assuming a value of 1.0
for the hull efficiency then the value of the propulsive efficiency for
a practical Hydrojet system would be between 0.72 and 0.76.

As discussed in (1.1), a ducted impeller would be expected to generate smaller vibratory surface forces than a comparable screw propeller, although the rotor forces generated may still be large. The reduction in surface forces, which is due to the symmetry of the boundary around the impeller, will only be fully achieved if the duct wall is sufficiently rigid.

The unsteady rotor forces for a ducted impeller can, in principle, be calculated by use of an unsteady propeller theory (modified suitably for the effect of the duct) together with a knowledge of the dynamic properties of the impeller drive and support system. Such calculations, while complex, have been carried out for the screw propeller (Ref. 4.4 and 4.5). It was intended that rotor forces would be estimated theoretically for comparison with values experimentally measured, but time did not permit this to be done. As it happened, a faulty dynamometer prevented the measurement of rotor forces, also (see 4.3.2).

To estimate the surface or duct forces it is necessary to know the pressure distribution on the duct wall, and this in turn requires knowledge of the unsteady pressure field of the impeller. Since the pressure field of a ducted impeller had not been previously investigated experimentally, a major portion of the experimental work of this project was directed to this end (see Section 5.0). A theoretical investigation of the pressure field was begun as part of the project, but as noted below, was not completed.

The calculation of the pressure field near a rotating impeller in a duct is, in incompressible flow, equivalent to obtaining a complete solution for the instantaneous flow field. It matters not whether

the solution is for the velocity field, the pressure field, or the potential field, since any one of these can be obtained (in principle at least) from the other. In pract ce, there may be advantages in obtaining one solution before the others.

The early analyses of ducted impellers (reviewed in Refs. 1.6 and 1.7) were based on the ring aerofoil theory of Dickman (Ref. 1.8) and Weissinger (Ref 1.9) with the impeller represented by an actuator disc. These analyses give no information on the unsteady flow field.

Lifting-line theories were put forward for ducted impellers by Ordway et al in 1960 (Ref. 1.10) and Morgan in 1961 (Ref. 1.11), and were subsequently further developed by these investigators (Ref. 1.12 and 1.13). The near-field solution of Ref. 1.10 was based on the following model:

(a)   bound vortices to represent the blades

(b)   helical vortex sheets to represent the shed blade vortices, and,

(c)   spiral vortices on a surface of rotation to represent the duct.

Using the Biot-Savart law, and the superposition of velocity fields for each of (a), (b), and (c) a solution was obtained in a series form. The zeroth harmonic field which determines the steady shroud load on a non-parallel duct, was worked out in detail. In the later work of Ref. 1.12, Ordway et al investigated the higher harmonic components of the flow field and showed that a solution for each was in principle obtainable. They indicated two procedures by which such solutions could be obtained but noted that these solutions would be difficult to work out in detail, and that the evaluation in any numerical case

would involve much computation.

The authors at the time unaware of Ordway et al's work began early in the project on a potential solution to the impeller-in-duct problem. Considerable effort was put into this work. Difficulty was experienced in elucidating the field, although it was early realized that a series solution would be possible. An attempt was then made to solve the problem using the Biot-Savart law and the superposition of velocity fields, but this approach had not proceeded far when the Ordway et al reports were received showing that Ordway had already used this approach to obtain a solution (at least in principle) to the higher harmonics of the potential field.

It was then intended to extend Ordway's work to obtain a solution in detail for the higher harmonics, and to develop a digital computer programme based on this. This work had begun by the date of printing of this report, and will be continued by the second author at the University of Calgary.

It is regrettable that the theoretical solution for the pressure field was not available to compare against the experimental data described in Section 5.0, at the date of writing. However, it is intended that this comparison will be later made and published.

2.0   IMPELLER DESIGN AND MANUFACTURE.

2.1   IMPELLER DESIGN.

2.1.1   Introduction.

Propeller design procedures in use today, do not attempt to determine the optimum propeller geometry for a given set of operating conditions, apart from one recorded exception given in Ref. 2.1.

The methodical series of propellers are based on an optimum value for one of the major variables and the optimum values for all other design variables are not determined. For example, from the design data for the NSMB (or Van Manen) screw series, the optimum diameter can be chosen and hence the corresponding pitch and mean blade area ratio can be determined to avoid cavitation under the operating conditions. In this series, the blade outline, blade sections, and variation of maximum blade thickness with radius have been previously fixed.

In some of the more theoretical design procedures, it is possible to calculate the circulation distribution, so that the energy loss caused by the induced flow is minimised. It is not possible, however, to determine from these theories an optimum blade shape for strength and for the desired circulation distribution.

The theoretical knowledge of propeller operation has progressed to a stage where an attempt should be made to develop a design technique based on these theories which would determine the

best propeller geometry to suit a given set of operating conditions. A technique of this magnitude would require many mathematical statements and decisions. If such a design is to be economical in both time and cost, the resources of a high-speed digital computer and store are necessary. With the advent of more rigorous and complex theoretical approaches to the design of propellers, a type of optimum design procedure will become necessary in the future, if full advantage is to be taken of the acquired theoretical knowledge.

A programme described in Appendix A 1 was an initial attempt at an optimizing design procedure. Although the design method used in this programme was not the most rigorous, the solutions given by the programme show that optimization could be usefully employed for more complex design theories. The programme was developed to study the feasibility of the Hydrojet propulsion unit.

2.1.2 <u>Hydrodynamic Model of the Impeller.</u>

Since the present research project was directed towards estimating the capabilities of a ducted propulsion system, it was considered that a simplified vortex-line theory could be satis- factorily applied to the design of the impeller.

The following theory is applicable to the design of ducted propellers where the induced circulation around the duct can be neglected. It can also be applied to the design of axial flow pump units.

Consider an impeller operating in a long cylindrical duct in which the fluid can be considered as irrotational upstream of the impeller. It is assumed that the impeller has neglible tip clear-ance. Thus the impeller diameter equals the duct internal diameter. The finite size boss is assumed to have neglible effect on the induced flow.

It is assumed that the axial velocity profile is uniform across the duct upstream of the impeller.

It is also assumed that for a sufficient distance upstream and downstream of the impeller, the duct is parallel. The impeller design is selected to have no axial component of induced velocity. The velocity diagram is as shown in Fig. 2.1.

It is considered to be sufficiently accurate for the inter-ference flow to be assumed constant circumferentially at any radius. This is equivalent to assuming the interference flow is generated by an infinite number of lifting-lines of variable strength in the radial direction. Using the Betz's criteria for minimum induced energy loss in the wake of an inviscous fluid, and the Kutta-Joukowsky relationship, the ideal thrust and torque gradients at any section can be derived as follows:-- (see Fig. 2.1)

$$\frac{dT_i}{dr} = 4\pi \rho \omega^2 r^3 \eta_i (1 - \eta_i) \qquad \ldots 2.1$$

$$\frac{dQ_i}{dr} = 4\pi \rho \omega V_a r^3 (1 - \eta_i) \qquad \ldots 2.2$$

2.4

If it is assumed that the circulation distribution for minimum energy loss is not greatly affected by the variation of profile drag with radius, then the actual thrust and torque gradient can be evaluated as follows:-- (see Fig. 2.1).

$$\frac{dT}{dx} = \frac{dT_i}{dx} (1 - \xi \tan \beta_i) \qquad \ldots 2.3$$

$$= K_1 \eta_i (1 - \eta_i)(1 - \frac{\xi}{\delta x \eta_i}) x^3 \qquad \ldots 2.4$$

and

$$\frac{dQ}{dx} = \frac{dQ_i}{dx} (1 + \frac{\xi}{\tan \beta_i}) \qquad \ldots 2.5$$

$$= K_1 \frac{Va}{\omega} (1 - \eta_i)(1 + \xi \delta x \eta_i)x^3 \qquad \ldots 2.6$$

where

$$\delta = \frac{\omega R}{Va} \qquad \xi = \frac{C_D}{C_L}$$

$$x = \frac{r}{R} \qquad K_1 = \frac{4\pi \rho \delta^4 Va^4}{\omega^2}$$

$$\tan \beta_i = \frac{1}{\delta \eta_i x}$$

The total thrust (T) and torque (Q) of the impeller can only be evaluated by summation over the blade length if the drag to lift ratio ξ is known at each section. Since this ratio depends on the blade profile which is in turn dependent on the strength, cavitation and hydrodynamic requirements, a simple expression for thrust and torque cannot be obtained.

2.5

An approximation to the impeller geometry can be obtained by assuming the drag to lift ratio constant with the radius. In this case integration gives the following equations for total thrust T and overall efficiency η_o.

$$T = A(1 - \eta_i)(\eta_i B - C) \qquad \ldots 2.7$$

$$\eta_o = \frac{\eta_i B - C}{B + \eta_i D} \qquad \ldots 2.8$$

$$= \frac{T}{A(1 - \eta_i)(B + \eta_i D)} \qquad \ldots 2.9$$

where

$$A = \frac{\pi\rho\, Va^4\, \delta^3}{\omega^2} \qquad\qquad C = \frac{4}{3}\,\xi\,(1 - K^3)$$

$$B = \delta\,(1 - K^4) \qquad\qquad D = \frac{4}{5}\,\xi\,\delta^2(1 - K^5)$$

$$K = \frac{\text{radius of boss}}{R}$$

2.1.3 Blade Element Properties.

(1) Blade element characteristics.

The design lift coefficients of the section (C_L) can be expressed as,

$$C_L = \frac{dL}{\frac{1}{2}\rho V_R^2\, c\, dr} = \frac{8\pi\,\delta(1 - \eta_i)x^2 R}{zc\sqrt{(x\,\delta\,\eta_i)^2 + 1}} \qquad \ldots 2.10$$

where c = chord of blade section.

The theoretical lift coefficient (C_{li}) required to develop the design lift is assumed to be greater than C_L by a factor μ_m, the viscosity factor. According to the potential theory of thi.. wing sections (see Chapter 5, Ref. 2.2), the theoretical lift coefficient of the section is a function of the camber to chord ratio $\dfrac{m_x}{c}$ only if the section operates at shock-free entry conditions, hence

$$C_{li} = l_m \frac{m_x}{c} \qquad \qquad \text{... 2.11}$$

The blade section chosen for this impeller was an NACA-16 thickness distribution with a mean line of $a = 1.0$ and the values for viscosity factor (μ_m) and lift camber factor (l_m) at shock-free conditions are given in Appendix A 1, eqn. 18 to 20 and also in Table 5.6, p 175 in Ref. 2.2 .

(2) Blade strength.

The stresses at a blade section were calculated by the simple theory for bending of a beam as suggested by Tingey (Ref. 2.3, also Ref. 2.2).

It is important to note that this theory can be applied only to designs where chordwise bending due to the pressure distribution over a section can be ignored. This implies that the blades should have relatively large thickness to chord ratio $(\dfrac{t_x}{c})$ and not excessively wide chords. The blade geometry chosen for the impeller is consistent with the assumptions of the stress calculation by Tingey.

(3) Cavitation.

Using the theory of thin wings, the cavitation parameter, the "pressure minima cavitation number" σ_p is determined for the given blade section as follows: (Ref. 2.2 p 209)

$$\sigma_p = (1 + 1.14 \frac{t_x}{c} + \frac{C_{li}}{4})^2 - 1 \qquad \ldots 2.12$$

The sectional cavitation number σ_s is defined by

$$\sigma_s = \frac{(P_r - e)}{\frac{1}{2} \rho V_R^2} \qquad \ldots 2.13$$

where

P_r = pressure at blade section radius r and at minimum immersion

e = saturated vapour pressure

When applying these equations to an actual impeller an overall factor f_o which makes allowance for irregular and viscous flow is introduced to effectively increase σ_p.

Thus

$$\sigma_s \geqslant f_o \, \sigma_p \qquad \ldots 2.14$$

where f_o = 1.2 (Ref. 2.2 p. 209)

A similar method was used by Matthews and Straszak to estimate the inception of cavitation in screw propeller designs. (Ref. 2.4).

2.1.4 Optimum Design.

The optimum combination of blade sections for a Hydro-jet impeller was chosen to be that which satisfies the following:--

(a)   The hydrodynamic equations for minimum energy loss.

(b)   The lowest possible profile drag providing that:--

(c)   The blade section is strong enough to limit the sectional stresses to a value equal to or less than the maximum design stress.

(d)   The blades must also operate free from cavitation.

(e)   As a consequence of meeting the above conditions, the weight of the impeller will be a minimum for the chosen operating conditions.

Details of the design procedure are given in Appendix A1.

Although the impeller dimensions calculated by this design method lead to an optimum blade section arrangement for the given conditions, it is not necessarily the optimum design for a given duty, for example, for a given thrust (T).

The optimum design must be selected by studying closely, the results of a series of systematically varied impellers, all designed for optimum arrangement and satisfying the requirements of a given duty. Before deciding upon the final impeller geometry, certain other factors

affecting the operation of an impeller or rotor-dynamic propulsion unit must also be taken into account - e.g.

(a) Is the largest diameter impeller that can be installed in the vessel also the optimum diameter?

(b) Is the number of blades and rotational speed conducive to exciting critical modes of vibration when the propulsion system is operating?

(c) What is the economical range of rotational speeds of the prime mover?

The sectional lift coefficient is another important variable which must be studied before selecting the final design.

The design programme given in this report does not achieve the ideal objective. This could be stated as "the selection of an optimum impeller geometry to suit a particular duty by considering every possible arrangement which satisfies all known laws, principles and facts associated with its operation." All these decision points could be inserted into a programme for the logical selection of the ideal impeller, and would require extremely careful planning. Although the complete optimum design is not specified directly by the programme of this report, it is considered that the technique given for selecting an optimum blade geometry is a radical departure from the usual propeller design procedures.

2.2   <u>IMPELLER CHARACTERISTICS AND MODEL IMPELLER</u>.

The impeller design method outlined in the previous section determines

the optimum blade dimensions which satisfy the design assumptions and the

given set of operating conditions.   Unfortunately it is not possible to

represent the parameters which govern the impeller characteristics by

dimensionless groups, as for each set of operating conditions there is only

one arrangement of blade dimensions which satisfy all the design require-

ments.

A design study was made of a twin Hydrojet propulsion unit to replace

an existing single screw propeller on a 19,000 tdw ore carrier. A drawing

of the proposed layout is given in the Appendix A5.

The main design requirements of the impeller were

    Thrust/Unit   - 44,800 lbf

    Velocity at impeller disc - 19.3 fps

To meet the above operating conditions, a number of impellers were

designed according to the procedure given in Section 2.1 by varying the

impeller radius, rotational speed and blade area ratio. The impeller

efficiency η_E for these various designs are shown in Figs. 2.2 to 2.4.

The blade section chord was assumed linear with radius, varying from CID

at the boss to COD at the blade tip.

A study of these characteristics shows the radius at which the

impeller efficiency is a maximum is not significantly affected by blade-

area ratio or geometry changes (Fig. 2.2).   Similarly, the optimum

rotational speed is not greatly affected by the varying impeller geometry

(Fig. 2.3) for the fixed impeller diameter and rotational speed.   Fig.

2.4 shows the small change in impeller efficiency due to a change in the

blade geometry.

2.11

The impeller chosen to meet the design conditions was as follows:--

Thrust/Unit	44,800 lbf
Velocity at impeller disc	19.3 fps
Diameter	15 ft
Blades	4
Rotational Speed	1.5 rps
Expanded Blade Area Ratio	0.543
Linear chord distribution	
Tip chord	5.0 ft
Boss chord	3.0 ft
Chord section	NACA-16, a = 1.0
Theoretical efficiency of the impeller	0.87
Thrust load coefficient	0.688

An 8 inch diameter model of this impeller is shown in Fig. 2.5 and Fig. 2.9 and a list of dimensions of the impeller is given in Table 4 of Appendix A1.

The value of the theoretical impeller efficiency compares favourable with that taken in Section 1.2.2 as an initial estimate.

2.12

2.3   <u>MACHINING TECHNIQUE FOR THE IMPELLER</u>.

Manufacturing technology, in general has progressed rapidly
over the past decade, but it has not significantly affected the
machining techniques used to construct model or prototype propellers.

Changes in manufacturing processes are necessary if accuracy
is to be increased and production time decreased. Accuracy is
important where measured values of a variable from model experi-
ments are to be used to predict the prototype values or are to be
compared with theoretical values.

The common method of machining an impeller or propeller is to
use a cutter which moves (relative to the blade) on a cylindrical
path with centre on the axis of the impeller. The cutter motion
is controlled by a follower moving over a series of templates which
may be either cylindrical or expanded-cylindrical sections depending
on the mechanism used to convert movement of the follower to the
cutter.

Another method, which is suited for the majority of milling
machines, is the spot-machining of points on the blade surface in
either a polar or a rectangular grid pattern. This method requires
considerable computation especially when cartesian co-ordinates are
used, because the object is naturally defined by polar co-ordinates.

In all the machining techniques commonly employed it is usual
to use only a small number of sections to define the complete blade
shape. Hand machining is thus necessary to "fair in" between the
machined regions.

Disadvantages of the above methods are:--

(1) The time taken to hand "fair in" between the accurately machined sections.

(2) The blade surface can only be as accurate as the templates.

(3) The accuracy is dependant on the size of the cutter since a correction should be made to the templates to define the locus of the cutter moving over a blade surface at the desired section. Because the template shape is usually that of a blade section, an appreciable error is introduced unless the cutter has a cutting edge radius small in comparison with the radius of curvature of the blade surface at the point being considered.

The ideal method of machining an impeller is by an automatically-controlled milling machine using a magnetic tape as an input medium for all machining instructions and control. The technique used to manufacture the model impeller associated with this research project, could be adapted to generate the above machining instructions.

Appendix A 2 gives a method of determining the co-ordinates of points on the locus-surface generated by the centre of a spherical cutter which would machine the surface of an arbitrarily defined impeller blade. The points are obtained in a rectangular grid pattern of a predetermined dimension.

The 8 inch diameter model impeller, Fig. 2.9, (scale ratio of 22.5) was machined in a Pantograph copying machine (Fig. 2.7 and 2.8) from a three-dimensional master template. This master template was four times larger than the model and was machined in a universal miller (Fig. 2.6) to dimensions calculated by the programme in Appendix A 2.

The master templates were used to increase the accuracy of the final impeller and to reduce the number of machining co-ordinates necessary to obtain the required accuracy.

The machined points were placed 0.25 of an inch in the radial direction and either 0.125 or 0.025 of an inch in a direction normal to it, depending on the rate of curvature of the surface at the point being machined. To define the blade surfaces 6550 points were used, ie. 3275 points for each blade surface. The spherical cutter used to machine the master templates was 1.25 of an inch in diameter.

The accuracy of the finished model impeller was within $\pm$ 0.001 of an inch. The accuracy of computation can be selected and depends on the size of the model and master templates.

A brief description of the machining technique used is given in Appendix A 3.

3.0   MODEL ARRANGEMENT AND TESTING PROCEDURE

3.1   MODEL ARRANGEMENT.

Investigations were conducted to determine the impeller characteristics and surface pressures on the duct of a simple two-dimensional Hydrojet model as shown in Fig. 3.1. This model was tested in the 18 inch diameter Research Water-Tunnel of the Department of Mechanical Engineering.

The model consisted of several plane cylindrical sections of 8 inch internal diameter, to which was attached a contoured entrance section and a converging exit nozzle. The duct from intake to exit was 4.625 impeller diameters in length and the impeller was located in a plastic section 2.75 diameters from the intake. The plastic section of the duct surrounding the impeller had a blade tip clearance of 0.0028 impeller diameters.

The entrance section was a portion of an NACA 0015 basic thickness profile with an NACA 250 mean line. (Ref. 3.1, Nozzle 19 in Table 2). The exit nozzle had an area ratio ($\frac{A_J}{A}$) of 0.745 which corresponds to the design thrust load coefficient of the impeller as expressed in equation 1.5 of Section 1.2.1.
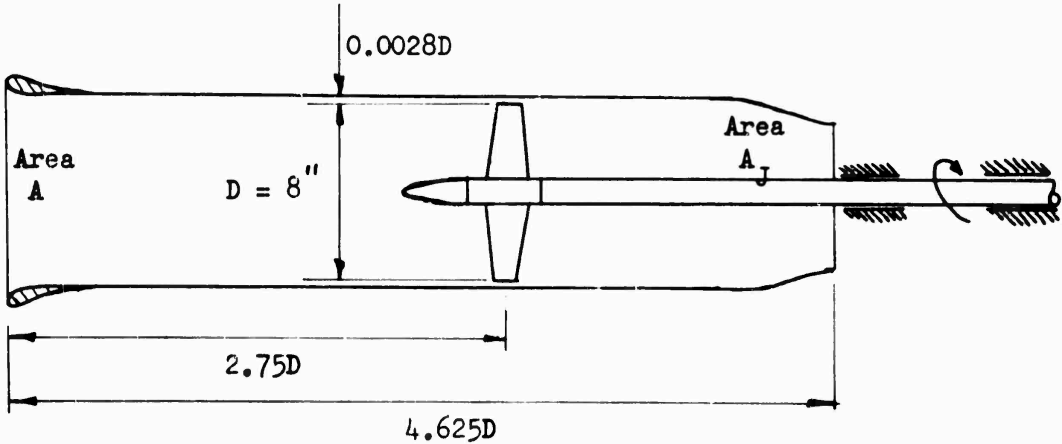
The pressure transducer (Section 4.1.2) could be mounted in any one of a series of locations placed on a plane parallel to the duct centre-line.

The other basic component of the model Hydrojet was the impeller dynamometer and drive shaft assembly. The drive shaft which housed the dynamometer was supported by bearings aft of the duct. Some difficulty was met with the design of these bearings because the impeller, dynamometer and drive shaft acted as a torsional pendulum and was excited by the slightest change in resistive torque of the bearing. However, the vibration of the dynamometer was reduced to workable levels by firstly inserting a carbon liner into the bearing and secondly by heavily damping the bearing supports. The damping was provided by lead weights which were attached to the supports and which were free to vibrate as dynamic absorbers.

3.2 DESIGN OF THE DYNAMOMETER.

The design requirements for the dynamometer were as follows,

(a)   The new system had to fit into the existing drive shaft without modification.

(b)   The system had to measure the mean values of torque and thrust.

(c)   The fluctuating components of the torque and thrust had to be measured.

The arrangement finally selected for the dynamometer is shown in Fig. 3.2 and 3.3.

The bearing which carried the impeller was elastically connected to the drive shaft by a thin-walled cylindrical sensing element. This allowed relative motion between the shaft and impeller and at the same time effectively supported the impeller.

A tapered-land hydrostatic bearing (Ref. 3.2) was chosen because the change in eccentricity of the bearing and journal is very small for a

change in the bearing load.   Thus the damping properties of the bearing
were very nearly constant and the damping was viscous.

As the impeller was effectively supported by the bearing, the design
of the sensing element was controlled by the maximum loading conditions of
the impeller, providing the natural frequencies of the dynamometer were
also acceptable.   Also another design requirement of the sensing element
was that its strain levels under normal operating conditions had to be
large enough to be detected by the measuring instruments.

The characteristics chosen for the dynamometer were as follows:--

TABLE 3.1

	THRUST	TORQUE
Normal max. loading - (Limited at present by electronic instrumentation)	100 lbf	200 lbf ins
Max. Design Loading	400 lbf	350 lbf ins
Natural Frequency with impeller in air	2000 cps	370 cps
Sensitivity of dynamometer and amplifier (Sect. 4.2)	0.031 volts/lbf	0.043 volts/lbf.in
Sensing element dimensions	1.300 in. dia.	
	1.300 in. length	
	0.030 in. wall thickness	
	Material - Cast Monel.	

The forces acting on the dynamometer were detected by a fully active
Wheatstone bridge circuit incorporating resistance wire strain gauges
supplied with a DC voltage.

Because the sensing element initially was open to the surrounding
water, the gauges were waterproofed by a thin coating (0.050 ins.) of a
silicone rubber compound.   This proved to be unsatisfactory because
the moisture content gradually increased over a period of several weeks
to a level that upset the balance of the D.C.

pre amplifiers in the recording instrumentation. (Appendix A7.)
For this reason an alternative method was used, which consisted of
forming an enclosed space above the strain gauges with a thin rubber
diaphragm (Fig. 3.3). The space was then filled with silicone oil
to exclude the entry of water into the space. This arrangement was
an improvement on the previous method.

Unfortunately after completing the model tests discussed herein
it was found that a small amount of water had entered the cavity and
that the silicone oil had affected the cement used to bond the strain
gauges to the sensing element. The torque and thrust results may thus
be in error (See Section 5.2.1).

3.3   MODEL TESTING PROCEDURE

Tests were conducted to determine the following:-

(a)   The fluctuating pressures acting on the inner surface of the
        duct near the plane of the impeller for,

        (i)   Uniform flow at the impeller.

        (ii)   Non-uniform flow at the impeller.

(b)   Impeller Performance Characteristics.

        (i)   Steady state values for thrust and torque.

        (ii)   Velocity in the wake of the impeller.

The above characteristics were investigated at both 15 and 20 rps of
the impeller, for various advance coefficients J_I, where

$$J_I = \frac{V_I}{nD}$$

V_I = duct velocity at intake (fps)

n = impeller rotational speed (rev per sec)

and   D = impeller diameter (ft)

When the model was tested under non-uniform inflow conditions, a
series of wire-mesh patches, which formed a velocity wake inducer

(Ref. 3.3), were located forward of the duct intake. The complete wake inducer could be rotated during these tests about a longitudinal axis of the duct. This enabled the complete pressure distribution on the duct surface to be measured by only one transducer which could be moved axially along the duct.

Since it is known that the induced vibratory pressure of an impeller is periodic in relation to impeller rotation, and that it has a fundamental frequency equal to the blade passing frequency (ie. rotational speed of the impeller times the number of blades), it was decided to express the pressure by a Fourier Series.

As facilities were available to process recorded analogue data into digital information, the Fourier components were determined analytically. The design and construction of a high-speed magnetic tape recording system with a Frequency Modulated (FM) recording mode was thus undertaken and is discussed in the following Section 4.0 and also in Appendix A7.

4.0   INSTRUMENTS AND APPLIED MEASURING TECHNIQUES.

The design and construction of much of the instrumentation for
measurement and data recording was undertaken for this research project.

The recording mode selected for this project was F.M. (frequency
modulated) to I.R.I.G. specifications.

The recorded F.M. analogue signal was converted to digital informa-
ation before analysing the data on a digital computer.

The recording instruments can be divided into the following basic
groups:--

(1)   Sensing elements - transducers

(2)   Signal amplifiers and conditioning units

(3)   Recording system - high-speed tape recorder

A simplified block diagram of the instrumentation is given in Fig. 4.1.

Details of each unit and its calibration are given in the following
sections and Appendix A7.

4.1   SENSING ELEMENTS - TRANSDUCERS.

4.1.1 Torque and Thrust Transducers.

Torque and thrust transducers were mounted in the dynamometer,
details of which are given in Section 3.2.

The impeller which was supported on a hydrodynamic tapered bearing
was elastically attached to the drive shaft via a thin-walled cylindrical
tube, or strain shell.

The sensing elements, resistance wire strain gauges, were cemented to the strain shell in the directions of the principal stresses, and were connected to form a fully-active Wheatstone bridge circuit which was sensitive to either axial or torsional loading.

The strain gauges in the torque and thrust bridges consisted of four 600 Ω Phillips strain gauges, PR 9812 with a nominal gauge factor of $K = 2.0$.

A direct current (D.C.) strain-gauge system was adopted, and the signals were voltage amplified in D.C. pre-amplifiers attached to the flywheel of the impeller drive shaft.

Monel-metal slip-rings with silver carbon brushes were used to transmit the signals to MOVADAS, the recording system.

4.1.2   Pressure Transducer.

The pressure transducer used was a Statham PM 222 TC $\pm$ 5-200 Bi-directional Differential Pressure Transducer which had a nominal output of 370 μV/psi/volt and a maximum excitation voltage of 3 volts.   The diaphragm of the transducer which was 0.25 of an inch in diameter, was flush mounted as an external surface of the transducer.   Because of its construction, the transducer had to be enclosed in a water-proof holder with only the sensing diaphragm and the signal leads open to the atmosphere.   It was found necessary, during the tests, to apply an internal pressure to the transducer diaphragm in excess of the static pressure at that particular point to ensure no possible entry of water into

the holder.

Before and after each series of measurements, the transducer was statically calibrated. The following is a brief specification of the transducer.

Table 4.1.

PRESSURE TRANSDUCER SPECIFICATION.

Model	Statham PM 222 TC $\pm$ 5-200
Pressure Range	$\pm$ 5 psid
Transduction	Resistance, balanced complete unbonded strain gaige bridge
Normal Bridge Resistance	200 Ω
Excitation	3 volts D.C.
Nominal Output	370 μV/psi/volt.

4.1.3   Event Marker - Transducer.

This simple transducer, namely a photo-electric cell was arranged to give a voltage spike once per revolution at a known position of the impeller. This voltage signal, after amplification, triggered a monostable multivibrator to generate a square pulse which was recorded, in F.M. form, on a track of the tape-recorder.

In the subsequent mathematical analysis, the phase of the Fourier components of the wave were determined with respect to the Event Marker signal.

The Units comprising the Event Marker are discussed in Appendix A 7.

4.2   SIGNAL AMPLIFIERS AND CONDITIONING UNITS.

The signal amplifier and conditioning units form a data acquisition system whic is called MOVADAS (Modulated Voltage Analogue Data Acquisition System).

MOVADAS consists of the following units (see Fig. 4.1.).

(1) D.C. voltage pre-amplifiers and mean-reading instruments.

(2) High-pass filter

(3) Driver amplifier

(4) Voltage to Frequency (V-F) Converter

(5) Programming Switch

Details of these units are given in Appendix A 7.

In order to obtain a signal capable of driving the Voltage to Frequency (V-F) Converter, the voltage output of the transducers were firstly D.C. amplified using balanced push-pull stages to gain stability and a satisfactory common mode rejection ratio. High-pass filtering was necessary to remove tunnel noise before further amplifying the AC components and converting the signal to a modulated frequency in the V-F Converters.

Prior to recording the desired F.M. signal on the tape, the programming switch inserted binary coded pulses to identify the

4.5

type of data and the data set or number. Calibration signals
were also fed into the V-F converter to give an instantaneous
calibration of the converter. The identification and calibration
signals were applied to all active data channels simultaneously so
that the resultant digital information could be cross correlated
between channels.

The F.M. signals in the range 54 Kc $\pm$ 40% were recorded at
60 ips. The analogue tape was later converted to digital inform-
ation at a rate of 4000 samples per second of actual recording
time.

The major difficulties encountered while developing the
measuring instrumentation are as follows:--

(1) D.C. Pre-amplifiers.

Because the voltage gains of the torque and thrust
amplifiers were approximately 2500 and 4000 respectively,
any small voltage change on the input side of the
amplifier caused large signal changes at the output.

Originally, the rotating pre-amplifiers and strain
gauges were supplied with power from external batteries
via slip-rings. This arrangement was found to be
unsatisfactory because:--

(i) Changes in brush to slip-ring resistance caused
the strain gauge supply voltage to fluctuate.

(ii) Thermal emf's were generated on the slip-rings.

(iii) Power leads cutting stray magnetic fields gener-
ated small voltages.

The noise was cut to acceptable limits by attaching to the rotating amplifiers, the complete power-supply unit, including batteries and a voltage regulation circuit.

The output from the amplifiers were the only signals transmitted through the slip-rings.

(2) Mean Reading Instrument.

Large fluctuations in the thrust and torque signals were recorded after the D.C. pre-amplifiers. It was not possible to record consistant mean readings on a normal volt-meter.

A consistant average was obtained by counting the number of cycles on the output of the V-F converter over a period of 10 seconds. For this test, the high-pass filter was removed from the normal recording circuit.

It was thought that the large fluctuations in the signals were caused by non-uniform flow at the impeller.

(3) High-pass Filter.

The level of the background tunnel noise was approximately equal to the magnitude of the maximum pressure signals due to the impeller. A frequency analysis of the total pressure showed that most of its components were below 60 cps. The major component of the pressure noise occurred between 30 and 35 cps.

The noise was due to changing static pressure in the working section caused by :--

(i) Average flow rate changing with time.

(ii) Vibrations transmitted to the working section and water tunnel structure from the drive motors, pumps and auxiliary units.

Since the frequency of the major component of the noise was below the blade passing frequency, filtering was adopted. After filtering out 50 cps and below, the pressure signal showed properties of a stationary periodic wave (refer Section 5.1).

The simple filter used did not have a sharp cut-off frequency, as it was only a single stage T filter. It was thus necessary to measure the complete transfer function of the filter and correct the measured signal. A typical plot of the transfer function components of one of the filters is shown in Fig. 4.2.

4.3 MATHEMATICAL ANALYSIS OF RECORDED INFORMATION.

After analogue to digital (A-D) conversion, the recorded digital information was identified and converted into words compatible to the word structure of the digital computer, CDC 6400 which was used in subsequent analyses (see Appendix A 7 and A 8 for details).

The list of digits which constituted a single experimental reading of one variable was termed a file. In each file there were a number of revolutions of the impeller, depending on the recording time. It was possible to choose from a complete file a list of numbers which corresponded to any one or more of the recorded revolutions of the impeller. This was possible because the identification pulses, from the programming switch, were recorded simultaneously on all active channels.

A Fourier analysis of the recorded signals was performed by considering the points as constituting a series of pseudo square waves whose Fourier coefficients can be expressed mathematically. The Fourier coefficients of the complex wave were determined by summing the coefficients of the pseudo square waves (see Ref. 4.1 and Appendix A 8)

The orientation of the reference axes used to describe the position of the impeller or a point on the duct surface is as follows:--

Consider a right handed set of axes OX, OY, and OZ with origin on the impeller axis and axes OY and OZ in the plane of the impeller (see Fig. 5.1). The plane YOZ was taken in these model studies to be the plane which contains the centroids of all the blade sections. (Section 2.3 of Appendix A 1 shows this to be a property of the impeller design).

The OX axis is in the same direction as the axial displacement of the impeller with respect to the fluid. The OY axis is

taken as the reference line for all angular measurements. The angular position of a given blade from the OY axis is θ and the position of a point in space is given by the coordinates X, r, γ.

4.3.1 Pressure Field.

The Fourier components of the pressure fluctuations at a point on the duct surface X, R_d, γ (see Fig. 5.1) were reduced to the following form, where R_d is the duct radius,

$$p = \sum_{i=1} A_i \cos(4 i(\theta - \gamma) + \varepsilon_i) \qquad \ldots 4.1$$

where A_i = modulus of pressure component of the ith harmonic of blade frequency, ie. single amplitude of vibratory pressure

θ = blade angle with respect to axis, Fig. 5.1

ε_i = phase-lead angle of ith harmonic

The magnitude of the pressures are also given in the form of non-dimensional coefficients K_{pi} and K_{pt} where

$$K_{Pi} = \frac{A_i}{\rho n^2 D^2} \quad \text{and} \quad K_{Pt} = \frac{P_t}{\rho n^2 D^2} \qquad \ldots 4.2$$

where P_t = single amplitude of total (all frequencies) vibratory pressure, peak to peak

r = propeller revolutions per second

D = propeller diameter

ρ = density of fluid

4.3.2 Vibratory Impeller Forces.

The direct measurement of fluctuating forces acting on an impeller propulsion system is extremely difficult because the forces must be determined from a knowledge of the vibrations of the propulsion system. This requires the complete dynamic properties of the impeller, drive and supporting system to be known. A further complication arises, however, due to a fundamental property of an impeller. The various modes of vibration of a propulsion system are cross coupled by the impeller.

The dynamics of this type of system are investigated, in part, in Ref. 4.4. Here a theoretical analysis is undertaken of an elastically supported impeller being excited by a sinusoidal gust velocity. Experimental values of the dynamic coefficients mentioned in this report are given in Ref. 4.5.

Consider a simple, elastically supported impeller vibrating about its longitudinal axis (ie. axial and torsional). The complete transfer function of an impeller-mass-spring system is not only dependent on the mechanical properties of the mass-spring system, but also on the geometry of the impeller.

The equations of motion describing this coupled system can be expressed in the following:-

$$\left[\ddot{\varepsilon}_Z M_Z + \dot{\varepsilon}_Z C_Z + \varepsilon_Z c^F_Z \right]$$

$$+ \left[\ddot{\varepsilon}_Z \boxed{\frac{F_Z}{\ddot{\varepsilon}_Z}} + \dot{\varepsilon}_Z \boxed{\frac{F_Z}{\dot{\varepsilon}_Z}} + \ddot{\varphi}_Z \boxed{\frac{F_Z}{\ddot{\varphi}_Z}} + \dot{\varphi}_Z \boxed{\frac{F_Z}{\dot{\varphi}_Z}} + \varphi_Z c^{FT}_Z \right] = F_Z$$

$$...4.8$$

$$\left[\ddot{\varphi}_Z I_Z + \dot{\varphi}_Z G_Z + \varphi_Z c_Z^T \right] +$$

$$+ \left[\ddot{\varphi}_Z \boxed{\dfrac{T_Z}{\ddot{\varphi}_Z}} + \dot{\varphi}_? \boxed{\dfrac{T_Z}{\dot{\varphi}_Z}} + \ddot{\varepsilon}_Z \boxed{\dfrac{T_Z}{\ddot{\varepsilon}_Z}} + \dot{\varepsilon}_Z \boxed{\dfrac{T_Z}{\dot{\varepsilon}_Z}} + \varepsilon_Z c_Z^{TF} \right] = T_Z$$

$$\dots 4.9$$

The first group of terms in both equations refer to an elastically supported impeller vibrating in air. These coefficients are called the dynamic mechanical coefficients. The second group of variables refer to the hydrodynamic and cross coupling properties of the impeller system, the dynamic hydro-mechanical coefficients. The definitions of the above quantities are given below in Table 4.2.

Combining the second group of variables in equations 4.8 and 4.9 as:-

$$\left[\ddot{\varepsilon}_Z \boxed{\dfrac{F_Z}{\ddot{\varepsilon}_Z}} + \dot{\varepsilon}_Z \boxed{\dfrac{F_Z}{\dot{\varepsilon}_Z}} \right] + \left[\ddot{\varphi}_Z \boxed{\dfrac{F_Z}{\ddot{\varphi}_Z}} + \dot{\varphi}_Z \boxed{\dfrac{F_Z}{\dot{\varphi}_Z}} + \varphi_Z c_Z^{FT} \right] =$$

$$= \left[\dfrac{1}{H_{H\varepsilon}} \right] \varepsilon_Z + \left[H_4 \right] \varphi_Z \qquad \dots 4.10$$

$$\left[\ddot{\varphi}_Z \boxed{\dfrac{T_Z}{\ddot{\varphi}_Z}} + \dot{\varphi}_Z \boxed{\dfrac{T_Z}{\dot{\varphi}_Z}} \right] + \left[\ddot{\varepsilon}_Z \boxed{\dfrac{T_Z}{\ddot{\varepsilon}_Z}} + \dot{\varepsilon}_Z \boxed{\dfrac{T_Z}{\dot{\varepsilon}_Z}} + \varepsilon_Z c_Z^{TF} \right] =$$

$$= \left[\dfrac{1}{H_{H\varphi_1}} \right] \varphi_Z + \left[H_3 \right] \varepsilon_Z \qquad \dots 4.11$$

and assuming that differential equations 4.8 and 4.9 are linear, with constant coefficients, they can be expressed as:-

Table 4.2 PROPERTIES OF THE ELASTIC SYSTEM.

Symbol	Description	Units.
	Dynamic Mechanical Coefficients	
ε_Z	Longitudinal displacement	ft.
φ_Z	Angular displacement	rad.
F_Z	Axial load – thrust	lbf.
T_Z	Torsional load – torque	lbf.ft.
M_Z	Effective mass of vibratory system in air	slug
C_Z	Damping in longitudinal direction	lbf.sec/ft.
c_Z^F	Stiffness in longitudinal direction	lbf/ft.
I_Z	Effective inertia of system in air	lbf.ft.sec^2
G_Z	Damping in torsional direction	lbf.ft.sec.
c_Z^T	Stiffness in "	lbf.ft/radian
c_Z^{FT}	Cross coupling stiffness between ε_Z and	"
c_Z^{TF}	φ_Z displacements	lbf/ft.

Table 4.2 continued.

<u>Dynamic Hydro-mechanical Coefficients</u> (Ref. 4.4, Table 1.3)

Symbol	Description	Units
$\dfrac{F_Z}{\dot{\varphi}_Z} = \dfrac{T_Z}{\dot{\varepsilon}_Z}$	Velocity coupling	lbf.sec.
$\dfrac{F_Z}{\ddot{\varphi}_Z} = \dfrac{T_Z}{\ddot{\varepsilon}_Z}$	Acceleration coupling	$lbf.sec^2$
$\dfrac{F_Z}{\dot{\varepsilon}_Z}$	Axial damping	lbf.sec/ft
$\dfrac{F_Z}{\ddot{\varepsilon}_Z}$	Axial entrained mass	slugs
$\dfrac{T_Z}{\dot{\varphi}_Z}$	Torsional damping	lbf.ft.sec
$\dfrac{T_Z}{\ddot{\varphi}_Z}$	Entrained moment of inertia	$lbf.ft.sec^2$

$$\left[\frac{1}{H_\varepsilon} + \frac{1}{H_{H\varepsilon}}\right]\varepsilon_Z + H_4\,\varphi_Z = F_Z \qquad \ldots 4.12$$

$$\left[\frac{1}{H_\varphi} + \frac{1}{H_{H\varphi}}\right]\varphi_Z + H_3\,\varepsilon_Z = T_Z \qquad \ldots 4.13$$

Here H_i represent the transfer function of a particular section i of the vibratory system

where

      $i = \varepsilon$ simple longitudinal system in air

      $i = \varphi$ simple torsional system in air

      $i = H\varepsilon$ hydrodynamic system for longitudinal displacement

      $i = H\varphi$ hydrodynamic system for torsional displacement

and $i = 3,4$ coupling between longitudinal and torsional displacement

A further simplification can be made by substituting

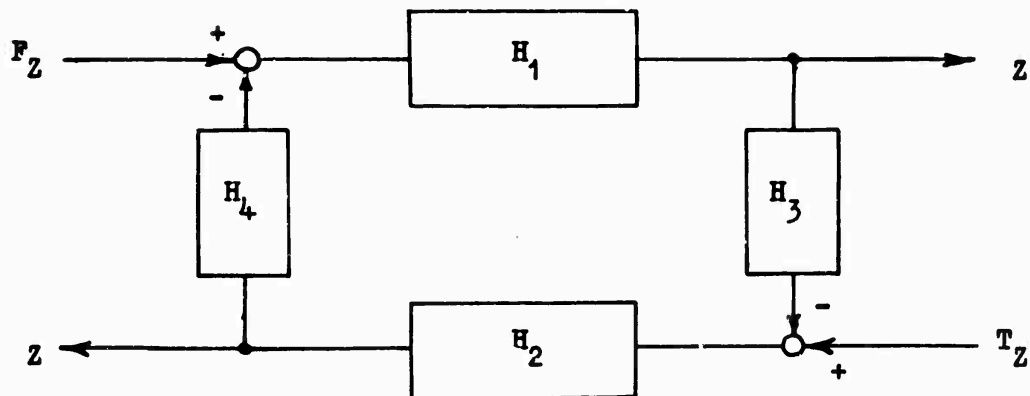$$\frac{1}{H_1} = \frac{1}{H_\varepsilon} + \frac{1}{H_{H\varepsilon}} \qquad \ldots 4.14$$

and

$$\frac{1}{H_2} = \frac{1}{H_\varphi} + \frac{1}{H_{H\varphi}} \qquad \ldots 4.15$$

into equation 4.12 and 4.13

$$F_Z = \frac{\varepsilon_Z}{H_1} + H_4\,\varphi_Z \qquad \ldots 4.16$$

$$T_Z = \frac{\varphi_Z}{H_2} + H_3\,\varepsilon_Z \qquad \ldots 4.17$$

This permits the impeller-mass spring system and associated hydro-dynamic effects to be illustrated by a block diagram as follows:--

The actual impeller loading can be calculated from measured displacements ε_z , φ_z by equations 4.16 and 4.17 once the respective transfer functions have been determined either mathematically or experimentally.

It was intended that the fluctuating forces acting on the impeller of the Hydrojet model would be measured in these studies, but this was not possible because of a faulty dynamometer (Section 3.2).

An outline of the method used to calibrate the dynamometer is given in Section 4.5.

4.4   SPHERICAL 5-HOLE PITOT AND ITS CALIBRATION.

Until now, the claibration of the 5-hole spherical pitot was
conducted in a fluid in which the relative direction of flow was
known accurately.   This necessitated the use of a towing tank,
in which the relative motion of carriage and water was precisely
known, or the use of a very accurate wind or water tunnel.

A method was devised to accurately calibrate a spherical
pitot in a flow whose direction is only approximately known.
Calibration is thus possible in a small wind tunnel, water tunnel
or duct.

The calibration procedure and theoretical analysis which is
given in detail in Appendix A 6, is briefly discussed in the
following section.

4.4.1   Theory.

The potential solution of the flow around a sphere gives the
pressure at a point as:--

$$\frac{p - p_o}{\frac{1}{2} \rho V^2} = 1 - \frac{9}{4} \sin^2 \beta \qquad \qquad \dots 4.3$$

where   p   =   pressure at point considered

         p_o =   free stream pressure

         V   =   magnitude of velocity vector $\bar{V}$ of free stream

         ρ =   fluid density

         β =   angular position of point from stagnation point

For three equispaced holes a, b, c on a great circle of a sphere Pien (Ref. 4.2) has shown that (see Fig. 4.3) --

$$C_{ph} = \frac{p_a - p_b}{\frac{1}{2} \rho V_h^2} = \frac{9}{4} \sin 2\alpha \sin 2\beta_h \qquad \ldots 4.4$$

$$C_{Ph} = \frac{p_a - p_b}{2P_c - p_a - p_b} = \frac{\sin 2\alpha}{1 - \cos 2\alpha} \tan 2\beta_h \qquad \ldots 4.5$$

where

p_a, p_b, p_c = pressures at a, b, c.

C_{ph}, C_{Ph} = pressures coefficients

α = angle between adjacent holes

V_h = orthogonally projected component of the velocity $\bar{V}$ onto the plane of the great circle

β_h = angle between V_h and the stagnation point

From measurements of p_a, p_b, p_c the value of β_h can be calculated from equation 4.5, whence V_h can be obtained from equation 4.4. If on the great circle through c orthogonal to that through a, b, c, two equispaced holes a' and b' are placed as shown in Fig. 4.3, the component V_v of the velcoity $\bar{V}$ in the plane of this circle can be determined from measurement of p_a', p_c', p_b' by equations analogous to 4.4 and 4.5. The three components V_x, V_y, V_z along the sphere axes OX, OY and OZ of the velocity $\bar{V}$ are then given by:--

$$V_x = V_h \cos \beta_h$$

$$V_y = V_h \sin \beta_h$$

$$V_z = V_v \sin \beta_v \qquad \qquad \dots 4.6$$

In Ref. 4.2 and 4.3 in place of equation 4.4 the appropiate relations for

$$\frac{p_c - p_a}{\frac{1}{2} \rho V_h^2} \qquad , \qquad \frac{p_c - p_b}{\frac{1}{2} \rho V_h^2} \qquad \qquad \dots 4.7$$

are used.   The first or second of these pressure coefficients is taken depending on whether V_h is on one side or the other side of the centre hole.   This introduces an unnecessary complication. Use of equation 4.4 is also recommended because its pressure coefficient has a greater variation at any given value of β_h than these other two coefficients, thus giving a greater sensitivity.

4.4.2   Calibration.

4.4.2.1   Initial Angular Calibration.

The pitot is set up in a flow whose direction is approximately known, so that it can be rotated about two axes OY, OZ which are normal to each other and to the nominal flow direction.   OY and OZ pass through the sphere centre and lie approximately in the plane of the holes.   The axis OX also passes through the sphere centre and is orthogonal to OY and OZ.   The axes OX, OY, OZ are

are called the pitot axes.

Values of the expression for C_{ph} and C_{Ph} versus β_h and C_{pv} and C_{Pv} versus β_v are obtained by rotating the pitot axes OY and OZ respectively.

The error introduced by the flow velocity $\bar{V}$, not being in the calibration plane will be quite small since the velocity in the calibration plane will differ from V only by $V(1 - \cos\phi)$ where ϕ is the angle of $\bar{V}$ to the calibration plane. Usually ϕ will not be more than a few degrees.

4.4.2.2   Orientation of Pitot Axes with reference to Datum Instrument Axes.

On the pitot base there will have been machined location faces. These can be used to define a set of orthogonal axes at the sphere centre, which will be called the datum instrument axes OXX, OYY and OZZ. The problem is now to determine the orientation or position of the pitot axes with reference to these known instrument axes. As shown below, this orientation can be determined in a stream whose flow direction is only approximately known, by three inversions of the sphere position, providing the pitot is set up in the flow so that the sphere can be rotated about OXX, OYY or OZZ without the centre of the sphere moving in space.

(1)   Rotation about OXX Axis.

The sphere is initially positioned so that the flow vector $\bar{V}$ is at some estimated angle ψ to the centre hole (of between 5° and 10°). The sphere is then rotated

successively by 90° about the instrument axis OXX.

By solving equations 12 to 15 of Appendix A 6 the orientation of the pitot axis OX with respect to the instrument axes can be determined.

(2) **Inversion about OYY axis**

The sphere is positioned so that the velocity $\bar{V}$ will make an angle $\theta \simeq 5^\circ$ with the XXYY plane as shown in Fig. 4.4. Since the flow direction is known approximately, an estimate of the value of θ can be made. The sphere is then rotated about OYY so that $\bar{V}$ will make an angle of approximately $-\theta$ with the XXYY plane. Using values of the pressures at the initial and final positions, the orientation of pitot axis OZ with respect to the instrument axes can be determined (by solving equations 24 and 25, Appendix A.6).

(3) **Inversion about OZZ axis**

By repeating the procedure outlined in the section above, but in this case, for inversion about the OZZ axis, the orientation of OY axis can be determined.

4.4.2.3   Calibration Assumptions.

The initial calibration referred to in section 4.4.2.1 is based on an assumption, that the flow velocity is in the calibration plane. The accuracy of calibration can be increased by repeating the calibration procedure now that the fluid direction with respect to the instrument can be calculated.

Another assumption is that the pressure relationship between the holes is only dependent on the velocity component which can be considered as existing in the respective plane of calibration and that the pressure distribution is independent of the magnitude of the velocity component in the other calibration plane.

This is true for a perfect sphere having infinitely small holes which lie on a great circle through the centre hole.

The calibration of this instrument should include a check on its accuracy for fluid velocities whose directions are not in in the calibration plane.

The velocity gradient of the free stream is also assumed to be small over the area of cross section of the sphere.

4.4.3   Construction Details.

The diameter of the spherical head was chosen to be 0.375 of an inch.   An angular distance between the centre hole and the side holes of 20° and a hole diameter of 0.024 of an inch was selected.

The major difficulty in constructing an accurate spherical pitot is to accurately position the pressure tapping holes in the sphere.   The following method of manufacture was used to partly alleviate this problem.

(1)   The head was rough machined to a cylindrical form.

(2)   This blank was mounted on a precision vertical drilling machine and pressure tapping holes were drilled parallel to the axes of the pitot head.

These holes were positioned so that a point on their centre line would be 20° to the axis of the spherical head when the head was machined spherical to 0.375 of an inch in diameter.

(3)   Small bore stainless steel tubes were inserted into the holes and soldered in place.

(4)   The head was accurately machined spherical.

4.5   <u>DYNAMIC CHARACTERISTICS OF THE DYNAMOMETER.</u>

Before a dynamic calibration could be undertaken, the linearity of the dynamometer had to be proven for various loading combinations of thrust and torque.   This test was conducted, and the dynamometer and associated recording instruments were shown to be linear with load.

The dynamic properties of an impeller-dynamometer system, as discussed in Section 4.3.2, can be broadly divided into the determination of -

(a)   The dynamic mechanical coefficients

(b) The dynamic hydro-mechanical coefficients

4.5.1   <u>Dynamic Mechanical Coefficients.</u>

A common method of determining the transfer function of a dynamic system is to excite the system with a sinusoidal force and measure the overall response of the system.   This method can be applied in nearly all cases, but certain restrictions and experimental procedures must be met, depending on the physical properties of the system and the force exciter.

However, the only possible way of applying an exciting force to the dynamometer, (Section 3.2) was by an external force exciter.   If the connection of this force exciter to the dynamometer, was to have a neglible effect on the actual transfer function of the latter, then the mass, stiffness and damping of the exciter had to be small in comparison with that of the dynamometer.

This was true for the axial mode but in the torsional mode, which had a low stiffness and natural frequency, this situation did not exist.   In this case, the dynamometer-plus-exciter system had to be considered as a compound system, each component of which had its own transfer function.

Here the torsional transfer function of the dynamometer was obtained by a vectorial substraction of the transfer function for the exciter from that of the exciter plus dynamometer system. This method of determining the vibration characteristics of a compound system is discussed in Ref. 4.6.

(a) <u>Transfer Function of the Exciter.</u>

The force exciter, which was used to determined the transfer functions, was an electro-magnetic loud-speaker coil assembly.

Two methods can be used to determine the transfer function of of electro-magnetic exciters. The experimental method was adopted for these studies in preference to a theoretical derivation. This required connecting the exciter to a known vibratory system and measuring the complete transfer function of the combined system.

A simple cantilever beam was selected as the known vibratory system. Its natural frequency and stiffness was chosen to be approximately equal to that of the dynamometer.

A certain portion of the mass of the exciter appeared to behave as a point mass loading on the beam. The magnitude of this mass was determined from a knowledge of the natural frequency of the system. Knowing this and the physical properties of the beam, the transfer function for the beam and effective mass loading was calculated. Now the vibratory characteristics of the exciter can be obtained by vectorial substraction of the transfer function of the beam from that of the combined system.

It was found that the exciter had only a small influence on the combined system and that it behaved as an extra mass loading.

(b) <u>Transfer Function of the Dynamometer in Air.</u>

Tests, similar to those above, were conducted to determine the dynamic mechanical coefficients of the dynamometer as expressed in equation 4.9. of Section 4.3.2.

The dynamometer-plus-exciter system was considered as a compound system, as discussed previously.

The mass or inertia added to replace the impeller during these tests was equal to that of the impeller in air.

4.5.2   <u>Dynamic Hydro-Mechanical Coefficients.</u>

It was anticipated that the following tests would be undertaken, but as previously mentioned, a fault in an electrical component of the dynamometer terminated these.

The values of dynamic hydro-mechanical coefficients were to be computed theoretically (Ref. 4.4) and compared with those determined experimentally from a knowledge of the free vibrations of the impeller-dynamometer when immersed in water (Ref. 4.7).

It is worthwhile to mention that the theory of Wereldsma (Ref. 4.4) is based on an unsteady two-dimensional airfoil theory presented by Von Karman and Sears (Refs. 4.8 and 4.9). This theory may be better adapted to ducted impellers than open water propellers, because in a ducted impeller the radial velocities and the velocity gradients over the blade length are small.

5.0   RESULTS OF MODEL EXPERIMENTS.

5.1   PRESSURE ON DUCT SURFACE.

The reference axis used to describe orientation of the impeller and the position of a point P (X, r, γ) is shown in Fig. 5.1. The right handed set of axes OX, OY, OZ with origin on the impeller axis has the axes OY and OZ in the reference plane of the impeller.

The reference plane, in this case, is the plane which contains the centroids of all the blade sections.

The direction of the OX axis is opposite to the fluid motion. All angular measurements are taken from the OY axis. The angular position of the impeller is given by θ (Fig. 5.1). The coordinates of a point on the duct surface are X, R_d, γ.

The induced fluctuating pressures p measured on the duct for the uniform in-flow conditions were taken at a fixed angular position of $\gamma = 0$ and various axial distances (X). The pressures at these points were expressed by the following equation --

$$p = \sum_{i=1} A_i \cos [4 i (\theta - \gamma) + \varepsilon_i] \qquad \dots 5.1$$

where A_i = magnitude of the ith harmonic of blade frequency pressure (i.e. single amplitude of the vibratory pressure).

θ = impeller blade angle with respect to the axes in Fig. 5.1.

γ = angular position of the point being considered (Fig. 5.1).

ε_i = phase-lead angle of ith harmonic component.

For the uniform flow conditions, the relationship above applied to all values of γ on the same axial section at X, because A_i and ε_i were independent of γ.

For the non-uniform in-flow to the impeller, however, the pressure

measurements were taken for various values of γ and X. The pressures were again expressed by equation 5.1, but for this type of pressure distribution the values of A_i and $\mathcal{E}_i$ were dependent on γ .

The test results are presented in a non-dimensional form which has been justified by other investigators (Ref. 5.1 and 5.3).

$$K_{Pi} = \frac{A_i}{\rho\, n^2\, D^2} \quad \text{and} \quad K_{Pt} = \frac{P_t}{\rho\, n^2\, D^2} \qquad \ldots 5.2$$

where K_{Pi} = pressure coefficient of ith harmonic of blade
frequency.

K_{Pt} = Pressure coefficient of total pressure.

P_t = half the peak to peak value of the total pressure
(all frequencies) (lbf/ft^2).

n = impeller rotational speed (rpm).

D = impeller diameter (ft).

ρ = density of fluid $(slug/ft^3)$.

5.1.1 Effect of Filtering the Signal and of its Periodicity.

The pressure measured by the transducer had two components. The periodic component in Fig. 5.2 was due to the induced pressure field of the impeller and the lower frequency component, apparently non-periodic, was generated by various external mechanisms remote from the impeller-duct system. The latter component had major frequencies between 30 and 35 cps. This was due to the excitation of the working section and supporting structure of the water tunnel at its natural frequency. The vibration was excited by force transmission through the pipe work from the main pumps and drive motors.

Because the level of the unwanted pressure fluctuations above 50 cps approached the noise level of the recording amplifiers, it was decided to select the operating conditions of the impeller so that the fundamental frequency of the induced pressure exceeded 50 cps. The impeller rotational speeds were thus chosen to be 15 and 20 cps, which corresponded to a fundamental frequency for the fluctuating pressure of 60 and 80 cps respectively.

It was decided to filter out the unwanted pressure component electronically, because without the use of a filter, it was difficult to study the induced pressure at distances greater than $\frac{X}{D} = 0.15$ where the noise to signal ratio exceeded 2. With the unwanted signal component removed it was possible to monitor the impeller induced pressure signal prior to recording. The recording accuracy was also improved because the signal due to the induced pressure was capable of driving the recording instruments over their full operating range.

A Fourier analysis of the filtered pressure signal was performed on the digital information obtained from the recording instruments. Over a period of 8 revolutions of the impeller, various samples of the recorded information were analysed and compared with those obtained from an analysis over the 8 revolutions. Fig. 5.3 shows the results of the Fourier analysis where the pressure coefficient for various samples (·, ⊙ , ..) are compared with the average pressure coefficient ( ) at the different harmonics of blade frequency. The pressure coefficients in Fig. 5.3 for the samples were computed from digital information between the NPI^{th} and the $(NPI + NP)^{th}$ revolution of the impeller. The values of NPI and NP for the samples are given in Fig. 5.3.

The results given in Fig. 5.3 show remarkable agreement with each other for the various harmonics of the blade frequency. Thus the pressure signals detected were stationary. A frequency analysis of the measured pressure is given in Fig. 5.4 for an impeller rotational speed of 20 cps. It can be seen that the pressure is periodic with a fundamental frequency of 80 cps. As this corresponds to the blade passing frequency, the results of Figs. 5.3 and 5.4 show that the pressure fluctuations were stationary and periodic.

Although the computed Fourier components were not significantly affected by the sample length, the results discussed in the following sections were the average components taken over 8 revolutions of the impeller for the uniform flow condition, and the average over 4 revolutions in the non-uniform flow conditions.

5.1.2 Effect of Reynolds Number.

The Fourier components of the pressure, namely the pressure coefficient and the phase angle, for impeller rotational speeds of 15 and 20 cps are given in Figs.5.8 and 5.12 for various values of advance coefficient (J_I).

The values for the measured pressure components are independant of the rotational speed. Thus it is assumed that the Reynolds number, at least over the small range applicable to model impellers, has no effect on the induced vibratory pressures of a ducted impeller.

It has also been shown (Ref. 5.1) that the free-space pressures of model open-water propellers are independant of Reynolds number.

5.1.3   <u>Vibratory Pressures with Uniform Flow.</u>

The pressure on the duct was measured for three advance coefficients J_I, equal to 0.74, 0.80 and 0.85 where

J_I = intake advance coefficient

= $\dfrac{V_I}{nD}$ where V_I = duct velocity at intake (fps)

n = impeller rotational speed (cps)

D = impeller diameter (ft)

The test results are presented in Figs. 5.5 to 5.17 and are discussed under the following headings:--

(a)   Vibratory pressure of the blade frequency harmonics.

(b)   Peak-to peak values of the total pressure.

(c)   Phase angle of the blade frequency harmonics.

(d)   Phase angle of the maximum pressure.

(a) <u>Vibratory Pressure of the Blade Frequency Harmonics.</u>

The magnitude of the Fourier components of the induced vibratory pressure acting on the duct surface is shown in Figs. 5.5 to 5.7 for the various advance coefficients.

The axial pressure distribution of the ducted impeller system shows similar characteristics to the free space pressures of an open-water propeller, (Ref. 5.2) but the absolute value of the pressure is far greater.   The attenuation in magnitude with axial distance from the impeller is also greater than that of an open-water propeller.

The major pressure region of a Hydrojet extends over a relatively small distance between + 0.3 to - 0.1 of the impeller diameter.

This length is comparible with the projected length of the impeller blade in the axial direction of $\frac{X}{D}$ =+0.043 to-0.048. The magnitude of the pressure outside this region is of the same order as the pressure which exists at much larger tip clearances ($\frac{r}{D}$ = 0.6 to 0.7) for an open-water propeller.

It is known (Ref. 5.2 and 5.3) that the pressure distribution near an open-water propeller in a uniform velocity field is dependent on,

(i)   the blade loading

(ii)   the blade thickness

The pressure distribution associated with blade loading is symmetrical about the propeller, while that attributed to the blade thickness effect is asymmetrical. The effect of this same asymmetrical pressure distribution was detected for the ducted impeller. (Figs. 5.5 to 5.8). For this reason, the pressure due to the blade thickness effects must have a significant influence on the resulting vibratory pressures of a ducted impeller.

The magnitude of the pressure coefficients (K_{Pi}) for the higher harmonics are large in relation to the fundamental. Values of the K_{Pi} for the second and third harmonics were approximately 60% and 25% respectively of the fundamental value. This large harmonic content is not present in the near pressure field of an open-water propeller with the same number of blades. (Fig. 21 of Reference 5.1).

For a ducted impeller however the blade frequency harmonics are important and must be considered if the peak to peak amplitudes

are to be measured or calculated.

It can also be seen (Figs. 5.5 to 5.7) that for a given blade frequency harmonic, the axial distance at which the maximum pressure occurs moves forward as the harmonic number increases. The phase angle of the harmonics also reveal a forward shift of the harmonics with increasing harmonic number (Fig. 5.9 to 5.11). A discussion of this is left to a following section (c).

(b) Peak to Peak Values of the Total Pressure.

In Fig. 5.8 the magnitude of half the peak-to-peak pressure coefficient is given for the total pressure at various advance coefficients. The peak-to-peak values of the total pressure were determined by synthesizing the actual total pressure from its Fourier components.

As the blade frequency harmonics are very nearly in phase behind the impeller and are definitely in phase forward of the impeller plane, (see following section) the peak-to-peak values of the total pressure (Fig. 5.8) are approximately the sum of the pressures for the odd harmonic components.

(c) Phase Angle of the Blade Frequency Harmonics.

The blade frequency pressure harmonics lead the impeller blade position by an angle ε_i, where i is the harmonic number (eqn. 5.1). Therefore, the maximum pressure of the harmonic components on the duct surface are at an angle ε_i to the impeller blade position in the direction of the angular motion of the impeller.

The determination of the phase angle of any experimentally

derived signal is difficult, and this was the case with the
measured pressure signals (Section 5.15). After carefully study-
ing the results and relating them to the hydrodynamics of an
impeller, the following interpretation of the results is given.

It can be seen from Figs. 5.9 to 5.17 that the pressure field
consists of two separate regions, one forward and the other behind
the impeller. Near the plane of the impeller there is a discon-
tinuity in phase of the induced pressure.

(i)   Forward of the Impeller, the phase angle of each blade
frequency is very nearly independant of axial distance $\frac{X}{D}$
and of advance coefficient of the impeller. This is clearly
shown in Figs. 5.9 to 5.11 where the results for J_I = 0.74
are given. The pattern of variation of the phase angle for
the higher harmonics and higher advance ratios is not so well
defined but the results do appear to follow the same trend
as the lower harmonics.

As previously mentioned on p.5.6, the induced pressure is
dependant on the blade thickness and on the blade loading.
For an open-water propeller, the effect of blade thickness has
been estimated from a source-sink distribution over the blade
surface (Ref. 5.2). Also the pressure due to blade loading
is effectively the pressure distribution of an array of
doublets whose axes are perpendicular to the helicoidal surface
swept out by the advancing blade. Thus the phase angle of
the blade thickness pressure component at any axial
position is constant with respect to the blade position while

the phase angle due to the blade loading component is dependant on the distance from the propeller.

For a ducted impeller, however, the blade thickness must control the total pressure field ahead of the impeller be ause the phase angle of the pressure harmonics are constant with distance.

It has been shown by Breslin (Ref. 5.2, Figs. 2a to 3b) that the blade thickness effect controls the magnitude of the pressure field forward of a propeller. However, only limited evidence has been put forward for the phase relationship of the pressure in this region. Other investigations (Refs. 5.3 and 5.4) have indicated that there is a region forward of a propeller where the phase is substantially independant of distance from the impeller.

However, the phase angle of the harmonic components of the pressure for the ducted impeller ceases to be constant as the blade frequency harmonic number increases. The phase angle for the 3rd blade frequency harmonic, shown in Fig. 5.11 decreases with axial distance from the impeller. The pressure component due to blade thickness effect in this case must have a reduced influence on the total pressure field.

(ii)   <u>In the Region of the Impeller Plane,</u> the trailing vortices
or blade loading effect suddenly affects the pressure field
and the phase angle of the Fourier components show a
discontinuity (Fig. 5.9).   The point at which this discon-
tinuity occurs is not constant but moves forward slightly
with increasing blade frequency harmonic.,(Figs. 5.9 to 5.11).
As the maximum pressure peak also moves forward with
increasing blade frequency harmonic, the effective location
of the bound vortices emanating from the impeller blades
would appear to move forward.

(iii)   Aft of the Impeller.   Although the phase angle (ε_i)

of the harmonics components ⁻igs. 5.9 to 5.15) are for

values between 0 and 2π, they may also be expressed by the

addition of multiples of 2π, i.e. $(\varepsilon_i \pm 2\pi n)$ where

$n = 1,2,3,\ldots$ This is possible because the fluctuating

pressures are periodic over 2π radians. For this reason,

the value of phase angles in the above figures are not

discontinuous at 0 and 2π, but the values do, in fact,

represent a continuous function.

Aft of the impeller, the phase angles of the pressure

harmonics decrease linearly with axial distance from the

impeller plane (Figs. 5.1 to 5.15). The phase change is

in the same direction as the helicoidal wake pattern gener-

ated by the impeller. This indicates that the pressure field

is mainly governed by the pressure associated with the blade

loading, i.e. the pressure due to the trailing vortices. The

trailing vortices have approximately constant pitch equal to

that of the impeller. It is expected that the pitch of the

trailing vortices should be constant in this ducted impeller

case, because previous investigators have show theoretically

and experimentally that they are constant for most open-water

propellers.

It is difficult to determine from the results a relationship

between the phase angle of various harmonic components after the

impeller. The indication is that they are not exactly in phase

(Figs. 5.9 to 5.11) for the region near the impeller. This

may be due to --

(a)   The effective location of the bound vortex lines moving forward.

(b)   Inaccuracies in measurement and computation of the phase angle.

With increasing advance coefficient J_I, the phase angle of the pressure has a tendency to be continuous from forward of the impeller to well aft (Fig. 5.16). For this to occur, the pressure field due to the trailing vortices must be insignificant in comparison with that due to the blade thickness. This is possible because at $J_I = 0.85$ the impeller loading, which in fact controls the magnitude of the pressures associated with the trailing vortices, is extremely small compared with the loading value at $J_I = 0.74$ (Fig. 5 25).

(d)   Phase Angle of Maximum Pressure.

The phase angle of the maximum pressures shown in Figs. 5.12 5.15, and 5.17 are very nearly equal to that of the first blade frequency harmonic, because there is little variation in phase angle between the harmonics.

5.1.4 Vibratory Pressures with Non-uniform Flow.

Pressure measurements were taken with the impeller operating in a non-uniform flow. The velocity distribution at the intake of the duct and forward of the impeller is shown in Figs. 5.18 and 5.19. From these figures it can be seen that the velocity distribution

... efficiency, ...yed from the intake to the impeller.

.... of the fluctuating pressure on the duct was taken at only one advance coefficient J_{lavge} = 0.74. The operating conditions were selected to maintain the same mass flow through the duct as in the previous test at J_l = 0.74 for a uniform flow condition. It would have been better to maintain a constant thrust loading condition between these two tests, but this was not possible due to the malfunction of the dynamometer. The pressure was measured at various angular positions between γ = 0 and $\frac{\pi}{2}$ (Fig. 5.1) because the velocity pattern was basically symmetrical about two normal diametral axes.

A frequency analysis of the pressure revealed that only blade sequence harmonics were significant as was the case for the uniform ....
....
....
....
....

....
....
....
....
....
....
....
....
....

decays more slowly than the cor esponding signal associated with the uniform conditions."

This statement, however, was based on a limited number of calcula-tions at a considerable distance from the propeller where $\frac{r}{D}$ = 0.6. The assumptions of this theory may not apply to a region extremely close to a ducted impeller.

On the other hand the phase angle of the pressure on the duct at various axial distances was different from the uniform case and did not correlate with the wake pattern at the impeller (Figs. 5.23 and 5.24)

5.1.5   Possible Measurement Errors.

Factors which affected the accuracy of the measured pressure components were --

(a)   Recording instrumentation and analysis.

(b)   A finite size pressure transducer.

(c)   Static pressure drop across the model.

(a) Recording Instrumentation and Analysis.

Although the analogue pressure signal and the event signal were recorded simultaneously on different tracks of a magnetic tape (Appendix A7), the sampling of the analogue signal and subsequent conversion to digital information was executed for each track in turn. Thus the digital data from each track was within one sample of the true event. When comparing information from two tracks, the phase relationship between them may be in error by up to $\pm$ one sample in the total number of samples per period of the event. As the analogue to digital conversion was 4000 samples per second

for all the tests, this corresponded to $\pm$ 1.8 degrees of phase

shift at 20 cps of the impeller.   Unfortunately the phase error

in the harmonics of the blade frequency was considerably greater

and equal

$$\pm \; 1.8 \; Z \; i \; \text{degrees,} \qquad \qquad \dots 5.3$$

$$\begin{aligned} &\text{where } Z = \text{ number of blades } (\;4\;) \\ &\text{and} \quad i = \text{ blade frequency harmonic number.} \end{aligned}$$

This represents a significant phase error for the higher

harmonics.   It should be noted that the magnitudes of the

pressure components are not affected by this inaccurate phase

relationship.

The accuracy of the recording instrumentation and subsequent

analogue to digital (A-D) conversion was extremely high.   The

voltage to frequency (V-F) converters were linear to 0.5% of the

correct value.   For an input voltage of $\pm$ 1.4 volts to the V-F

converters, i.e. the normal input voltage range, the digital

information after A-D conversion had a range of approximately

700 units.   Also, at 4000 samples per second, which was the digital

sampling rate for these tests, there were at least 8 digital

samples per cycle of the 6th blade frequency harmonic.   Thus the

computational errors due to aliasing were small even for the higher

harmonics that were considered.

(b) <u>Pressure Transducer.</u>

The measured signal from the transducer was not a true 'point

measurement' but was in fact a reading which was dependant on the

pressure distribution on the diaphragm of the transducer.   As

previously discussed, the pressure distribution in the region of
the impeller showed considerable change in both magnitude and phase
with axial distance and it is in this region the accuracy of the
measured signal was doubtful.

In order to estimate analytically the accuracy of the recorded
pressure, the transducer diaphragm is assumed to be a uniform
circular plate, rigidly supported at the edge. Also the measured
signal is assumed to be proportional to the deflection of the
centre of the plate.

Consider the deflection of the plate due to the following
pressure distributions acting on it.

(i)   Linear pressure variation across the plate.

(ii)   Fluctuating pressure with a linear change in its
        magnitude and phase across the plate.

(i) Linear Pressure Variation.

Consider a linear pressure variation from P_1 to P_2
across the disc.
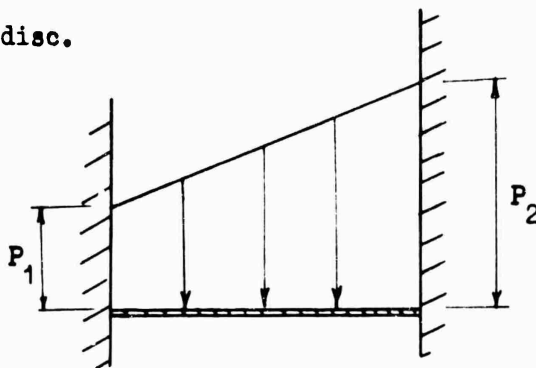
The deflection of a simply supported plate under the
above loading conditions is given in Ref. 5.5 (p.256 eqn(f)).
There the deflection of the plate at the centre is depen-
dant on the mean pressure i.e. $\frac{1}{2}(P_1 + P_2)$ and not on the

distribution, providing it is symmetrical.

This solution will also apply to the centre of a plate with fixed edges as above.

Forward of the impeller, the pressure on the transducer was approximately linear with constant phase, Therefore the measured components of the pressure in this region are effectively point measurements. However, the pressure measurements behind the propeller where large variations in magnitude and phase were detected, are inaccurate as shown in the following.

(ii) Linear Change in Magnitude and Phase on the Plate.

Consider a slowly varying sinusoidal pressure acting on a plate with the same boundary conditions as for (i) above. The magnitude and phase of this pressure is assumed to vary linearly across the disc. The deflection at the centre of the disc (w) due to this pressure (P) acting on a small unit area dx by dy is given in Ref. 5.5, p.290 viz.

$$w = \frac{P}{8 \pi D} (b^2 \log \frac{b}{a} + \frac{a^2 - b^2}{2}) \qquad \ldots 5.4$$
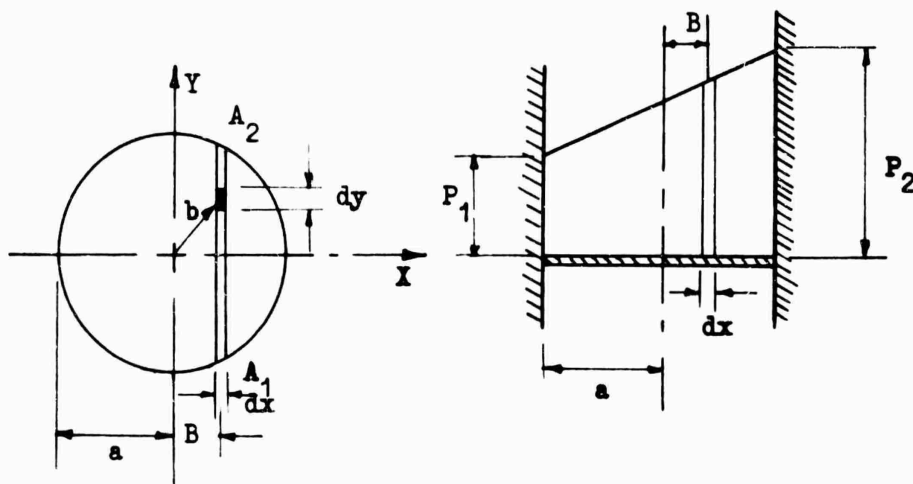
Assuming the pressure is linear with distance x

i.e. between A_1 and A_2 , the magnitude and phase are constant.
The resultant deflection (w') of the centre of the plate
due to the pressure loading from A_1 to A_2 is;

$$w' = \frac{P}{8 \pi D} \int_{A_1}^{A_2} (b^2 \log \frac{b}{a} + \frac{a^2-b^2}{2}) dx \, dy \qquad \ldots 5.5$$

where D = flexural rigidity of the plate.
Substituting $b = B \sec \theta$ and $y = B \tan \theta$ into equation 5.5
and evaluating between A_1 and A_2

$$w' = \frac{PB^3}{4\pi D} \left[\sqrt{(\frac{a^2 - B^2}{B^2})} \, (\frac{2a^2}{9B^2} - \frac{8}{9}) + \frac{2}{3} \arccos \frac{B}{a} \right] dx$$
$$\ldots 5.6$$

Assuming a phase distribution similar to that measured
aft of the impeller, then the response of the transducer
can be determined by an integration in the x direction.

From Fig. 5.10 the change in phase for a change in
$\frac{X}{D}$ of 0.031 (i.e. dimension of the transducer) is approxi-
mately 0.6π for the region aft of the impeller.

A numerical solution of equation 5.6 with the above
distribution of pressure was obtained. Under these condi-
tions the deflection of the centre of the plate was reduced
by 4.8% and the phase lead by 1.8 degrees compared to a
uniform pressure distribution equal to $\frac{1}{2}(P_1 + P_2)$ and no
phase change across the plate.

Thus the size of the transducer does affect the accuracy
of the pressure measurements in a region aft of the impeller.
Here the recorded pressures of the Hydrojet should be

increased by approximately 5%.

5.2   IMPELLER CHARACTERISTICS.

5.2.1   Impeller Performance Characteristics.

Unfortunately the values of thrust and torque coefficients given in Fig. 5.25 may be significantly in error. As mentioned in Section 4.1.1 the voltage signals from the dynamometer were amplified by the rotating D.C. pre-amplifiers before the voltage signals were measured. Due to the extremely large voltage gain of these amplifiers, there was considerable voltage drift during the measurement of the thrust and torque signals. The zero readings of the amplifiers taken before and after each experimental reading showed a voltage drift equivalent to approximately 10% and 2% of the measured values of thrust and torque respectively. In determining the values of torque and thrust, the drift was assumed linear with time. However, assuming the experimental values given in Fig. 5.25 are true values, then the experimental values are lower than the theoretical values at the design advance coefficient as shown below,

		Theoretical	Experimental
Intake Advance Coefficient $J_I = \dfrac{V_J}{nD}$		0.82	0.82
Thrust Coefficient $K_T = \dfrac{T}{\rho\, n^2 D^4}$		0.198	0.123
Torque Coefficient $K_Q = \dfrac{Q}{\rho\, n^2 D^5}$		0.0311	0.0204
Impeller Efficiency $E = \dfrac{J_I K_T}{2\pi K_Q}$ (at $J_I = 0.82$)		0.834	0.77
Maximum Experimental Impeller Efficiency (at $J_I \approx 0.74$)		--	0.95

Although there is a large variation between the theoretical and the experimental values for thrust and torque, the value of advance coefficient, at which the theoretical value of thrust is produced, is only 0.792. This represents a decrease of less than 4% in the design advance coefficient. Assuming the measured values are correct, the results indicate that the pitch of the impeller should be increased by approximately 1.04 to maintain the design conditions.

Although the measured impeller efficiency, at the design advance coefficient, was considerable less than that calculated, the maximum experimental efficiency was considerably greater and was equal to 0.95. If the measurements were in error by 12% then the maximum efficiency would be approximately 0.79. This value, although much lower than the theoretical efficiency, is considerably greater than an equivalent open-water propeller. For example, an open-water efficiency of 0.64 can be expected for a propeller of the Troost B-55 Series, which has approximately the same dimensions and operating conditions as the impeller tested in these studies.

The results indicate that a favourable impeller efficiency is obtainable from a ducted impeller, but further tests must be conducted to accurately determine the correlation between the theoretical and experimental performance characteristics.

5.2.2 Velocity in the Wake of the Impeller.

By measuring the velocities in the wake behind the impeller, the calculated load distribution along the blade may be checked. The results of such a wake survey with a 5-hole spherical pitot (Section 4.4) are given in Fig. 5.26.

In Fig. 5.26 the axial velocity (V_A) and the tangential velocity (V_T) are given for various radial distances at two advance coefficients. These velocities are not as predicted in Section 2.1. The theoretical design assumed the axial velocity distribution was constant and the tangential velocity was linear with radial distance. This variation between theory and practice is to be expected because of the limitations of the simple theoretical analysis.

It has been shown in Ref. 5.6 that large discrepancies also exist between the experimental and theoretical values of the wake velocities for open-water propellers, even when they are compared using the most rigorous propeller theories. Other workers, however, have obtained good agreement between theory and experiment (Refs. 5.7, 5.8).

6.0   CONCLUSIONS.

6.1   IMPELLER-INDUCED VIBRATORY PRESSURES.

Although the fluctuating pressures induced by a ducted impeller are similar in nature to that of an open-water propeller, several important differences do exist.

(1)   The harmonic content of the 2nd and 3rd blade frequency harmonics of the impeller-induced pressure is approximately 60% and 25% respectively of the 1st harmonic pressure. Thus theoretical and experimental determination of pressures at points which are extremely close to an impeller, i.e. about 0.3% of the impeller diameter, must include the blade frequency harmonic components.

(2)   Although the maximum pressure coefficient $\dfrac{P_t}{\rho\, n^2 D^2}$ is approximately 0.5, its magnitude rapidly attenuates to 10% of its maximum value at distances of $\dfrac{X}{D}$ equal to + 0.2 and - 0.1 from the impeller plane.

(3)   The blade thickness controls the pressure field forward of the impeller and results in a constant phase angle with respect to the blade position for all the harmonic components of the pressure.

(4)   Aft of the impeller, both the blade thickness and the blade loading, influence the pressure field. When the blade loading is high, the pressures associated with the trailing vortices control the pressure, but as the thrust loading approaches zero, the blade thickness effects become significant.

(5)   A marked discontinuity in the pressure distribution occurs near the plane which contains the mid-points of the blade sections of the impeller. Behind the impeller plane, the phase is constant

with respect to a uniform pitch helical surface which is, in fact, the trailing vortices of the blades. The position of the discontinuity in the pressure field, i.e. where the trailing vortices appear to emanate from the blade, has a tendency to move forward with an increase in the blade frequency harmonic component.

For this reason, the bound vortex lines, which represent the impeller in a theoretical model, must be situated at the mid-point of the blade sections.

(6)   For a non-uniform inflow velocity distribution at the impeller, the resultant induced pressure is dependant, to a first approximation, on the mean velocity component existing over blade length.

(7)   Care must be excercised when measuring pressures aft of an impeller, because the response of a finite size transducer is dependant on the phase relationship of the pressures across the diaphragm of the transducer. For example, the pressure measured behind the impeller with a transducer which has a diaphram diameter of 0.03 of the impeller diameter, is approximately 4% lower than the true pressure. However, the phase of the pressure is only in error by about 2 degrees.

6.2   IMPELLER EFFICIENCY.

There is substantial evidence that impeller efficiencies in the order of 0.90 are possible from a ducted impeller. The experimental value of the maximum impeller efficiency was 0.95, but this unfortunately may be an optimistic estimate because of instrumentation errors. A simple vortex-line analysis of the impeller predicted an efficiency

of only 0.83.

However, further experimental studies must be conducted to determine the actual performance charact ristics of the ducted impeller.

6.3   FEASIBILITY OF A HYDROJET.

Only two characteristics of a Hydrojet propulsion unit were considered in these studies. They were the propulsive efficiency and the impeller-induced vibratory pressures on the duct surface.

The propulsive efficiency of a Hydrojet suitable for large displacement vessels is expected to exceed 0.75 providing the ratio of duct length can be reduced to twice its diameter, then the propulsive efficiency is significantly increased to approximately 0.80.

Before accurate predictions can be made for the propulsive efficiency of a Hydrojet propulsion unit, detailed investigations into the frictional resistance of a duct-impeller system and also into the characteristics of the impeller are necessary.

The other characteristic of the Hydrojet that was considered was the impeller induced pressures on the duct surface. Although the magnitudes of these pressures were extremely high, the extent of this intense fluctuating pressure field was very small. Before it is possible to say whether the resultant forces due to the pressure and hence the vibration levels of the ship are acceptable, detailed studies of the duct structure surrounding such an impeller must be undertaken. It is anticipated that such a structure can be designed to effectively cancel the cyclic forces due to the induced pressures of an impeller operating in a uniform velocity field. This would then leave only those forces due to the non-uniformity of the wake to force excite the hull

Since it was shown that the duct need only extend fore and aft of the impeller a distance of about 0.4 of the impeller diameter to contain the most intense portion of the fluctuating pressure field within the duct, the efficacy of the Kort nozzle in reducing surface-pressure vibration forces is evident. It might appear that the Hydrojet has little advantage over the Kort nozzle. The Hydrojet, however, has the following advantages:-

(1)   Integral construction of the duct with the hull, giving higher strength and greater damage protection.

(2)   A longer intake section which could be used to give a more favourable flow distribution at the impeller during seaway conditions, when separation is likely to occur at the intake lip.

(3)   The intake scoop could be designed to take in relatively more low-energy boundary layer water than the open screw, thus contributing to an increase in overall efficiency.

(4)   It may be possible to use "rim drive" on the impeller, with an annular gear or electric-motor rotor being formed around the impeller. Such rim drive would remove one of the present blade strength limitations and would allow the use of thinner blade sections and higher power loadings.

(5)   Thrust deduction should be less for the hydrojet (See Ref. 1.2).

(6)   Cavitation control may be possible by slightly enlarging the duct near the impeller section.

The Hydrojet, however, suffers from the disadvantages of a higher duct skin friction-loss and a more complex structure than the Kort nozzle.

This report has shown that relatively shot ducted-propulsion
systems should generate substantially lower vibratory forces than
an equivalent open screw. It has also indicated that the efficiency
should be comparable with the open screw and may well be higher. It
appears that the Hydrojet and Kort-nozzle configurations have certain
relative advantages, and further work on both, together with comparative
studies, would be desirable.

REFERENCES.

0.1   NORRIE, D.H.   Studies in Marine Propulsion Vibration.

        Doctor of Philosophy Thesis, University of Adelaide, Mechanical

        Engineering Department.   July, 1964.

0.2   BROWN, N.A.   Periodic Propeller Forces in Non-uniform Flow.

        Massachusetts Institute of Technology, Dept. of Naval Architecture

        and Marine Engineering.   Report No. 64-7, June, 1964.

1.1   BRESLIN, J.P.   Review of Theoretical Predictions of Vibratory Pressures

        and Forces Generated by Ship Propellers.

        Stevens Institute of Technology, Davidson Laboratory, Note 717.

        (Prepared for the Second International Ship Structures Congress,

        Delft. July 1964.)

1.2   HALE, M.R. and NORRIE, D.H.   Hydrojet Propulsion Reduces Vibration.

        Engineering, 24th July, 1964.

1.3   GASUINAS, A and LEWIS, W.P.   Hydraulic Jet Propulsion - A Theoretical

        and Experimental Investigation into the Propulsion of Seacraft

        by Water Jets.

        Presented to Ordinary Meeting of the Institution of Mechanical

        Engineers, Portsmouth, 24th. October, 1963.

1.4   GONGWER, C.A.   The Influence of Duct Losses on Jet Propulsion Devices.

        Jet Propulsion, Vol. 24 No.6, 1954, p385-6.

References Continued--

1.5   VAN MANEN, J.D.   Fundamentals of Ship Resistance and Propulsion.

            Part B. p120. Netherlands Ship Model Basin,

            Publication 132a.

1.6   VAN MANEN, J.D.   Recent Research on Propellers in Nozzles.

            Journal of Ship Research, n2, pp13 - 46, 1957.

1.7   SACKS, A.H. and BURNELL, J.A.   Ducted Propellers - A Critical

            Review of the State of the Art.

            Progress in Aeronautical Sciences, Vol.2, Pergamon Press 196

1.8   DICKMAN, H.E.   Grundlagen zur Theorie ringformiger

            Tragflugel

            Ingenieur - Archiv. No.11, pp.36-52, 1940.

1.9   WEISSINGER, J.   Zur aerodynamik des ringflugels, deutsche

            versuchsantalt fur luftfahrt.

            E. V. Bericht, Nr.2, Mulheim, 1955.

1.10 ORDWAY, D.E., SLUGTER, M.M. and SONNERUP, B.O.U.

            Three-dimensional Theory of Ducted Propellers.

            THERM Report TAR-TR 602, Ithaca, N. Y., 1960.

1.11 MORGAN, W.B.   A Theory of the Ducted Propeller with a

            Finite Number of Blades.

            Inst. of Eng. Res., University of California, Berkeley, 1961

1.12   ORDWAY, D.E. and GREENBERG, M.D.   General Harmonic Solutions

for the Ducted Impeller.

THERM Report TAR-TR 613, Ithaca, N. Y., 1961.

1.13   MORGAN, W.B.   Theory of the Annular Aerofoil and Ducted

Propeller.

4th Symposium on Naval Hydrodynamics, 1962.

2.1   BRITISH PROPELLER DESIGN.

Marine Engineer and Naval Architects, Vol.88 No.1069,

April, 1965.

2.2   O'BRIEN, T.P.   The Design of Marine Screw Propellers.

Hutchinson & Co., Ltd. London, 1962.

2.3   TINGEY, R.H.   Marine Engineering, Vol.1 Chap.IX

(Editor - Seward, H.L.) Society of Naval Architects

and Marine Engineers, 1942.

2.4   MATTHEWS, S.T. and STRASZAK, J.S.C.   Optimum Length and

Thickness of Propeller Blade Sections for Cavitation

and Strength Considerations.

National Research Council of Canada. Mech. Eng. Report,

M. B.-231   April, 1961.

3.1   VAN MANEN, J.D. and SUPERINA, A.   The Design of Screw

Propellers in Nozzles.

International Shipbuilding Progress. Vol.6,No.55, March,1959.

Ref rences Continued--

3.2   MANNAM, J., FOWLER, J.H. and CARPENTER, A.L.

                Tapered Lands Hydrostatic Journal Bearings.

                I. Mech. E. Lubrication and Wear, 3rd Convention, London, 1965.

3.3   McCarthy, J.H.   A Method of Wake Production in Water Tunnels.

                David Taylor Model Basin, Report 1785, October, 1963.

4.1   CLARKZ, A.P.   Computation of the Coefficients of a Fourier Series

                Expansion of a Function defined by Sampled Data Points.

                Weapons Research Establishment, Tech. Memo. T.RD 71, ADDS.

4.2   PIEN, P.C.   The Five-Hole Spherical Pitot Tube.

                David Taylor Model Basin. Report 1229. May, 1958.

4.3   SILOVIC, V.   The Five-Hole Spherical Pitot Tube for Three Dimensional

                Wake Measurements.

                Hydro-Og Aerodynamisk Laboratorium, Lyngby, Denmark.

                Report No. Hy-3, May, 1964.

4.4   WERELDSMA, R.   Dynamic Behaviour of Ship Propellers.

                Internationale Periodieke Pers, Rotterdam. April, 1965.

4.5   WERELDSMA, R.   Experiments on Vibrating Propeller Models.

                Journal of Ship Research, 1965

                also Netherlands Ship Model Basin Publication No. 252.

4.6   PENDERED, J.W. and BISHOP, R.E.D.   Extraction of Data for a Sub-

                system from Resonance Test Results.

                Journal of Mechanical Engineering Science, Vol.5, No.4, 1963.

References continued -

4.7   LEIBOWITZ R C. and KENNARD, E.H.   Theoretical and Experimental
                determination of Damping Constants of One-to Three Dimensional
                Vibrating Systms.
                David Taylor Model Basin.   Report 1770, June 1964.

4.8   KARMAN, TH. VON and SEARS, W,R,   Airfoil Theory for Non-uniform Motion.
                Journal of Aeronautical Sciences, 1938.

4.9   SEARS, W.R.   Some Aspects of Non-stationary Airfoil Theory and its
                Practical Application.
                Journal of Aeronautical Sciences, 1941.

5.1   TACHMINDJI, A.J. and DICKERSON, M.C.   The Measurement of Oscillating
                Pressures in the Vicinity of Propellers.
                David Taylor Model Basin, Report 1130.   April, 1957.

5.2   BRESLIN, J P.   Review and Extension of Theory for Near-Field Propeller
                Induced Vibratory Effects.
                Fourth Symposium on Naval Hydrodynamics, Vol.2 Washington DC
                August, 1962.

5.3   BRESLIN, J.P. and KOWALSKI, T.   Experimental Studies of Propeller-
                Induced Vibratory Pressures on Simple Surfaces and Correlation
                with Theoretical Predictions.
                Journal of Ship Research, Vol.8, No.3, December 1964.

5.4   TSAKONAS, S; BRESLIN, J.P. and JEN, N.   Pressure Field around a
                Marine Propeller Operating in a Wake.
                Steven Institute of Tech. Davidson Laboratory, R-857, May 1962.

References continued --

5.5   TIMOSHENKO, S. and WOINOWSKY-KRIEGER, S.   Theory of Plates and Shells.
      McGraw - Hill Book Company.

5.6   JOHNSSON, C.A.   Comparison of Propeller Design Techniques.
      Fourth Symposium on Naval Hydrodynamics.
      Washington, DC.   August 1962.

5.7   DICKERSON, M.   Induced Velocities Forward and Aft of a Propeller.
      DTMB Report 1310,   March 1959.

5.8   BEVERIDGE, J.L.   The Radial Distribution of Propeller Thrust from
      Model Wake Measurements.
      DTMB Report 1136,   November 1958.

ACKNOWLEDGEMENTS

providing the research scholarships, which Mr. M. R. Hale held
during post graduate study.

The U.S. Government Department of the Navy and the David Taylor
Model Basin for the financial assistance which made this research
possib¹ .
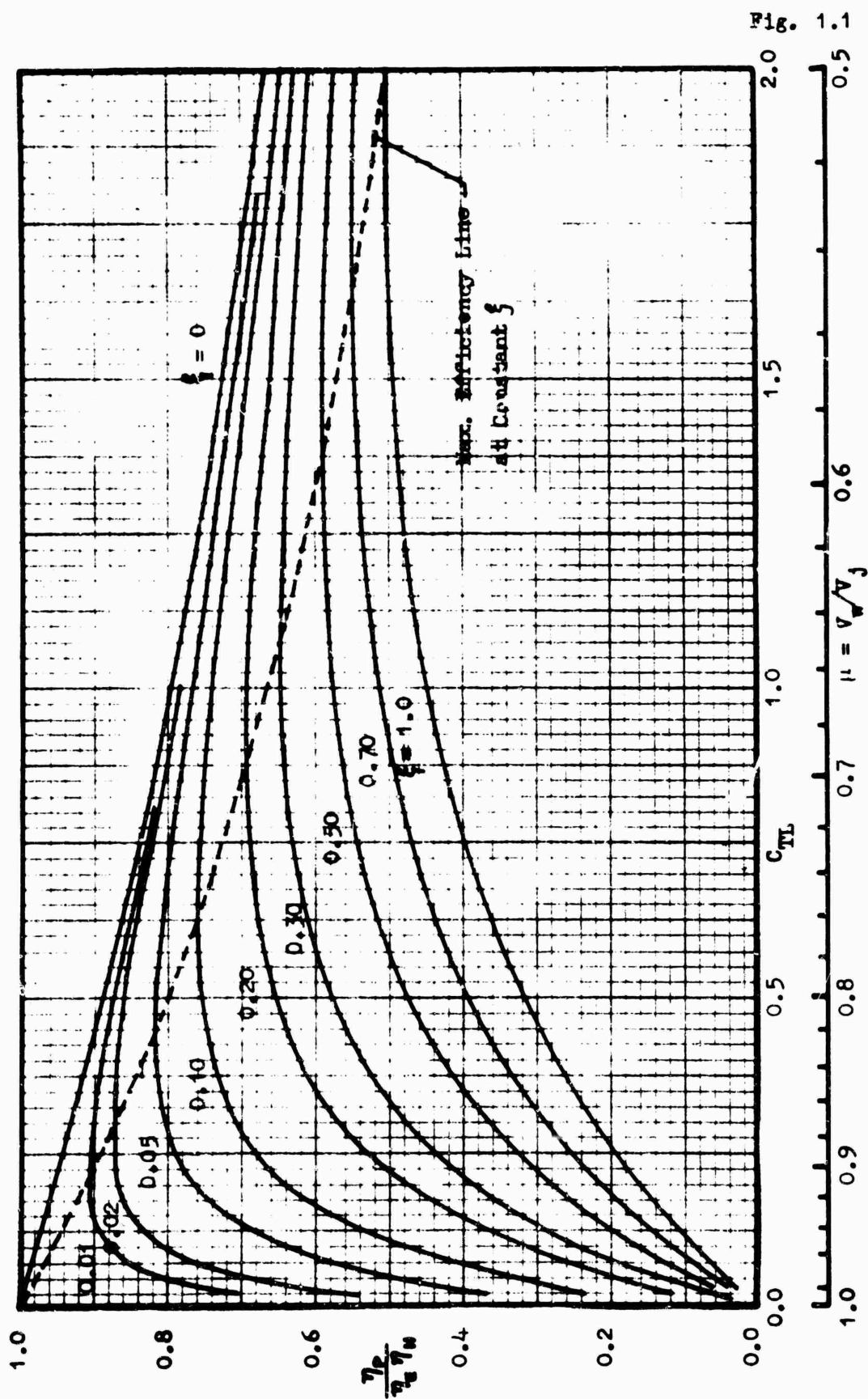
Fig. 1.1 - Estimated Performance of Hydrojet Propulsion Unit. (Assuming $K_A = 1$)

Fig. 1.1
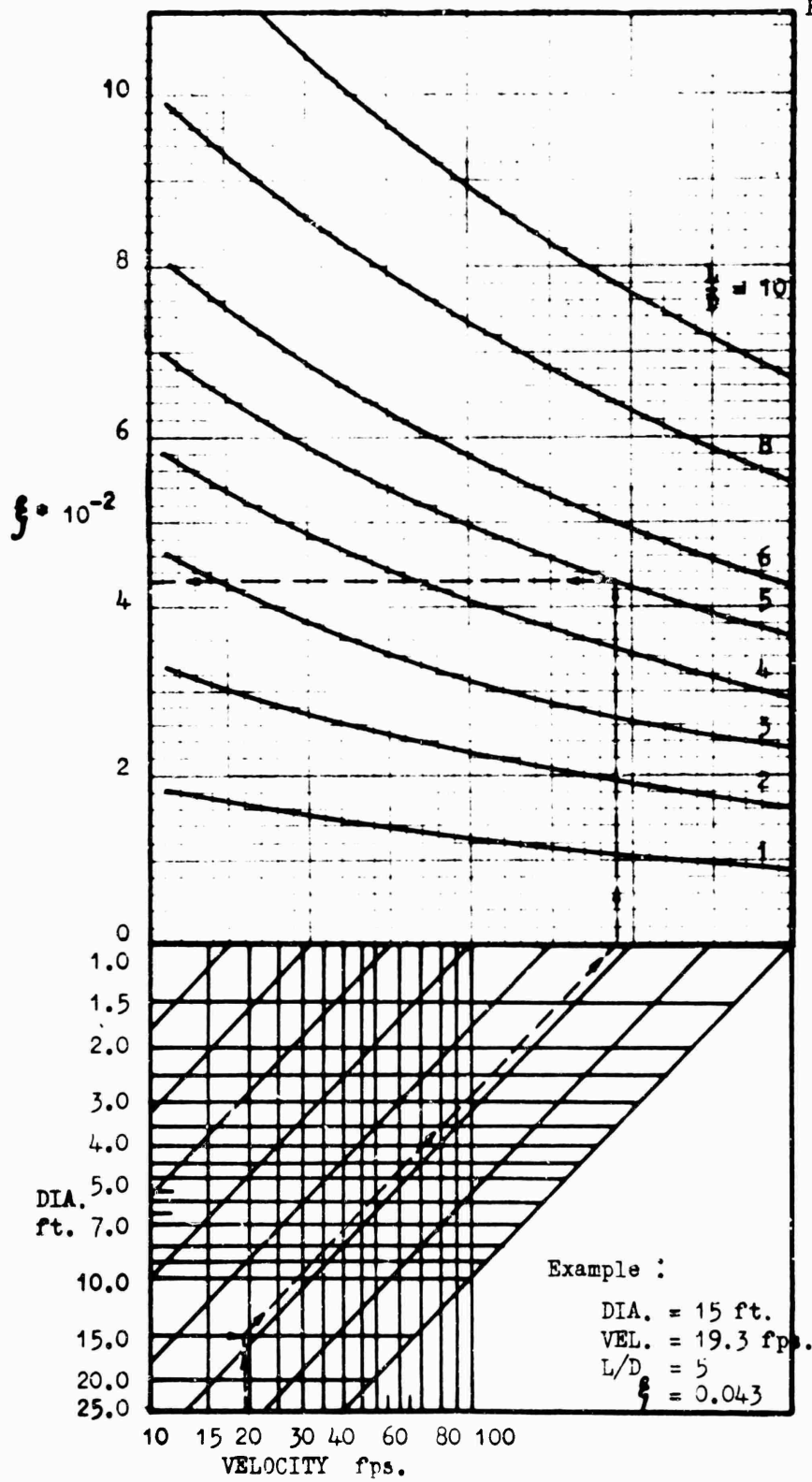
Fig. 1.2 - Estimated Ducting Loss Factor ξ.

Based on, (1) ρ = 1.99 slug/cubft.
(2) C_F ATTC. (1947) Mean Friction Line.
(3) Equivalent straight duct.

Fig. 2.1
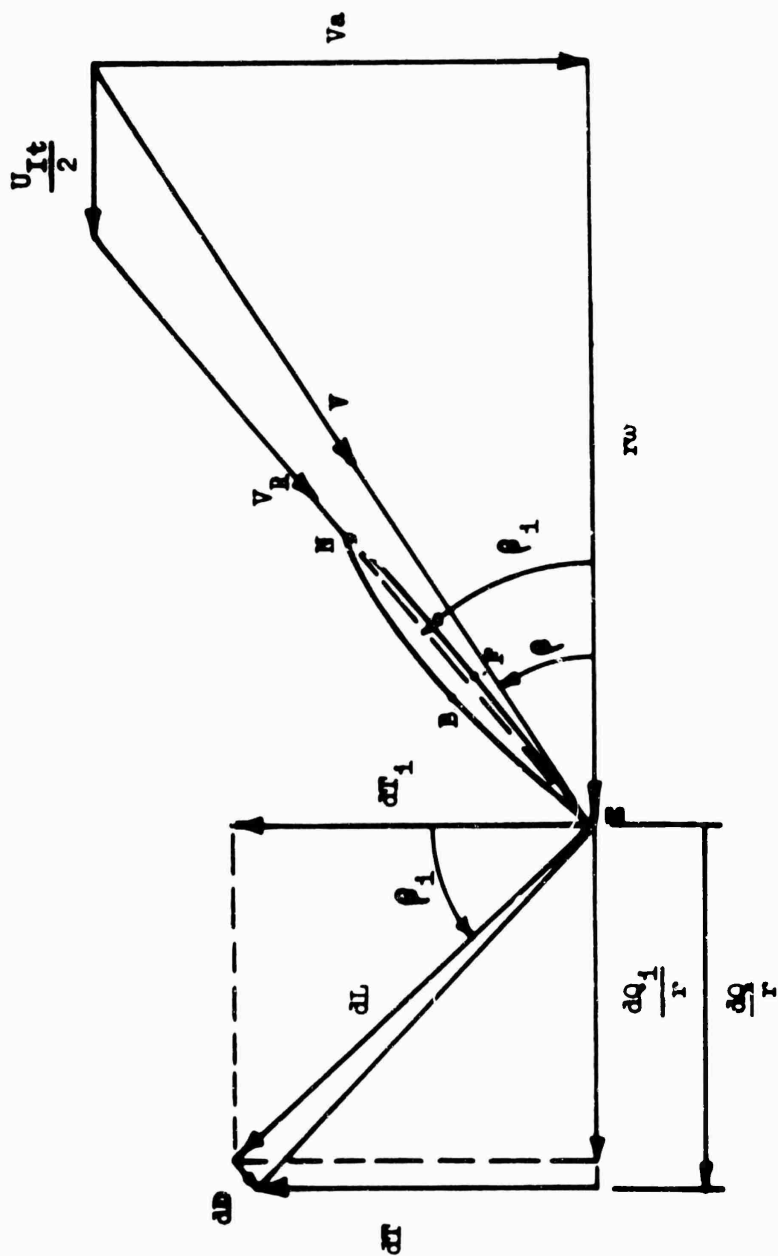
Fig. 2.1 - Velocities and Forces at Blade Section.

Fig. 2.2
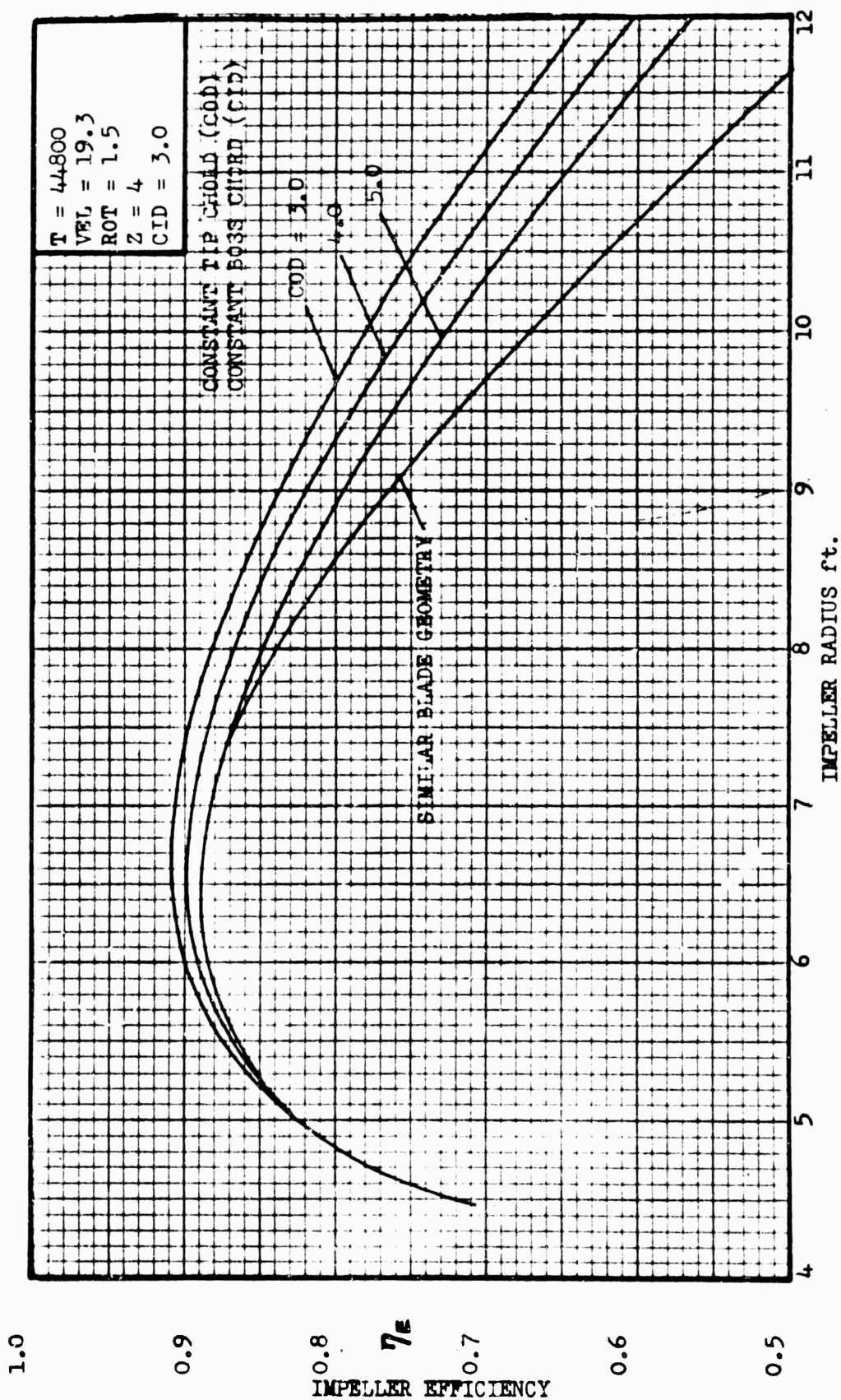
Fig. 2.2 - Optimum Efficiency for Varying Radius.
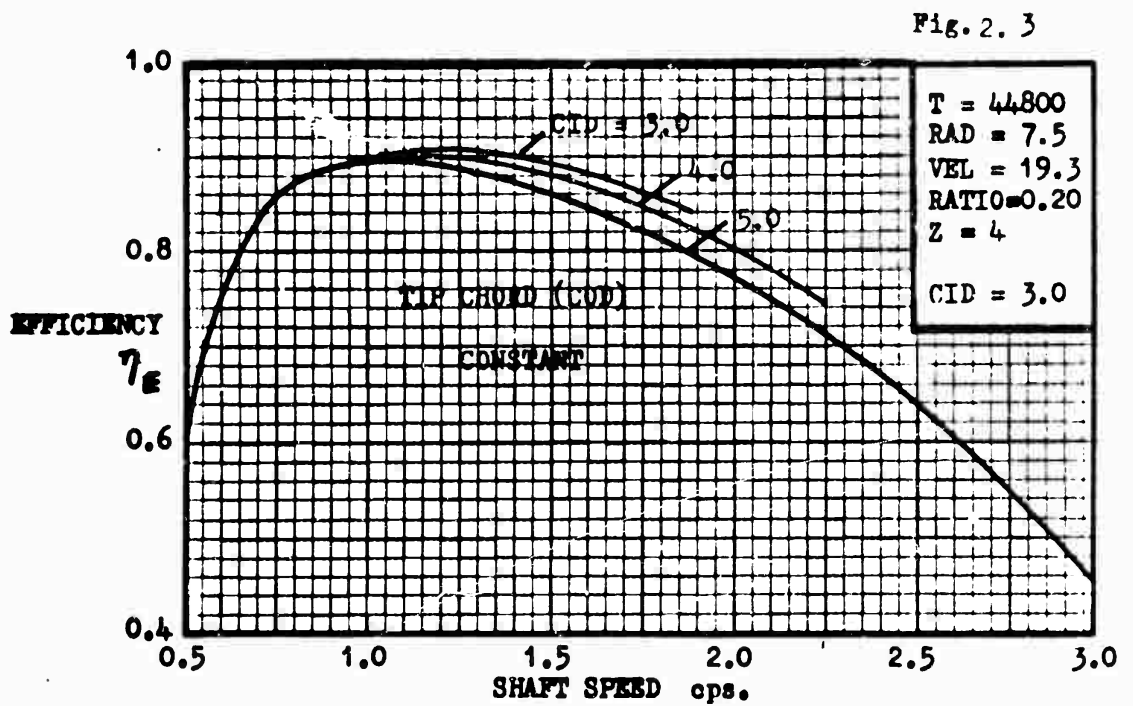
Fig. 2. 3

Fig. 2.3 - Optimum Efficiency at Varying Shaft Speed.
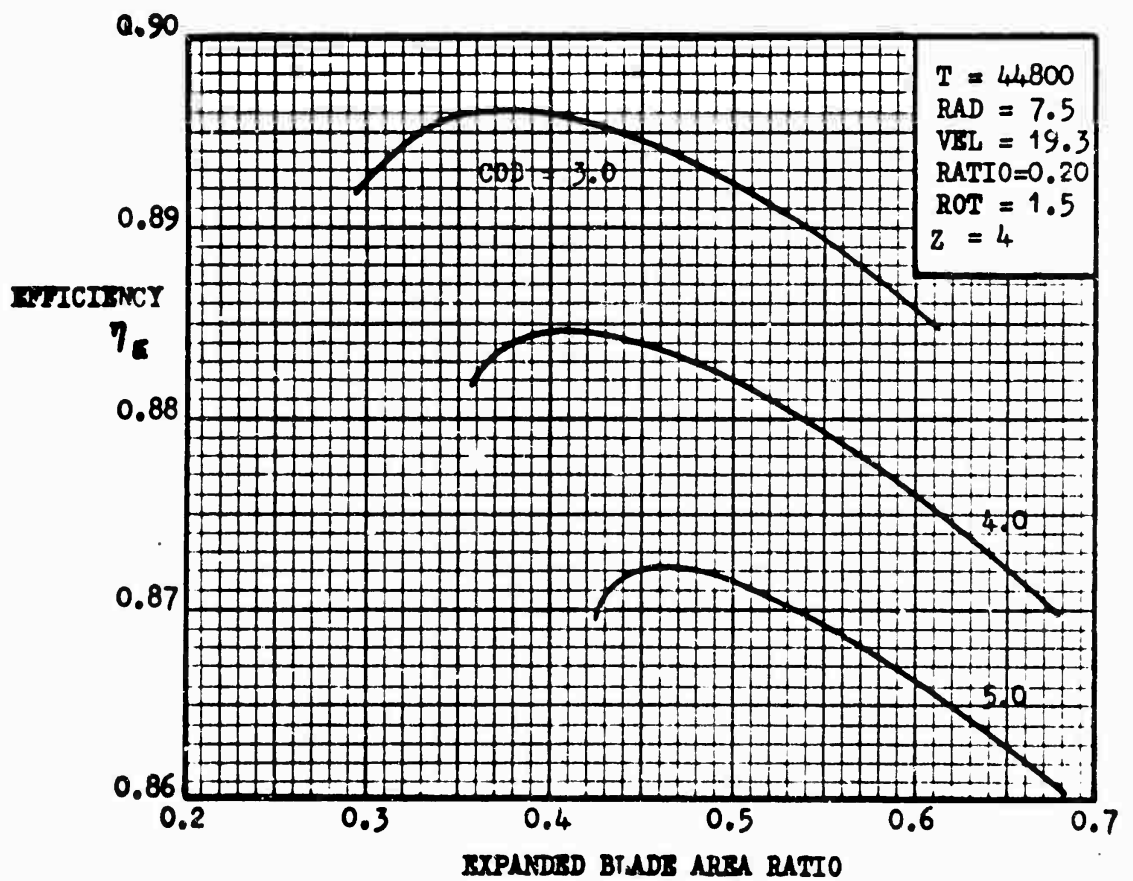
Fig. 2.4 - Optimum Efficiency with Varying Blade Geometry.

DETAILS OF EXPANDED BLADE SECTIONS

LE RAD   RADIUS

LE RAD	RADIUS
0·002	4·00
0·002	3·60
0·002	3·20
0·002	2·80
0·003	2·40
0·005	2·00
0·008	1·60
0·011	1·20
0·014	0·80

1·0 R
0·9 R
0·8 R
0·7 R
0·6 R
0·5 R
0·4 R
0·3 R
0·2 R

LINE OF MAXIMUM THICKNESS

0·128
0·114
0·100
0·102
0·123
0·156
0·175
0·196
0·218

DEVELOPED
BLADE OUTLINE

PROJECTED
BLADE OUTLINE

PROJECTED BLADE OUTLINE

TRANSVERSE VIEW
LOOKING FORWARD

PLAN VIEW OF BLADE

LONGITUDINAL SECTION THROUGH BOSS

TAPER 24 in 12

DIAMETER	8·000	EXP. AREA RATIO	0·583
PITCH (constant)	Y·000	M.W.R	0·008
NO. BLADES	4	BLADE THICKNESS RATIO	
ROTATION	R.H.	MEAN L/DT	0·11·3
P/D RATIO	0·901	THICKNESS FORM	NACA 16
MERIDIAL RATIO	0·50	BLADE SECTIONS	

UNIVERSITY OF ADELAIDE

Fig. 2.6

Fig. 2.6 - MACHINING MASTER TEMPLATES FOR IMPELLER.

Fig. 2.7 - MACHINING MODEL IMPELLER IN COPYING MACHINE.

Fig. 2.8
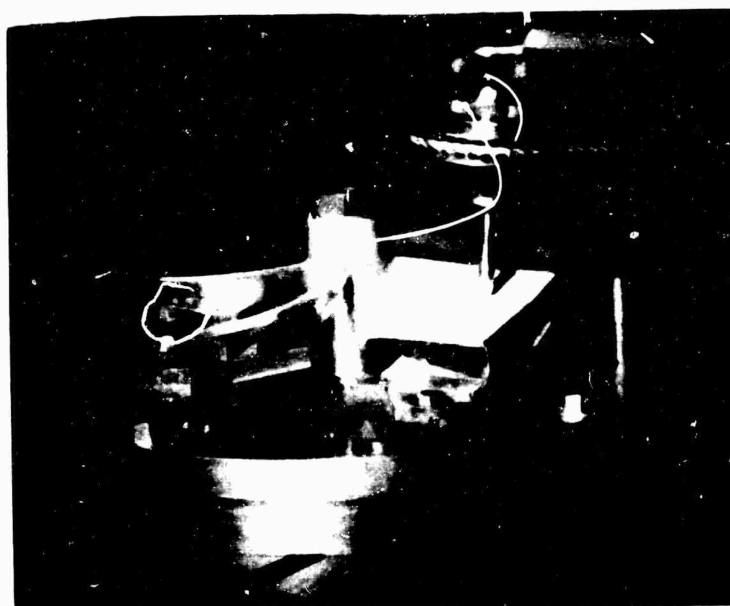
Fig. 2.8 - MACHINING MODEL IMPELLER.
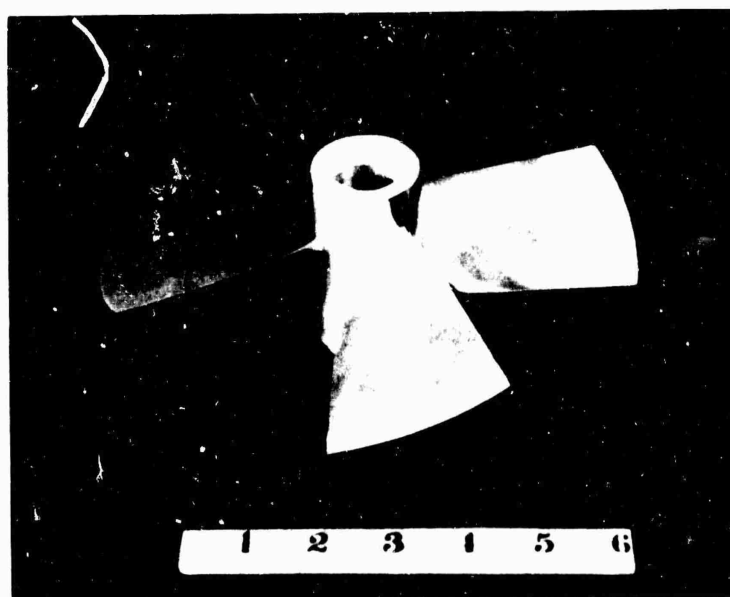
Fig. 2.9 - MODEL IMPELLER.

Fig. 3.1
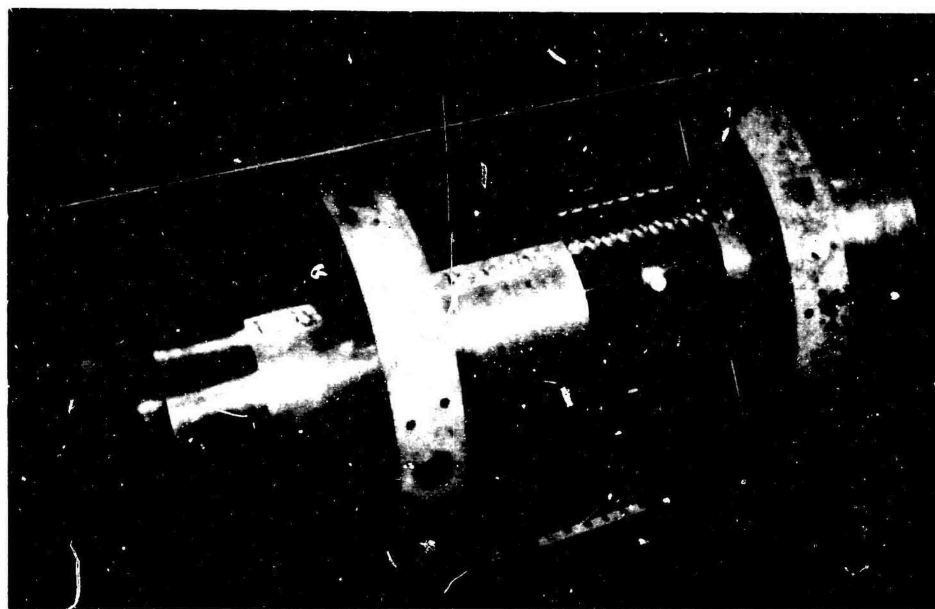
Fig. 3.1 — MODEL DUCT ARRANGEMENT.
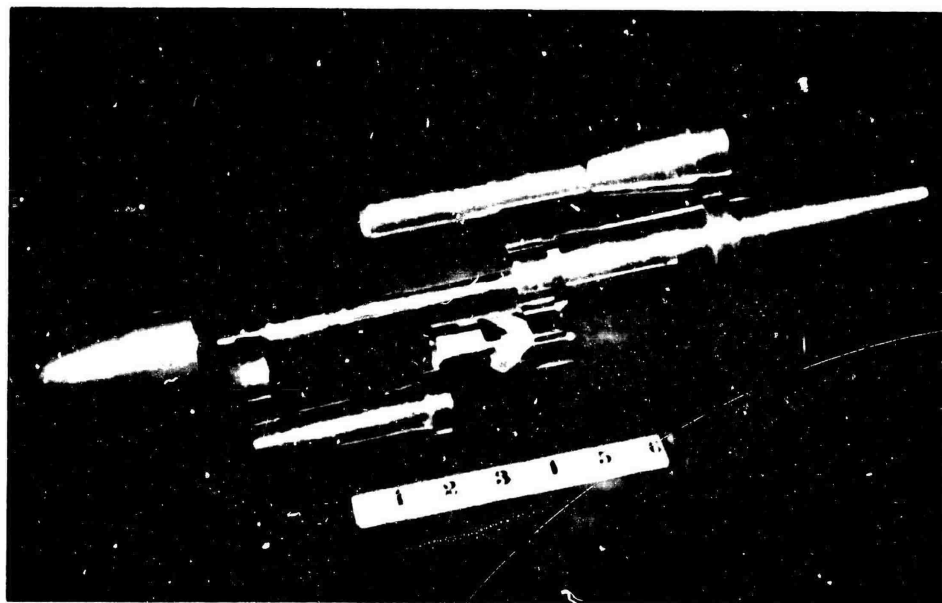
Fig. 3.2 — VIEW OF DYNAMOMETER BEFORE ASSEMBLY.

WATER SUPPLY FOR
TAPERED BEARING

DRIVE SHAFT

IMPELLER SUPPORT SHAFT

TAPERED HYDROSTATIC BEARING

IMPELLER SHAFT

THIN RUBBER DIAPHRAM

WATERPROOF CAVITY

SENSING ELEMENT WITH
STRAIN GAUGES ATTACHED
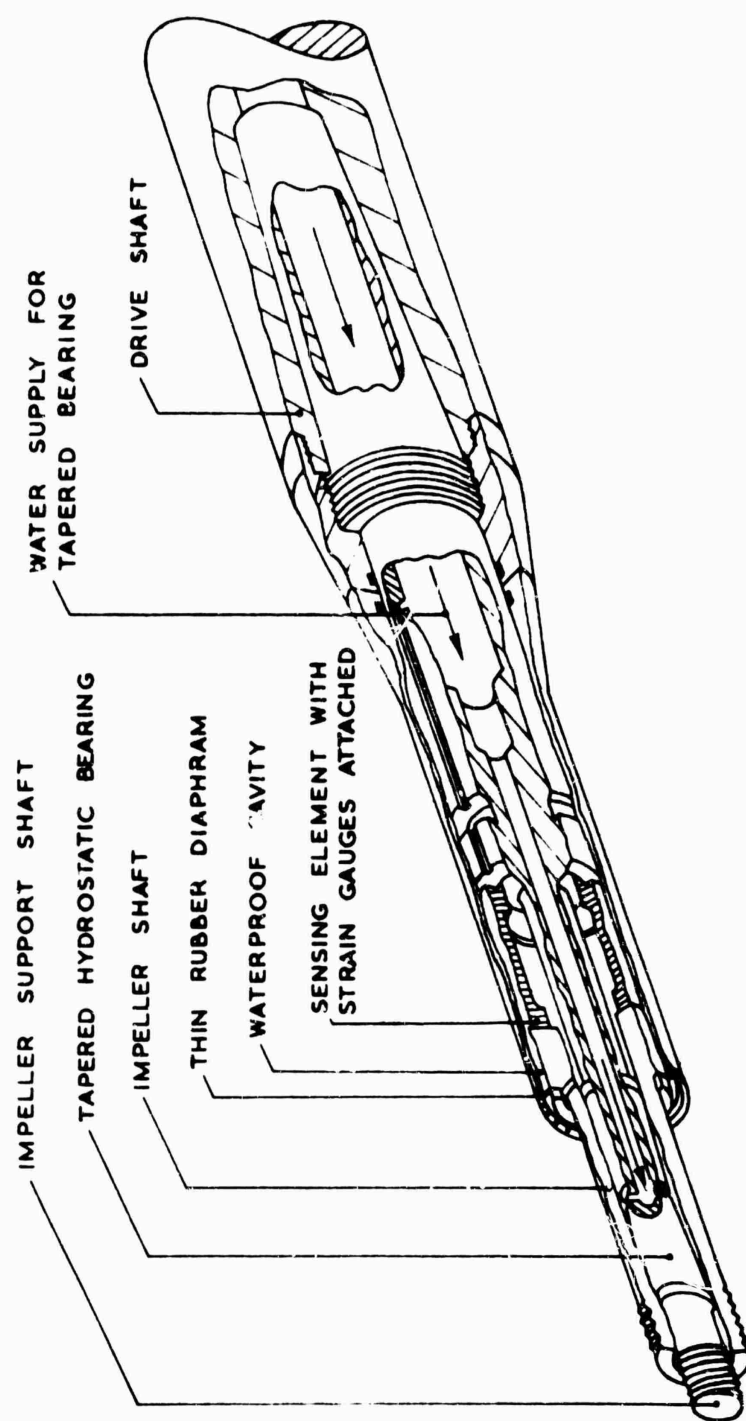
FIG. 3.3   CROSS SECTION OF DYNAMOMETER

Fig. 4.0
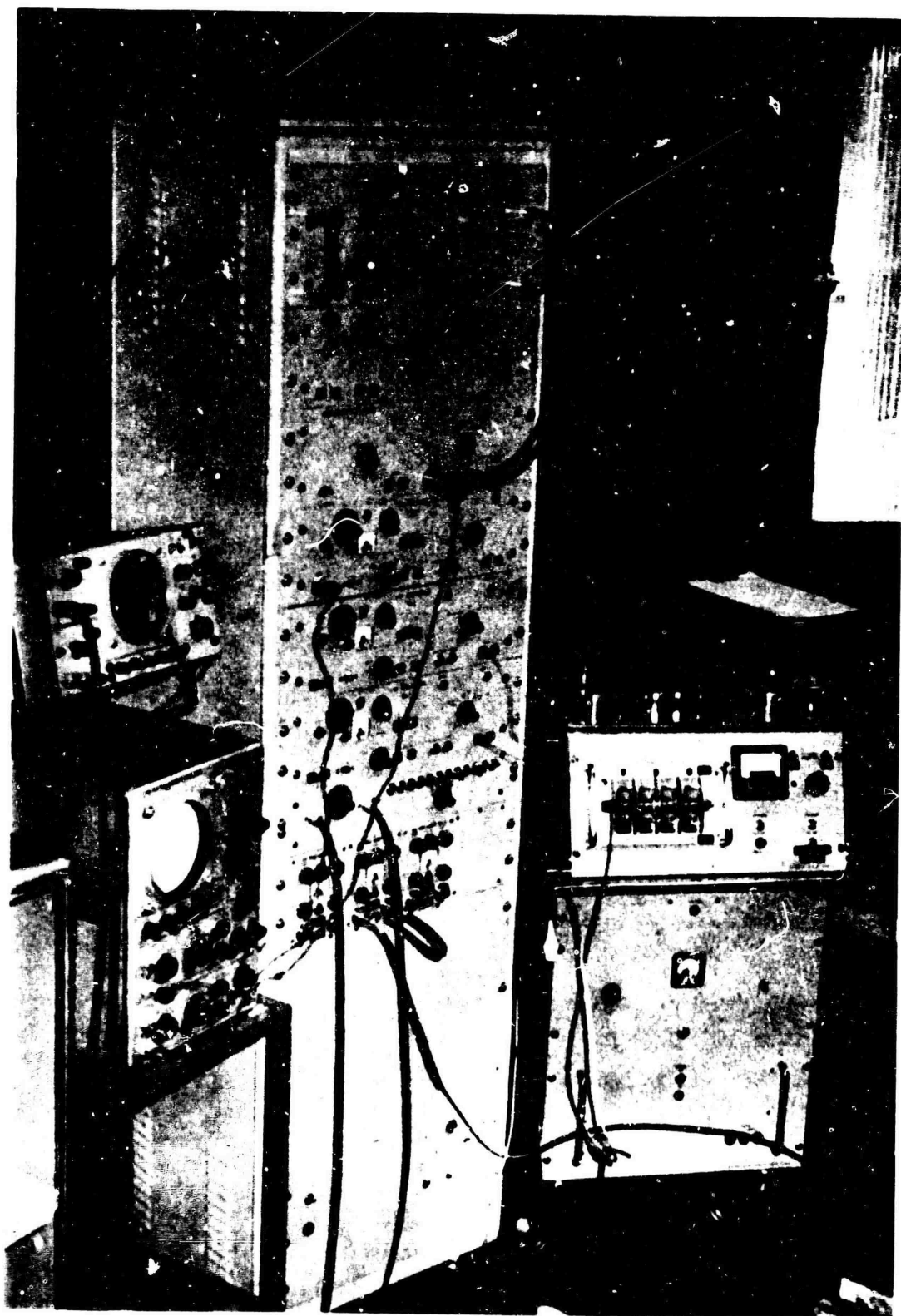
Fig. 4.0 — GENERAL VIEW OF THE INSTRUMENTATION.
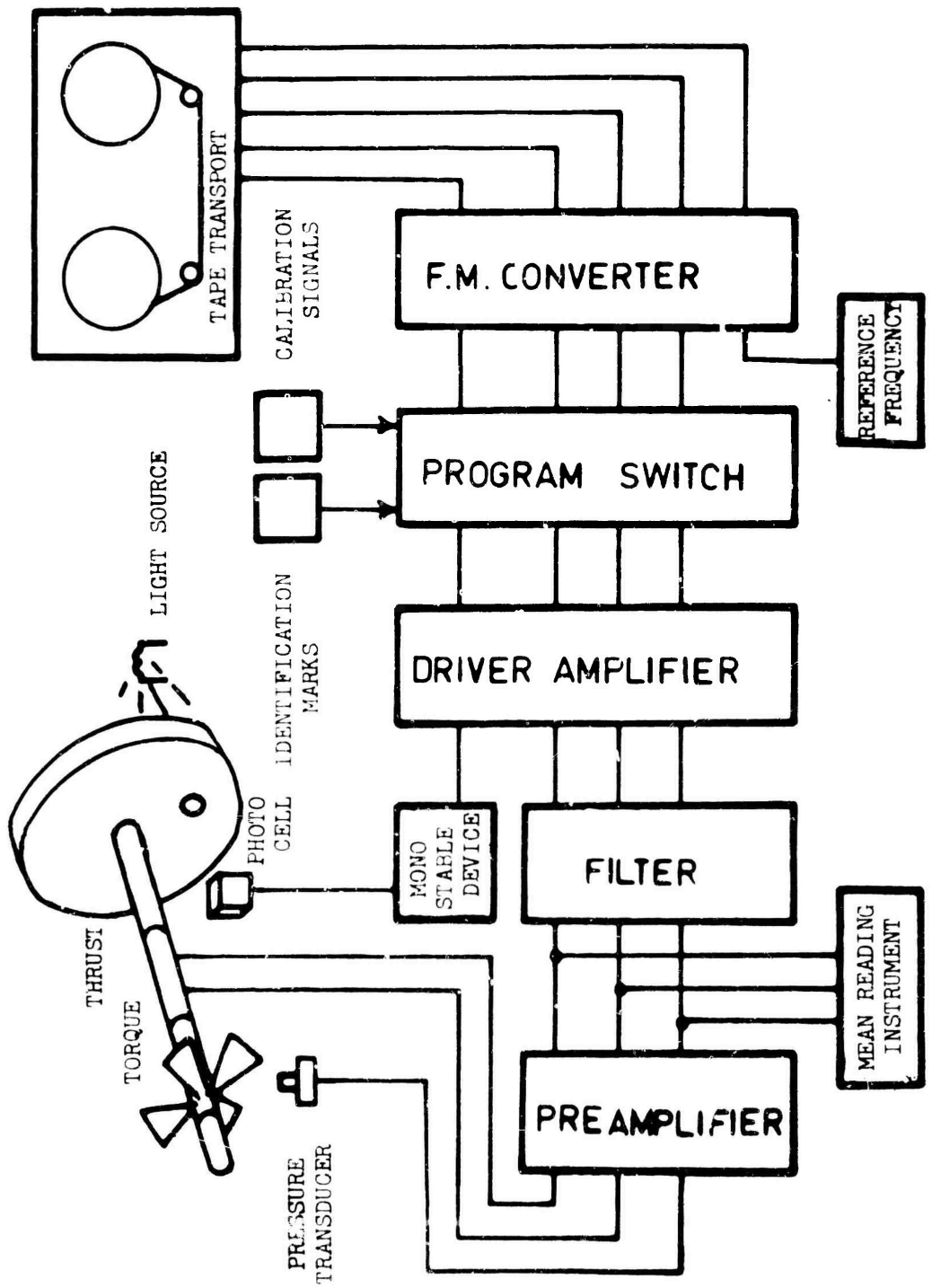
Fig. 4.1 – Block Diagram of Instrumentation.

PHASE ANGLE LAG (DEGREES)

Fig. 4.2

MODULUS

PHASE

FREQUENCY (cps)

MODULUS
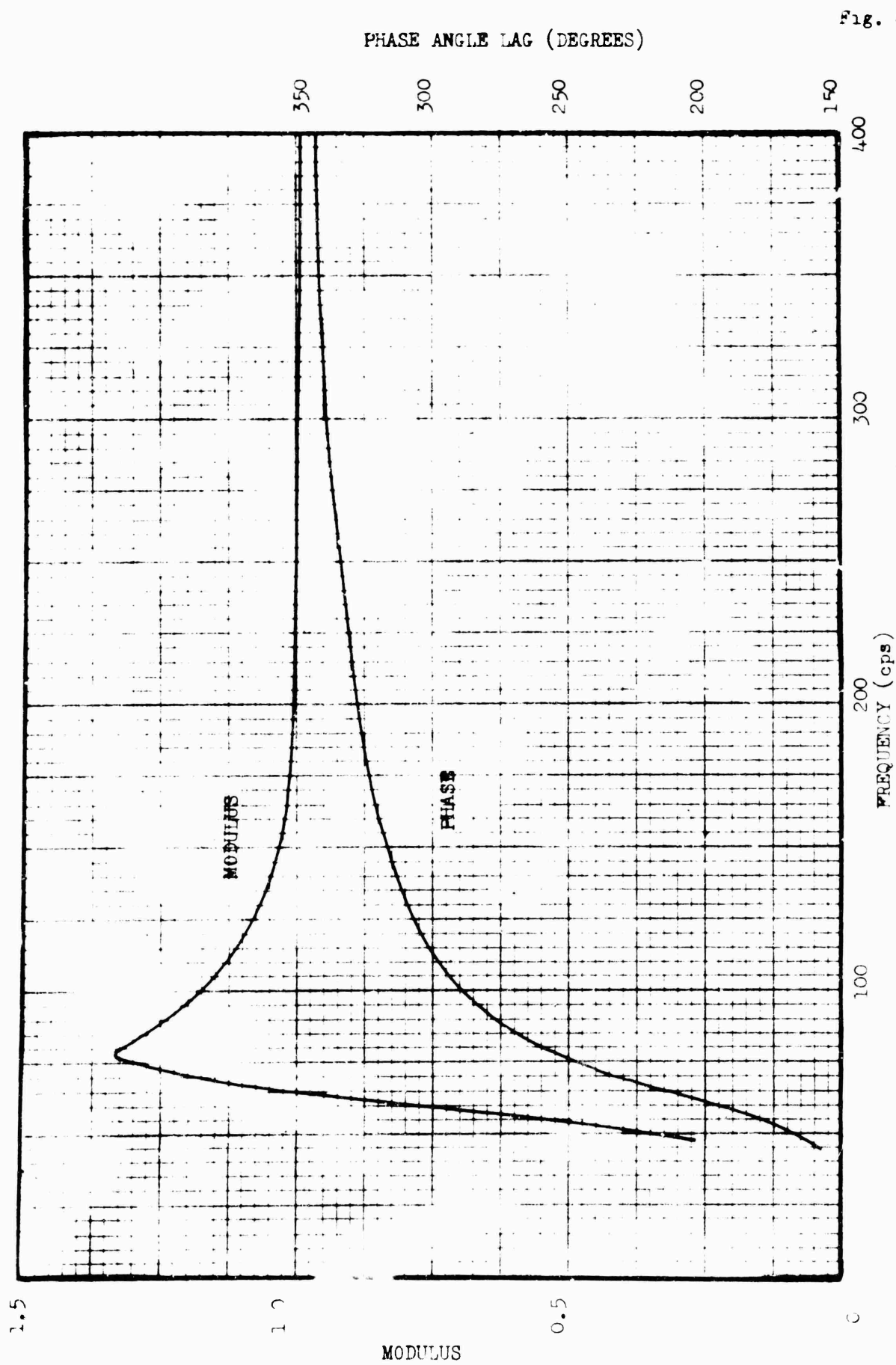
Fig. 4.2   -   Typical Transfer Function Characteristics of the High-pass Filter.

Fig. 4.3
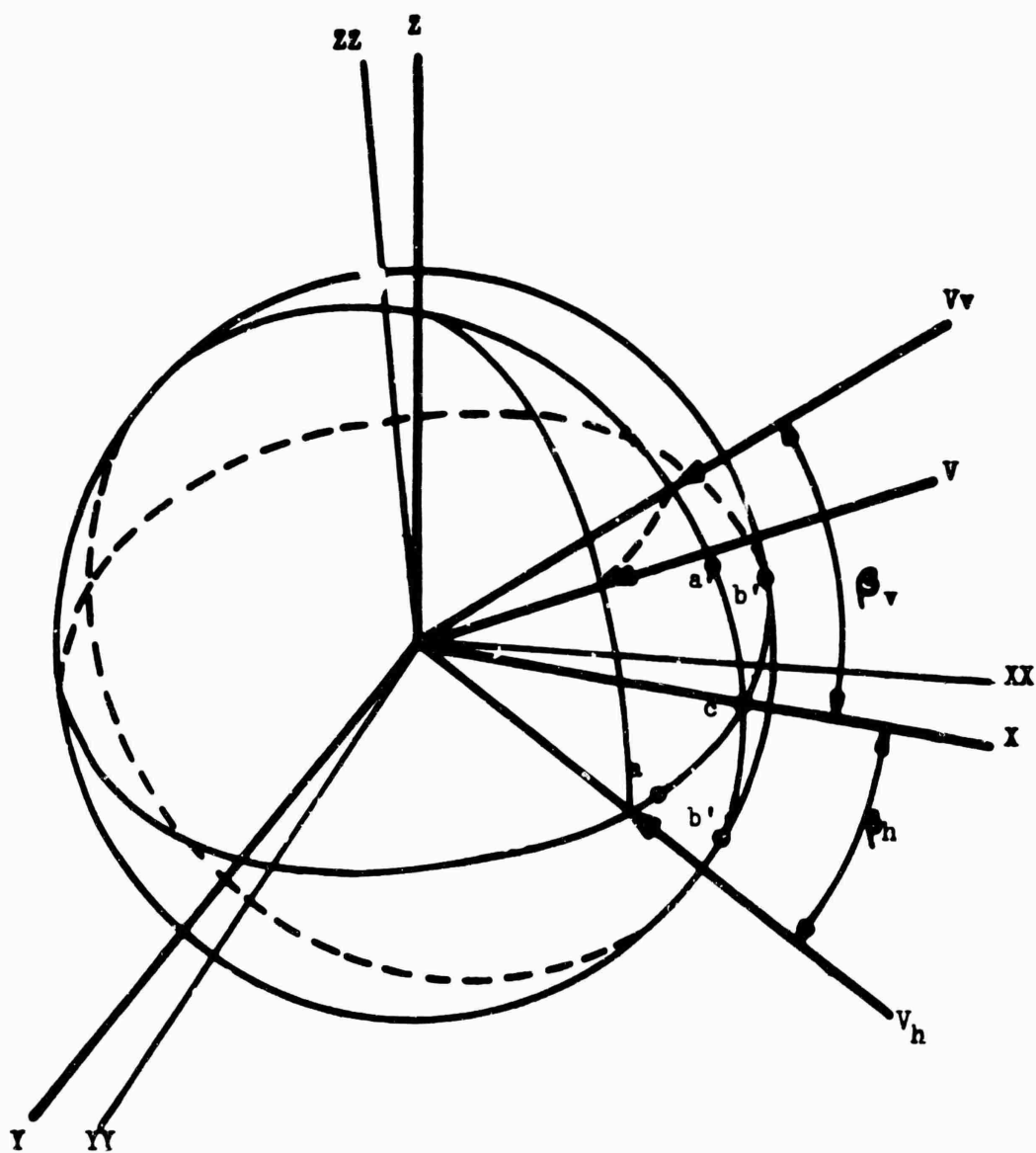
Fig. 4.3 - Orientation of Velocity components and pressure points
to the Axes.

Fig. 4.4
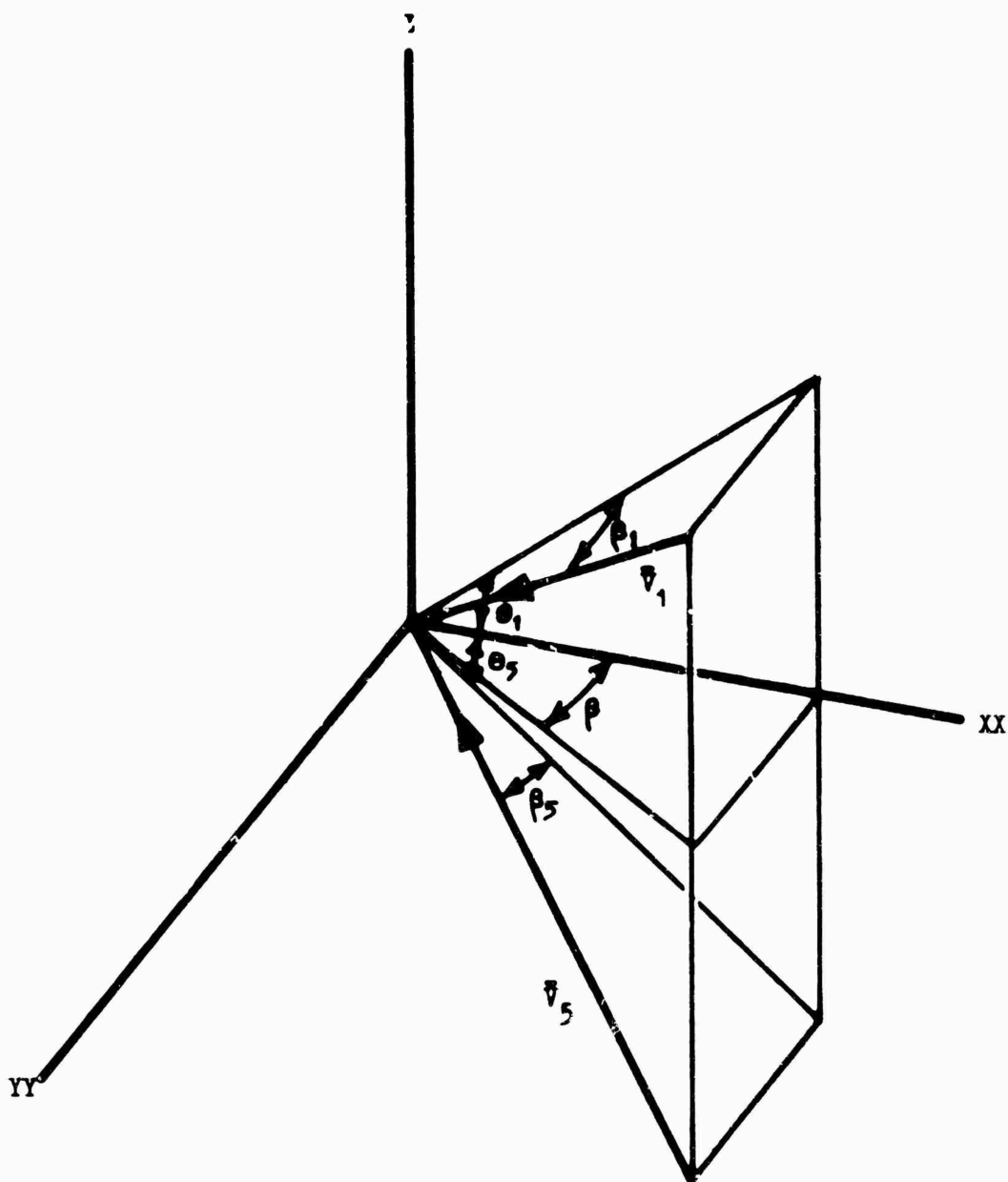
Fig. 4.4 - Inversion about OYY Axis.

Notation of Velocity Components with respect to
the Instrument Axes.

Fig. 5.1
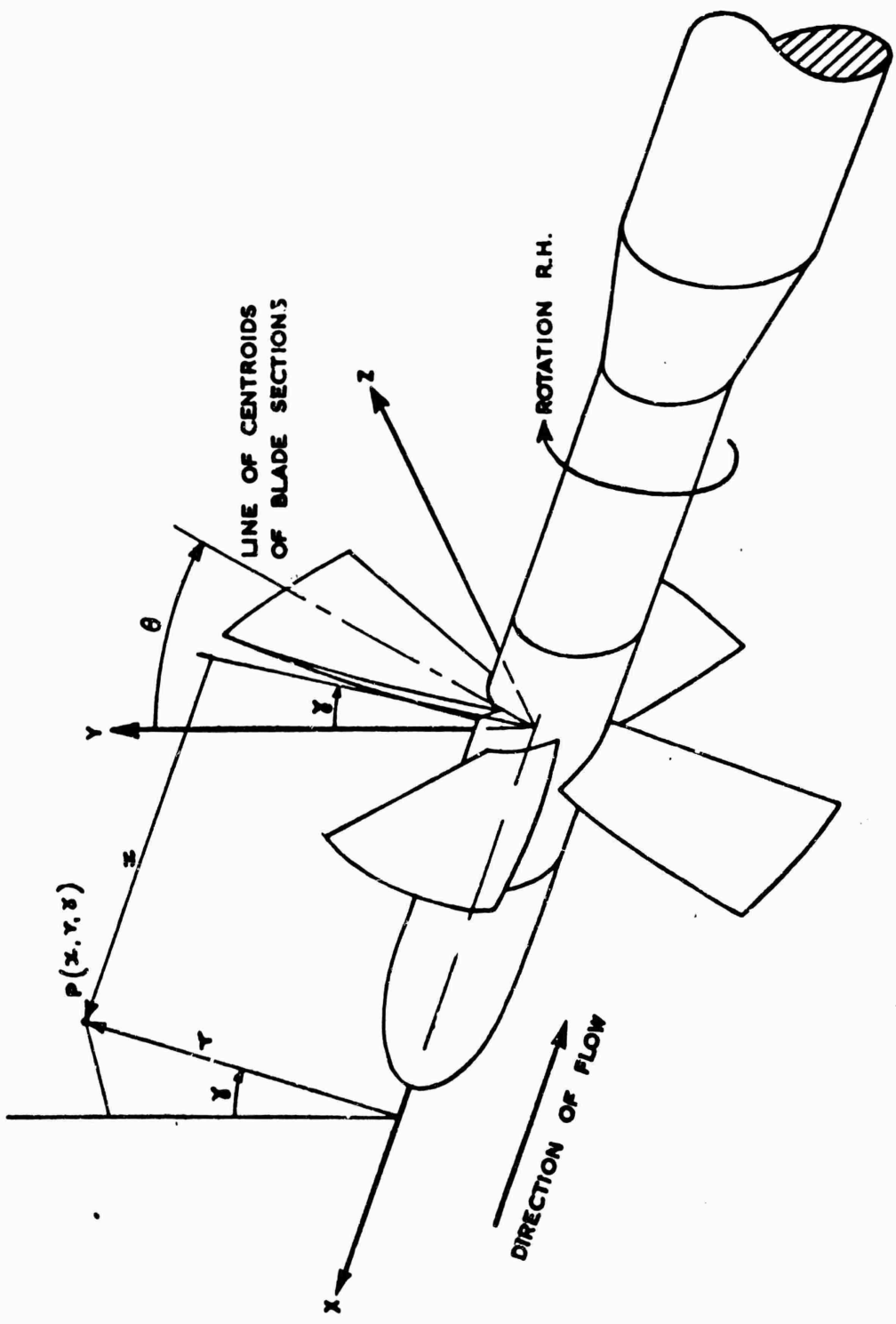
Fig. 5.1 - Orientation of axes of impeller

Fig. 5.2

1 REV.   θ = 0°   1 REV.   θ = 0°

1·0 psi.   1·0 psi.

$\frac{X}{D}$ = 0·1 NO FILTER $\frac{X}{D}$ = 0·1 FILTERED

1 REV.   θ = 0°

1·0 psi.

$\frac{X}{D}$ = 0·0 NO FILTER

1 REV.   θ = 0°   1 REV.   θ = 0°

0·5 psi.   0·5 psi.

$\frac{X}{D}$ = −0·1 NO FILTER $\frac{X}{D}$ = −0·1 FILTERED
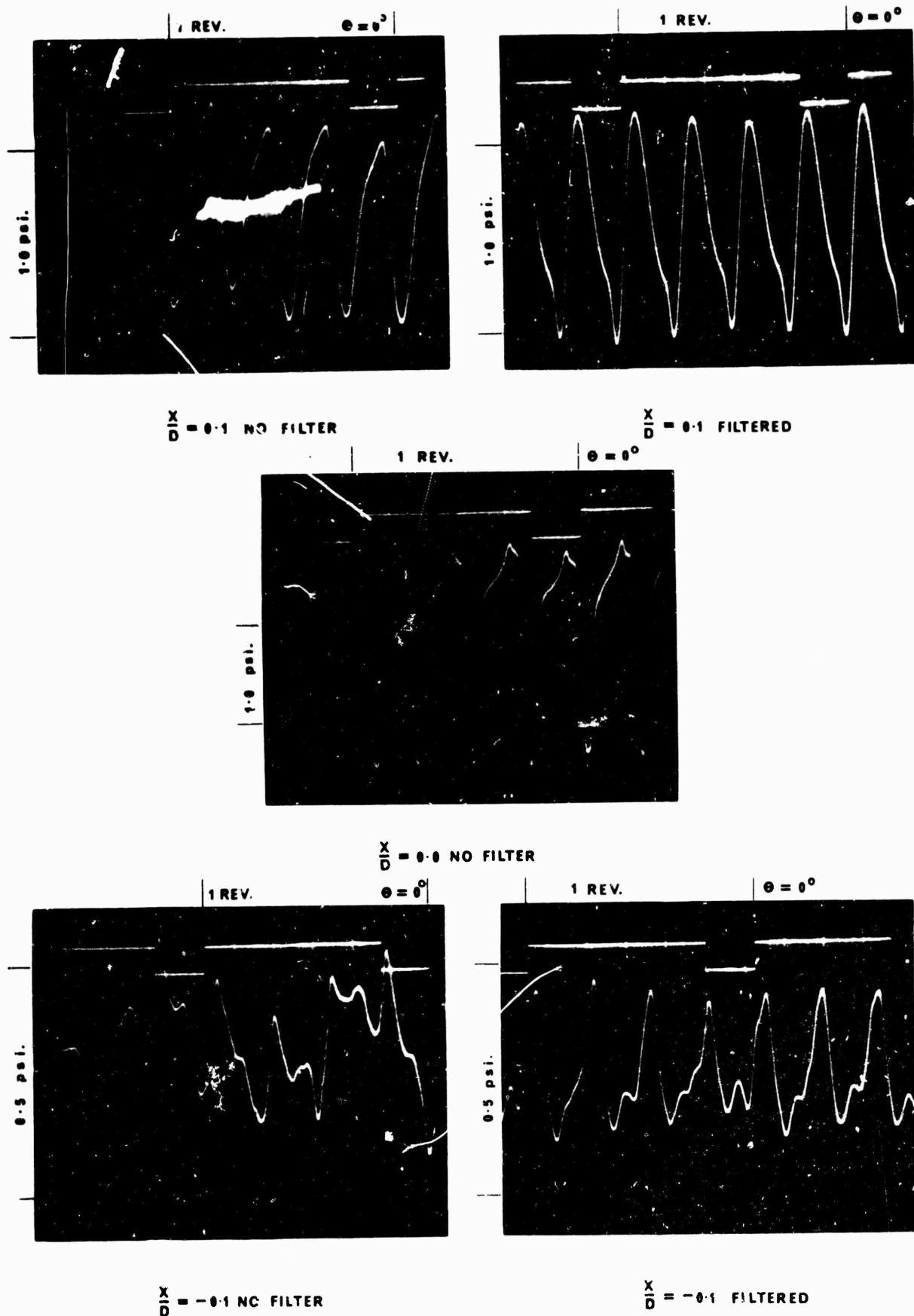
Fig. 5.2 — TYPICAL PRESSURE SIGNALS FOR UNIFORM FLOW J_1 = 0·74, N = 1200 rpm., $\frac{Rd}{D}$ = 0·5028

UNIFORM FLOW
IMPELLER – 4 BLADES

$\frac{R_d}{D}$ = 0·5028

$\frac{X}{D}$ = 0·10

J_1 = 0·74

		NPI=1	NP=8
▼	=	1	
▣	=	1	2
●	=	4	2
▲	=	7	2

PRESSURE COEFFICIENT

K_p

0·18
0·16
0·14
0·12
0·10
0·08
0·06
0·04
0·02

BLADE FREQUENCY HARMONIC NUMBER

1   2   3   4   5   6
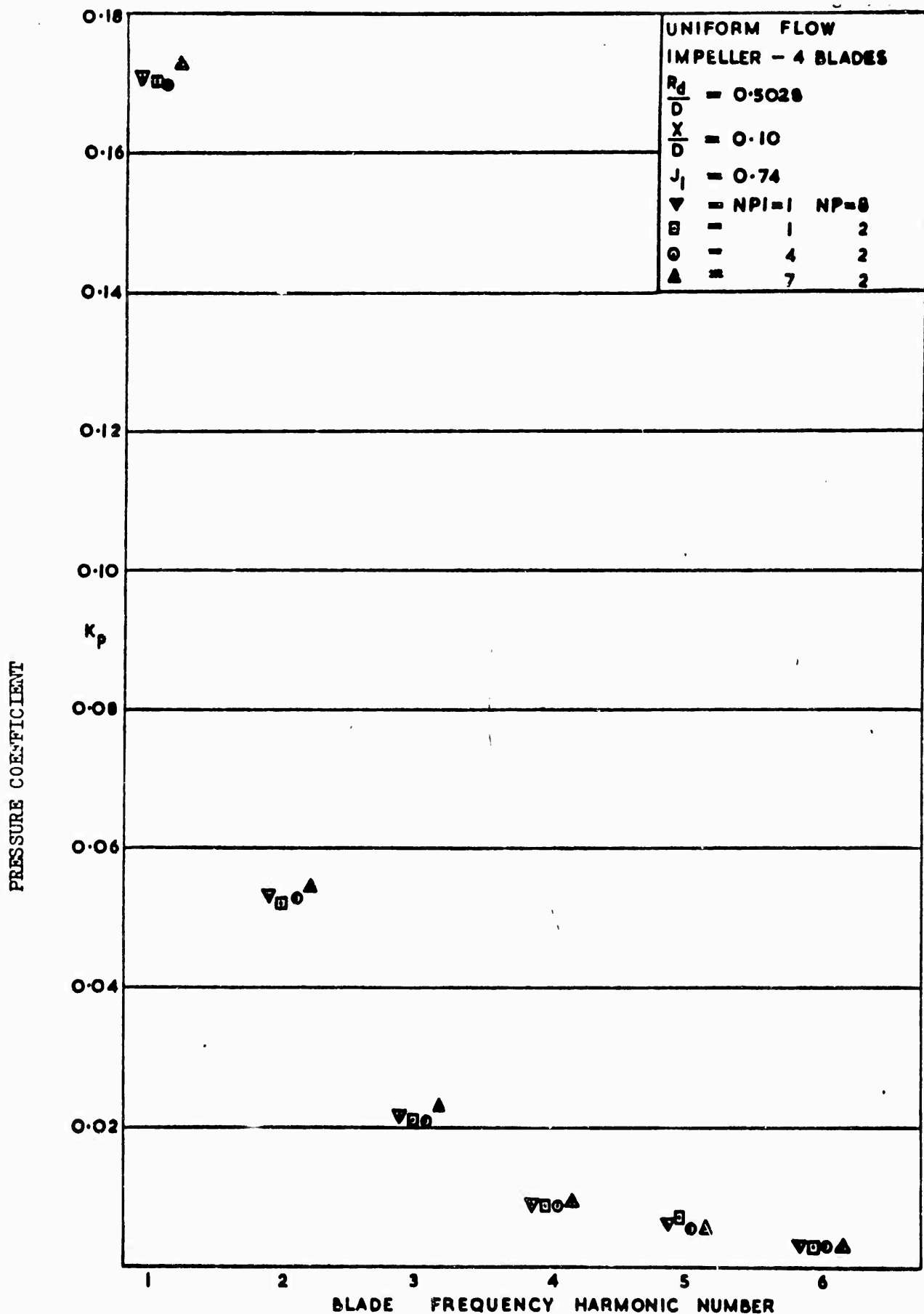
Fig. 5.3 – Periodicity of Recorded Pressure.
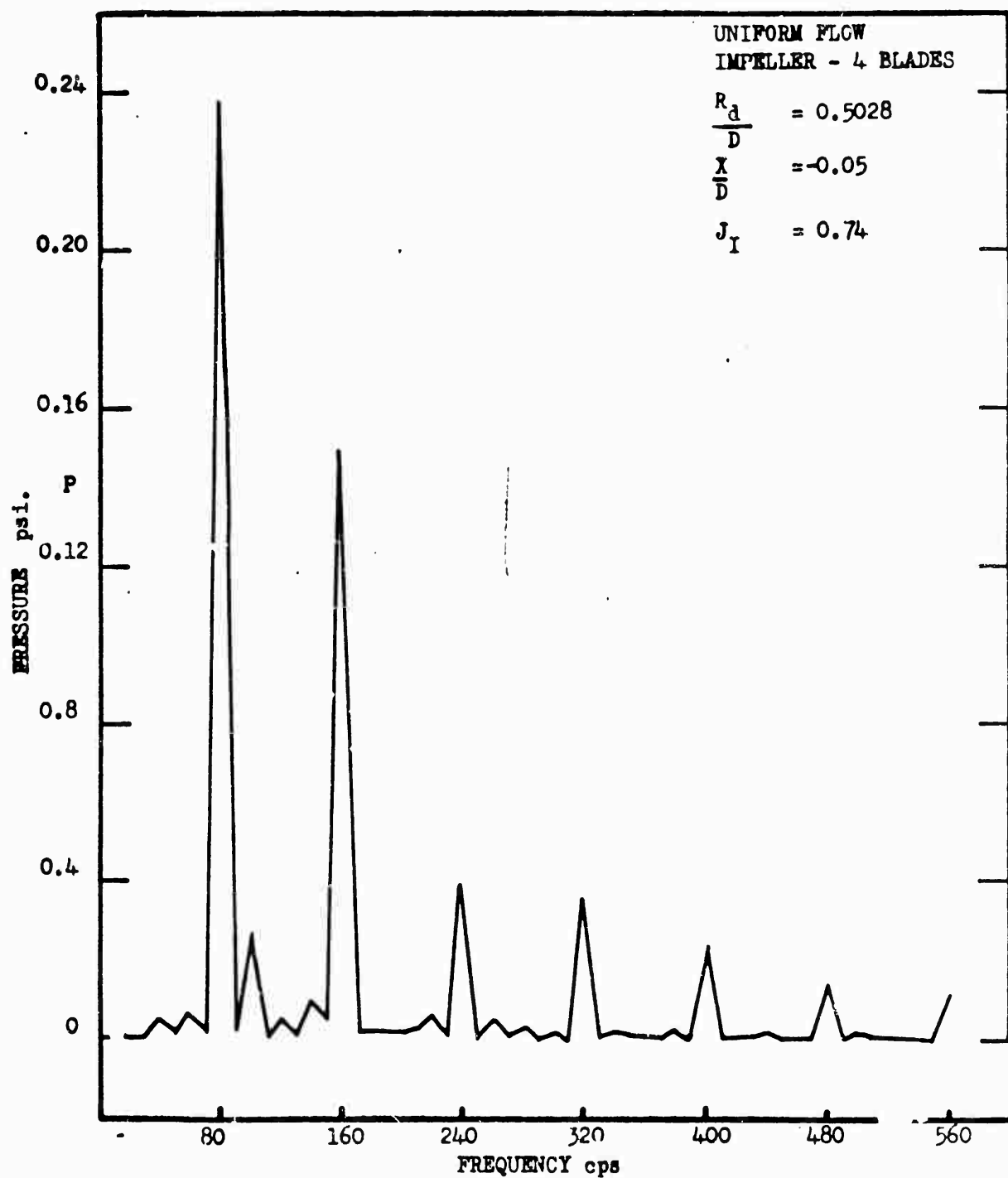
Fig. 5.4

Fig. 5.4 - Frequency Spectra of Pressure

Fig. 5.5
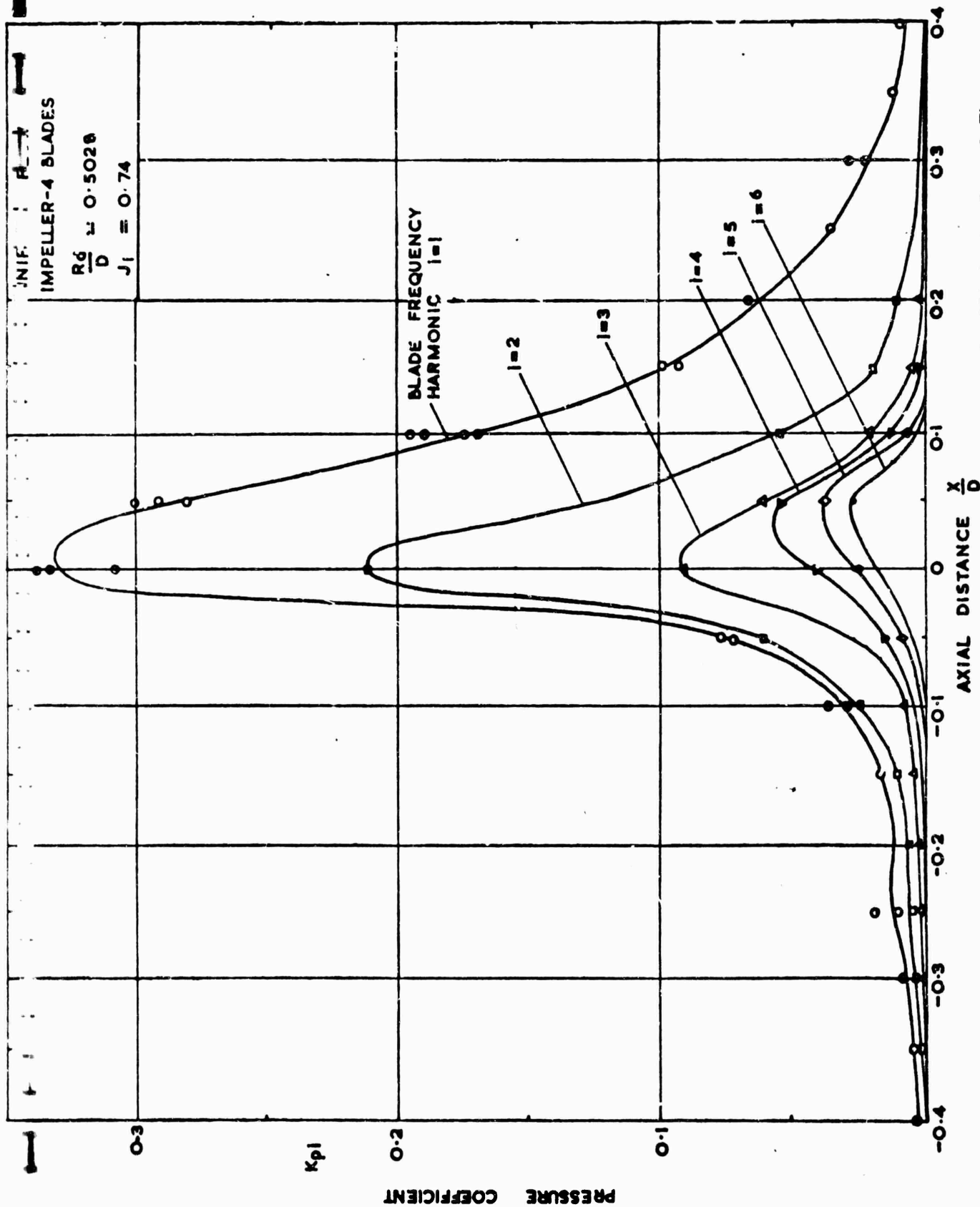
Fig. 5.5 - Axial Variation of Blade Frequency Harmonic Pressure Coefficient. $J_I = 0.74$.

UNIFORM FLOW
IMPELLER – 4 BLADES
$\frac{R_M}{D}$ = 0·5028
J_1 = 0·80

BLADE FREQUENCY
HARMONIC $I = 1$

$I = 2$
$I = 3$
$I = 4$
$I = 5$
$I = 6$

AXIAL DISTANCE $\frac{X}{D}$

PRESSURE COEFFICIENT

K_{pi}

0·3
0·2
0·1

0·4 0·3 0·2 0·1 0 -0·1 -0·2 -0·3 -0·4
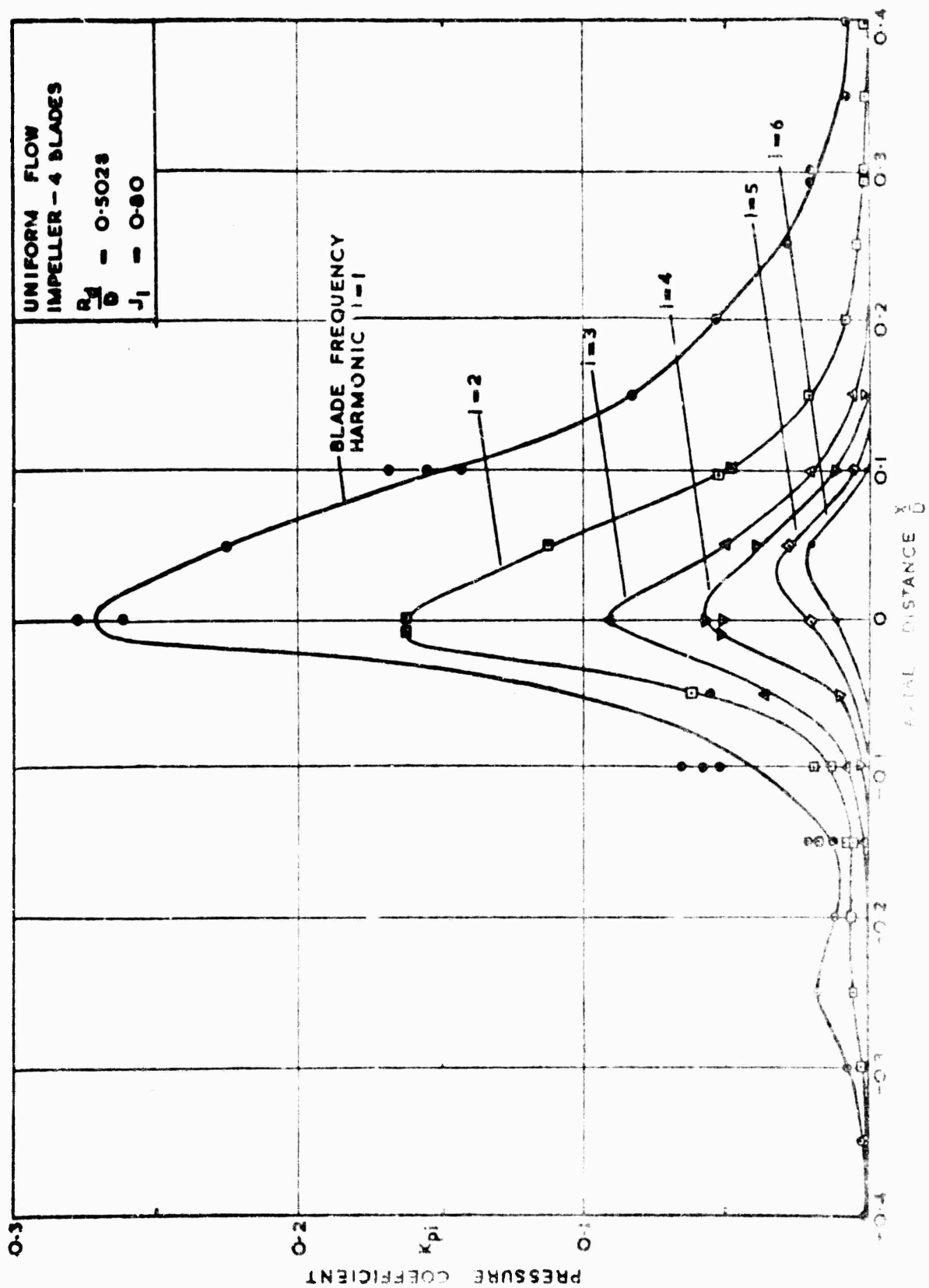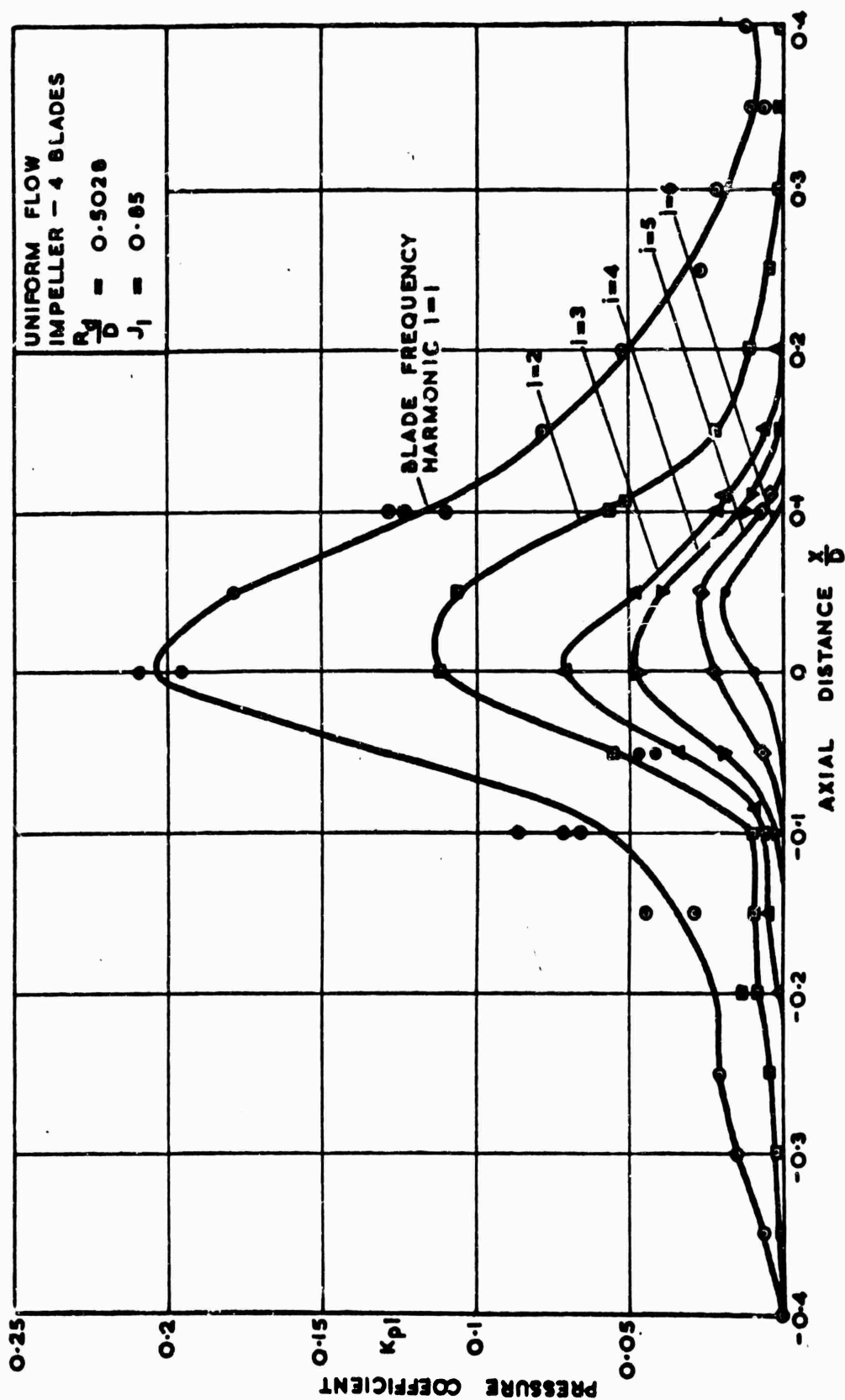
Fig. 5.7 - Axial Variation of Blade Frequency Harmonic Pressure Coefficient. $J_I = 0.85$.

Fig. 5.7
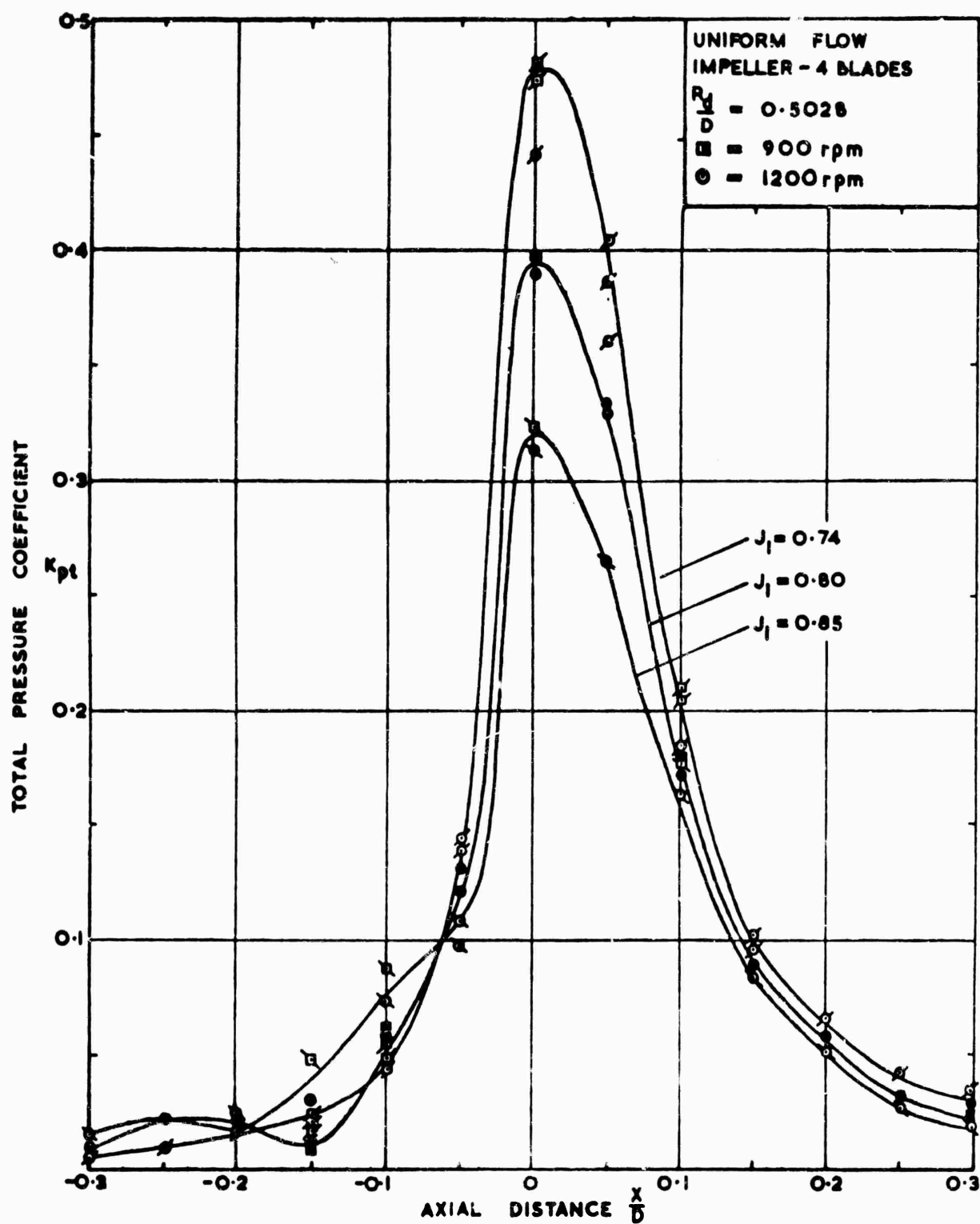
Fig. 5.8

Fig. 5.8 - Axial Variation of the Total Pressure Coefficient.

Fig. 5.9
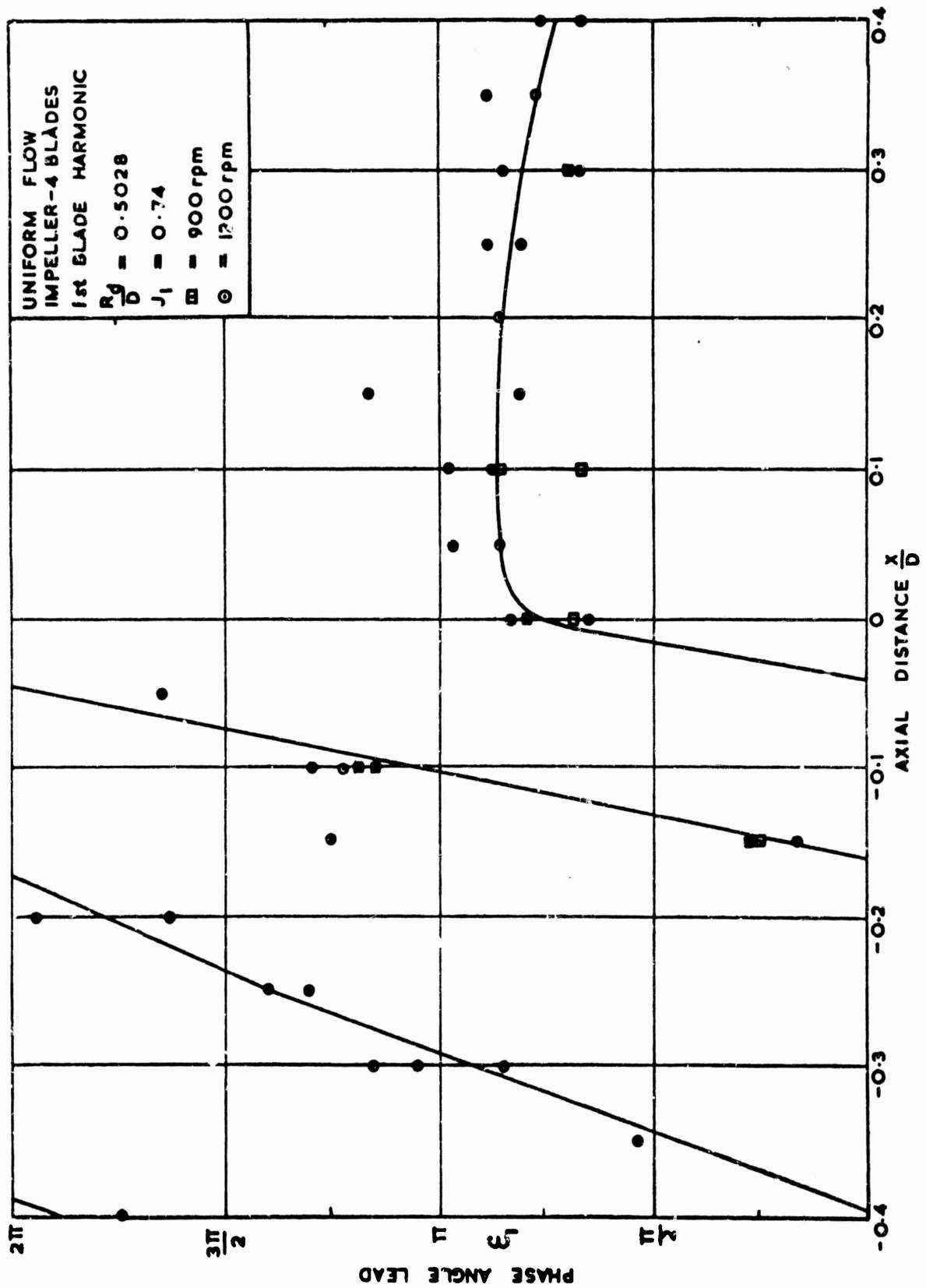
Fig. 5.9 - Axial ...ation of Phase Angle (Lead) For 1st Blade Frequency Harmonic. $J_I = 0.74$
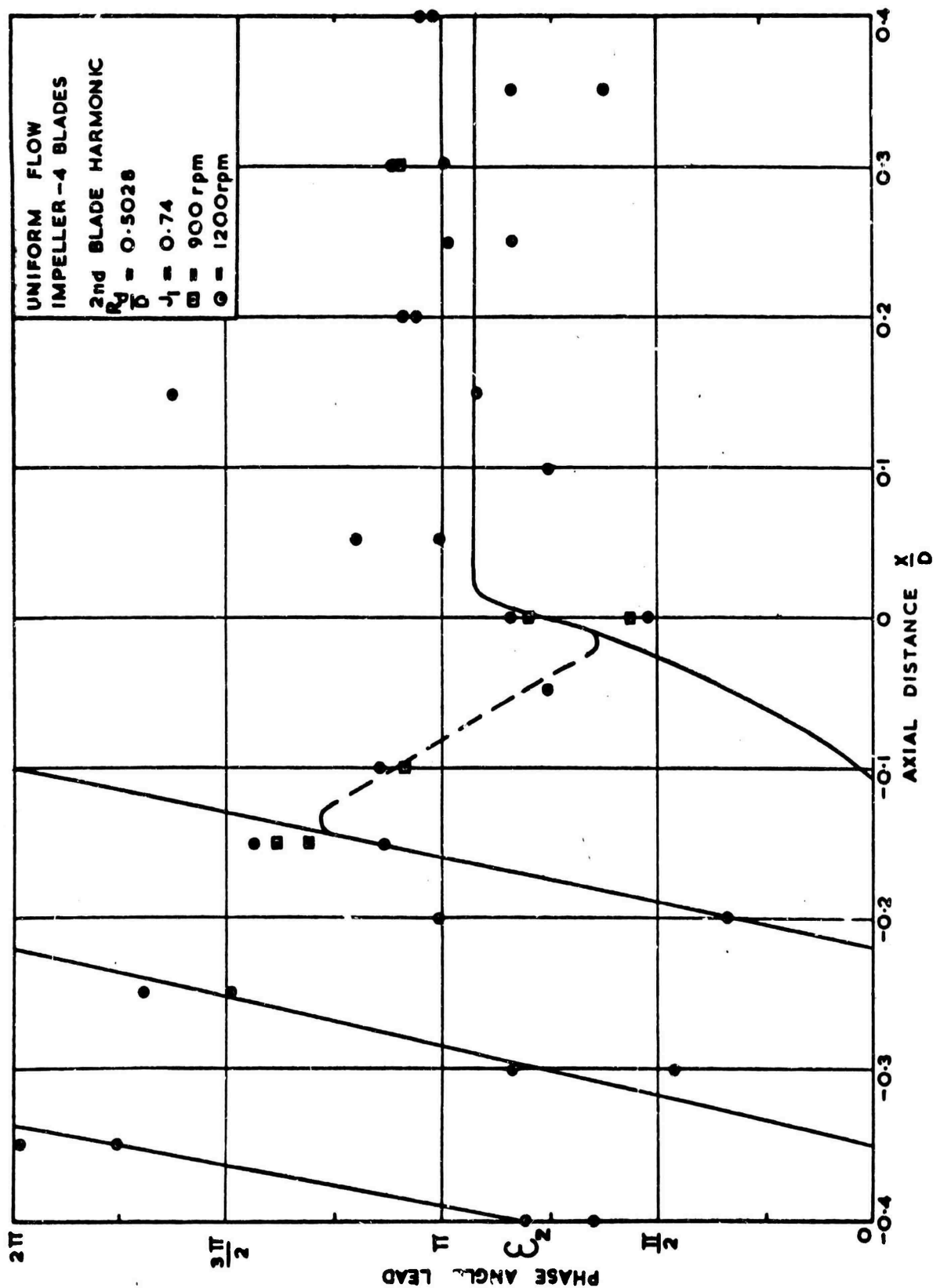
Fig. 5.10

Fig. 5.10 - Axial Variation of Phase Angle (Lead) for 2nd Blade Frequency Harmonic. J_I = 0.74.
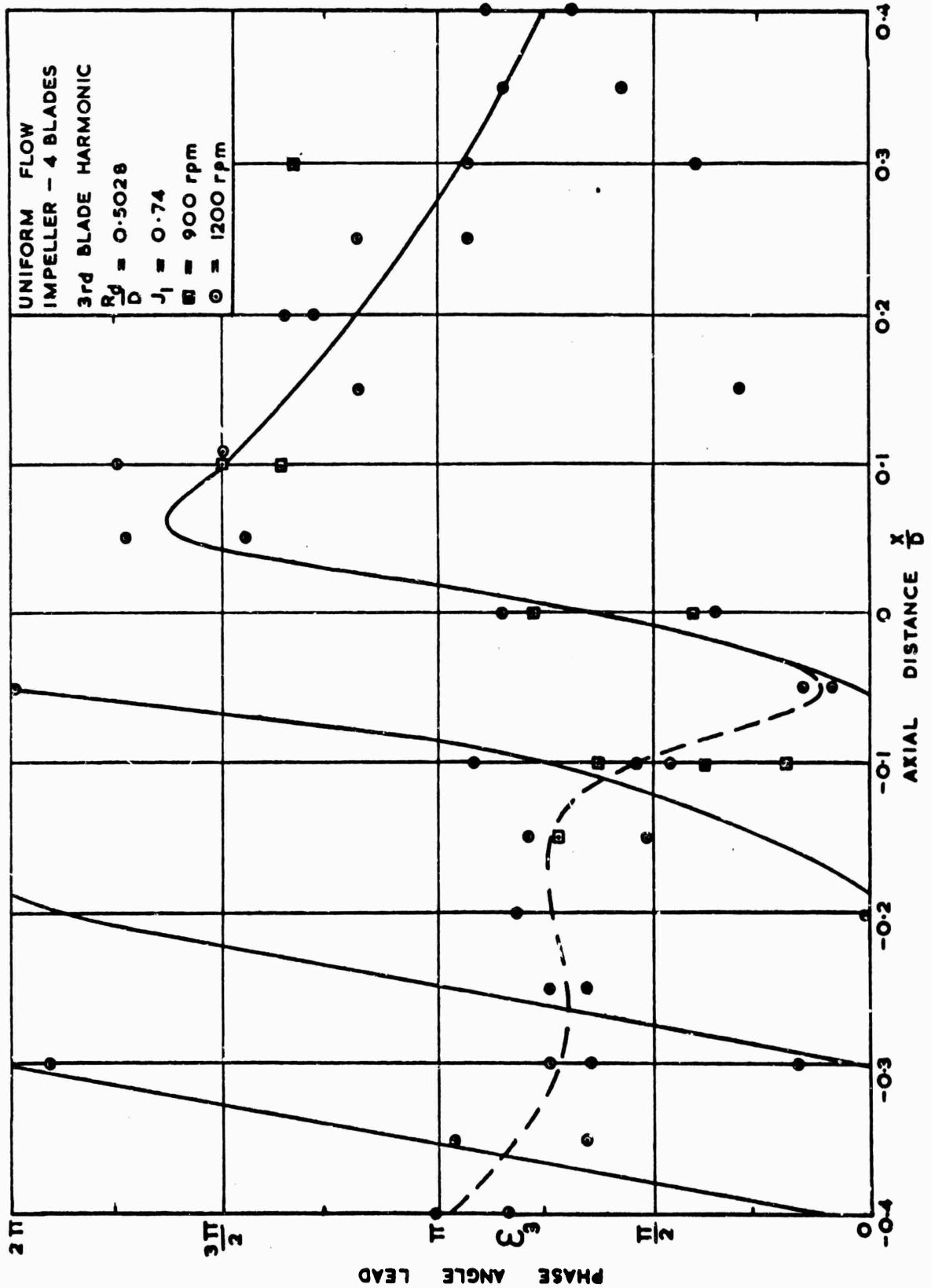
Fig. 5.11

Fig. 5.11   —   Axial Variation of Phase Angle (Lead) for 3rd Blade Frequency Harmonic. $J_I = 9.74$
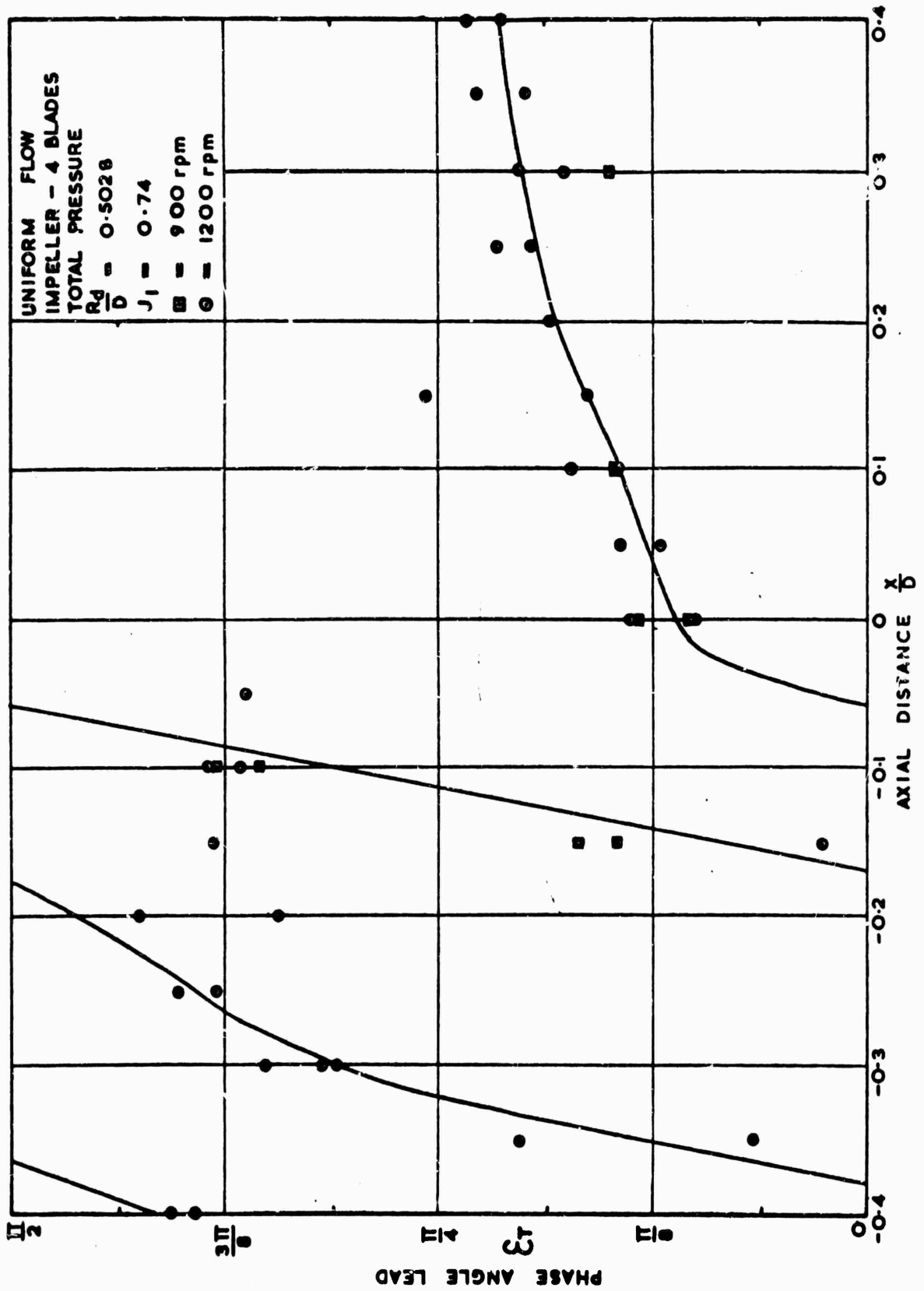
Fig. 5.12 - Axial Variation of Phase Angle (Lead) for Total Pressure.

Fig. 5.13
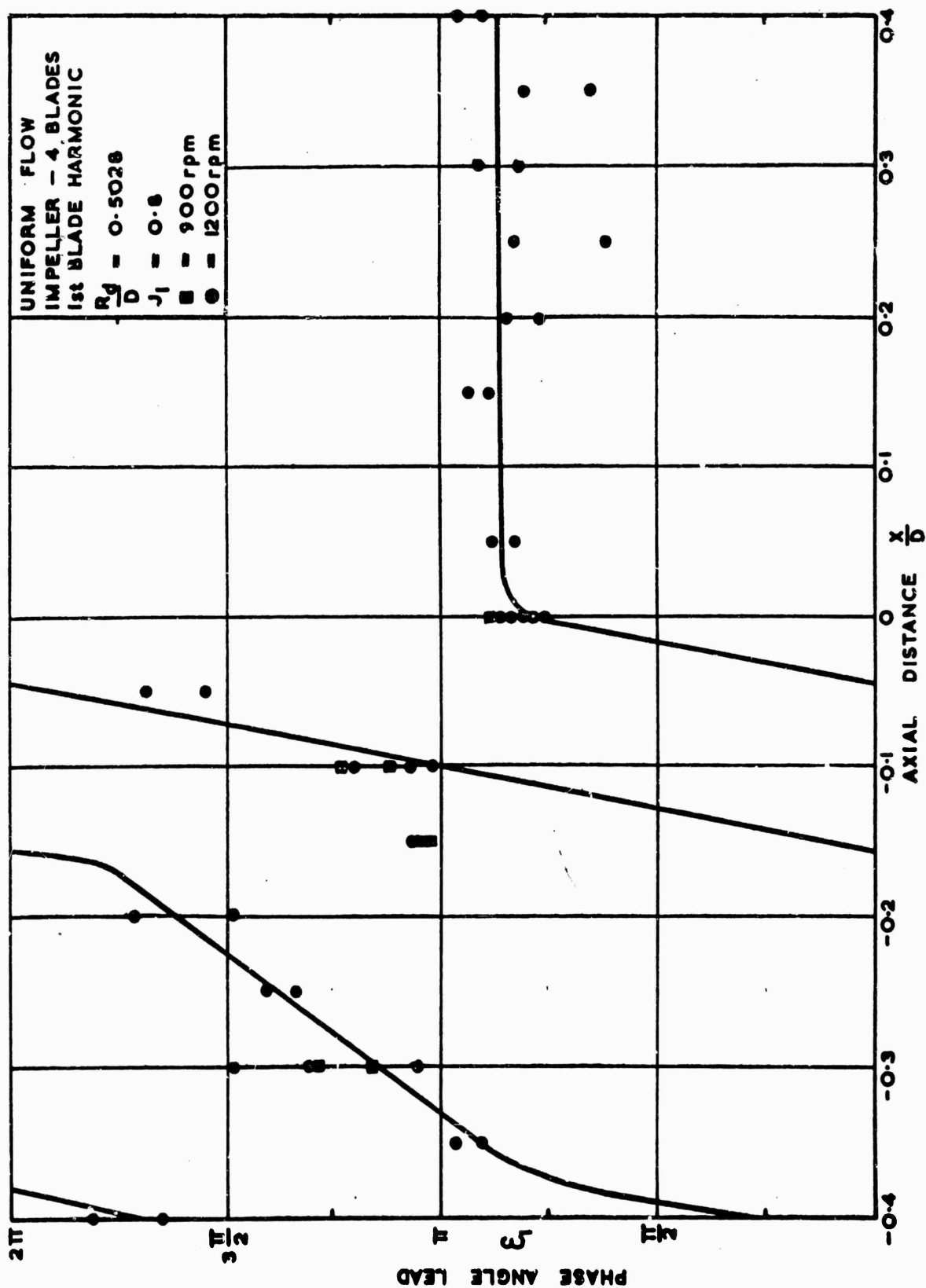
Fig. 5.13 - Axial Variation of Phase Angle (Lead) for 1st Blade Frequency Harmonic. $J_I = 0.80$.
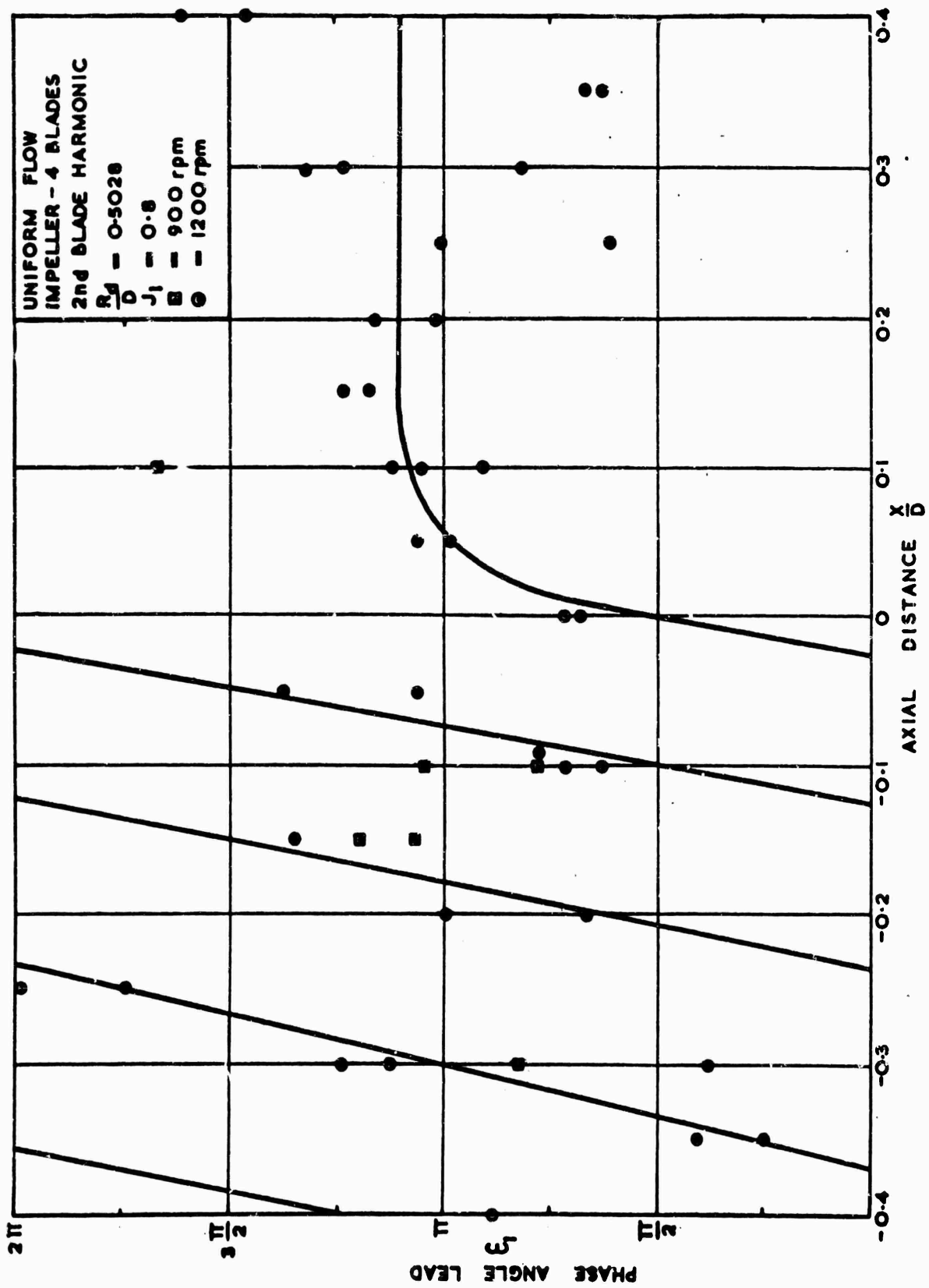
Fig. 5.14 - Axial Variation of Phase Angle (Lead) for 2nd Blade Frequency Harmonic. $J_I = 0.80$.
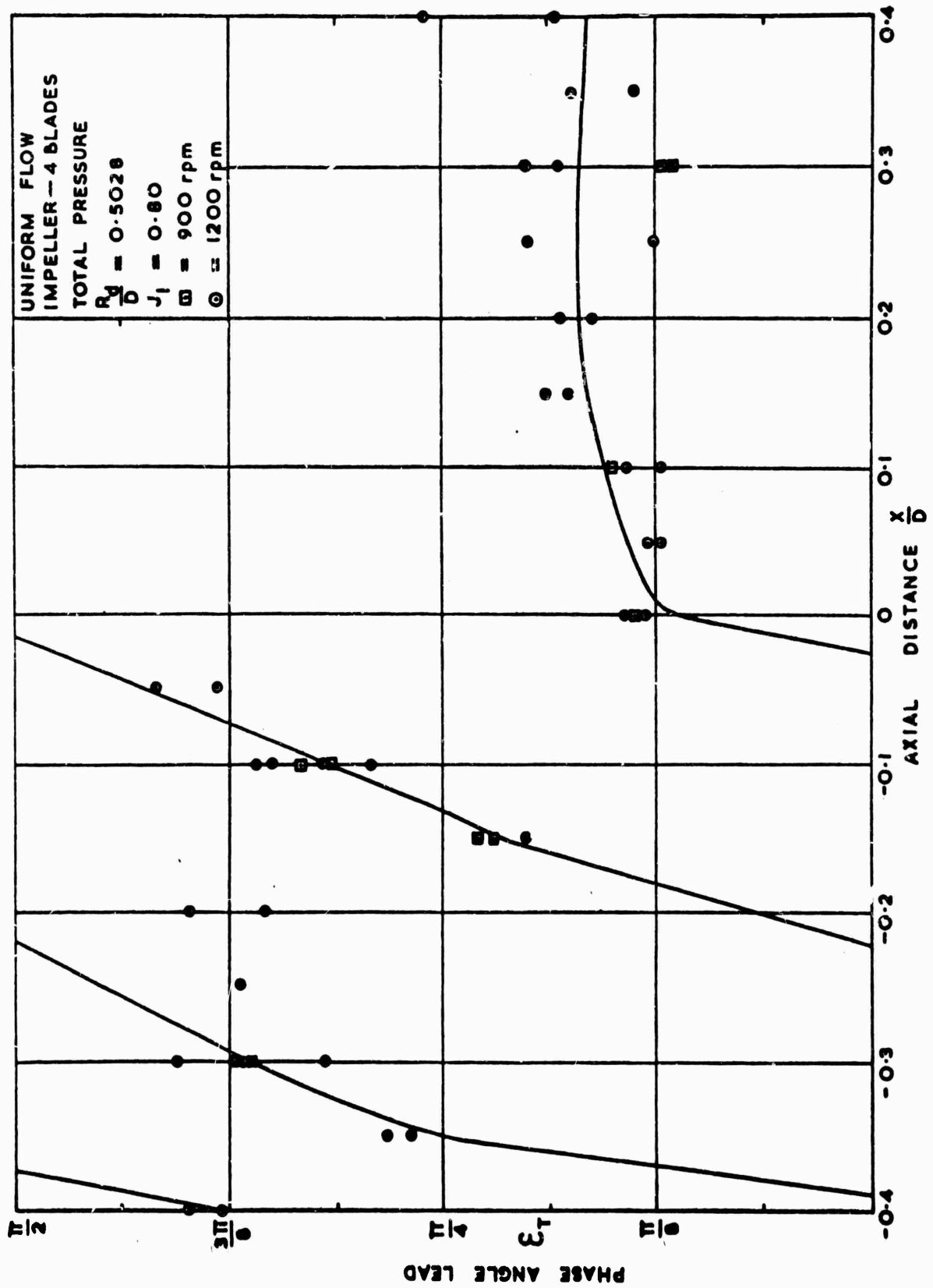
Fig. 5.14

Fig. 5.15 - Axial Variation of Phase Angle (Lead) for Total Pressure. J_I = 0.80.

Fig. 5.15
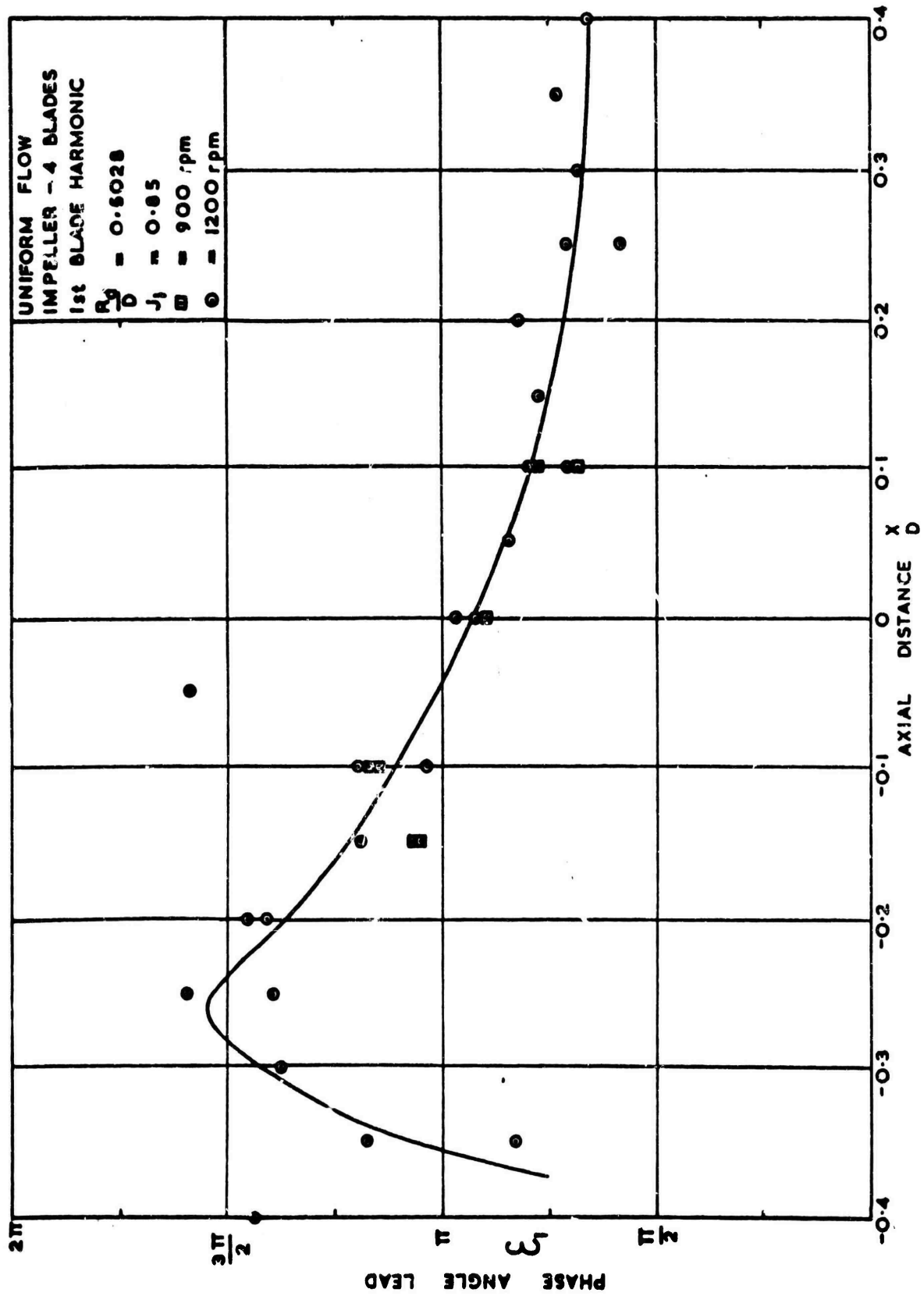
Fig. 5.16

Fig. 5.16 - Axial Variation of Phase Angle (Lead) for 1st Blade Frequency Harmonic. $J_I = 0.85$.
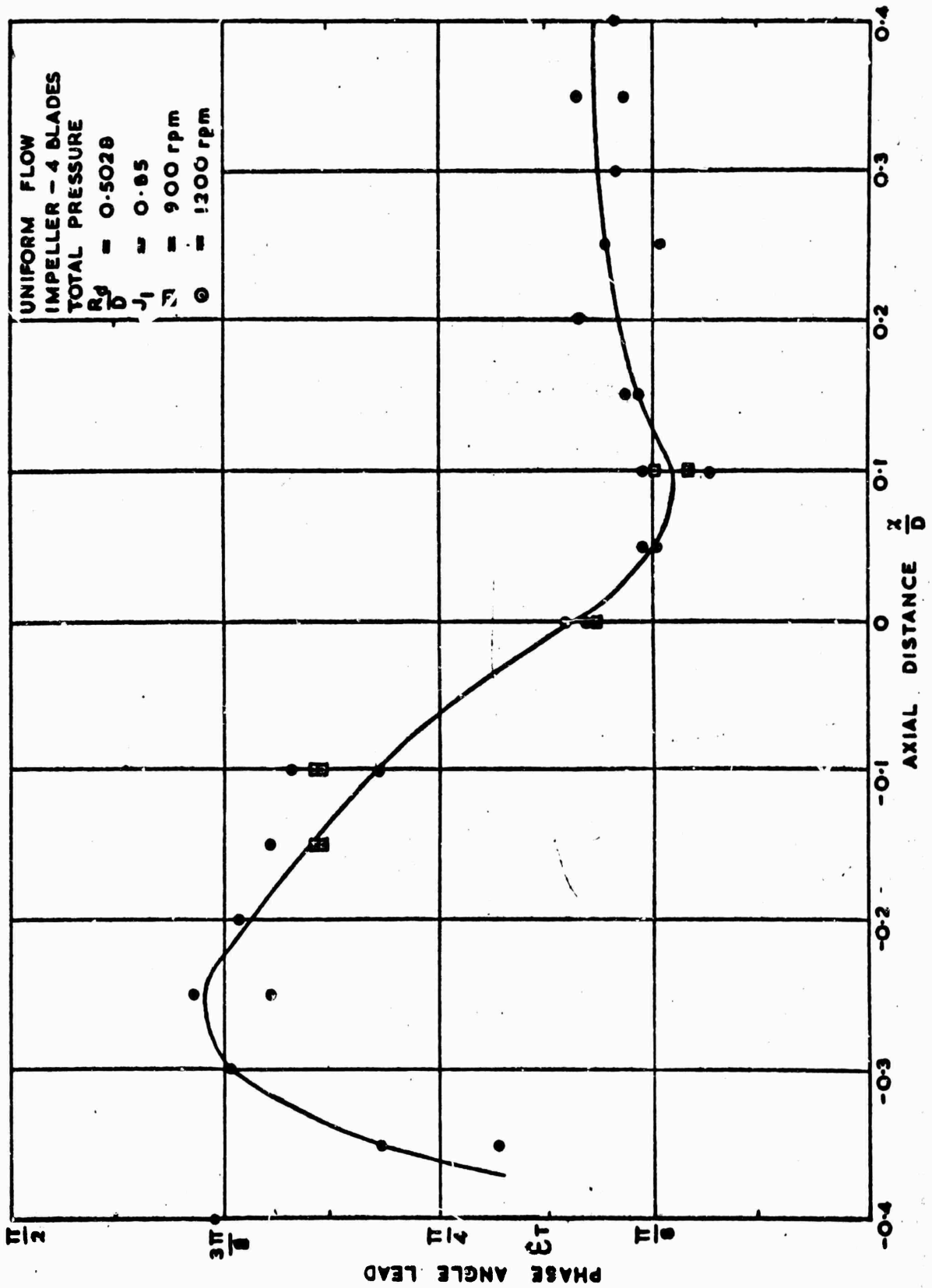
Fig. 5.17.- Axial Variation of Phase Angle (Lead) for Total Pressure. $J_I = 0.85$.

Fig. 5.18.
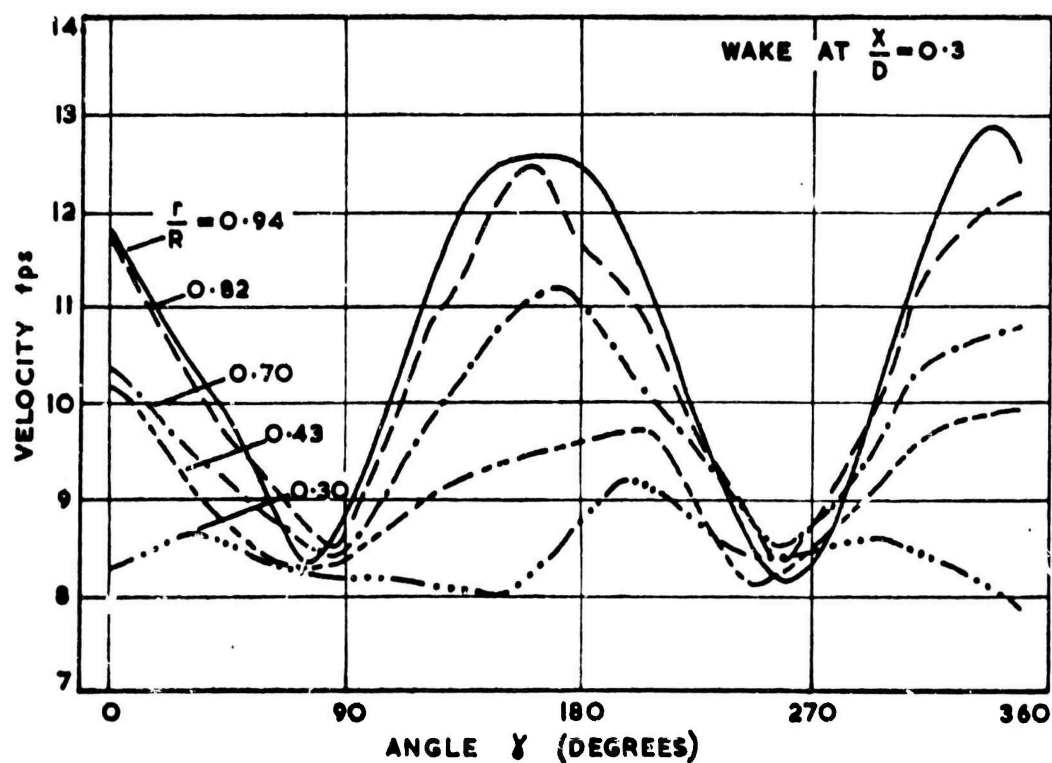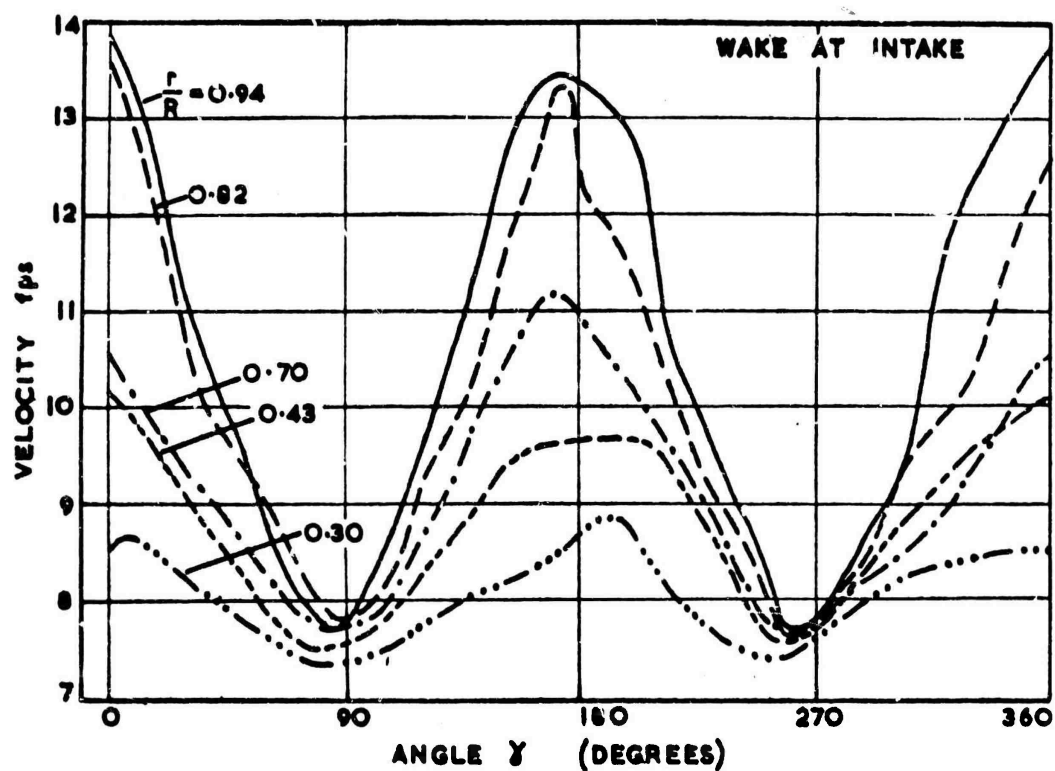
Fig. 5.18 - Velocity Profile in the Duct for Wake-2.

Fig. 5.19
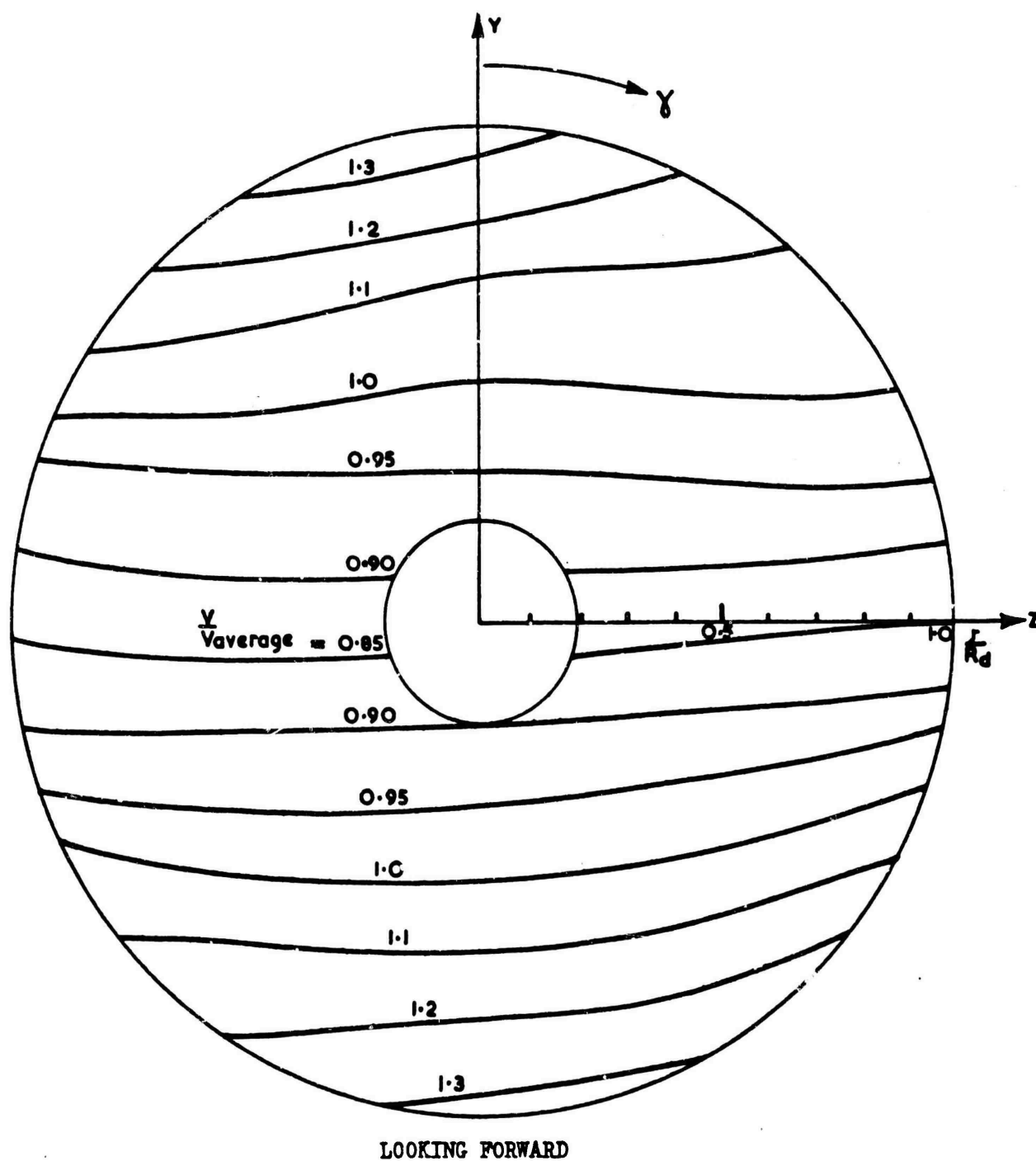
Fig. 5.19 - Velocity Profile at the Impeller for Wake - 2.
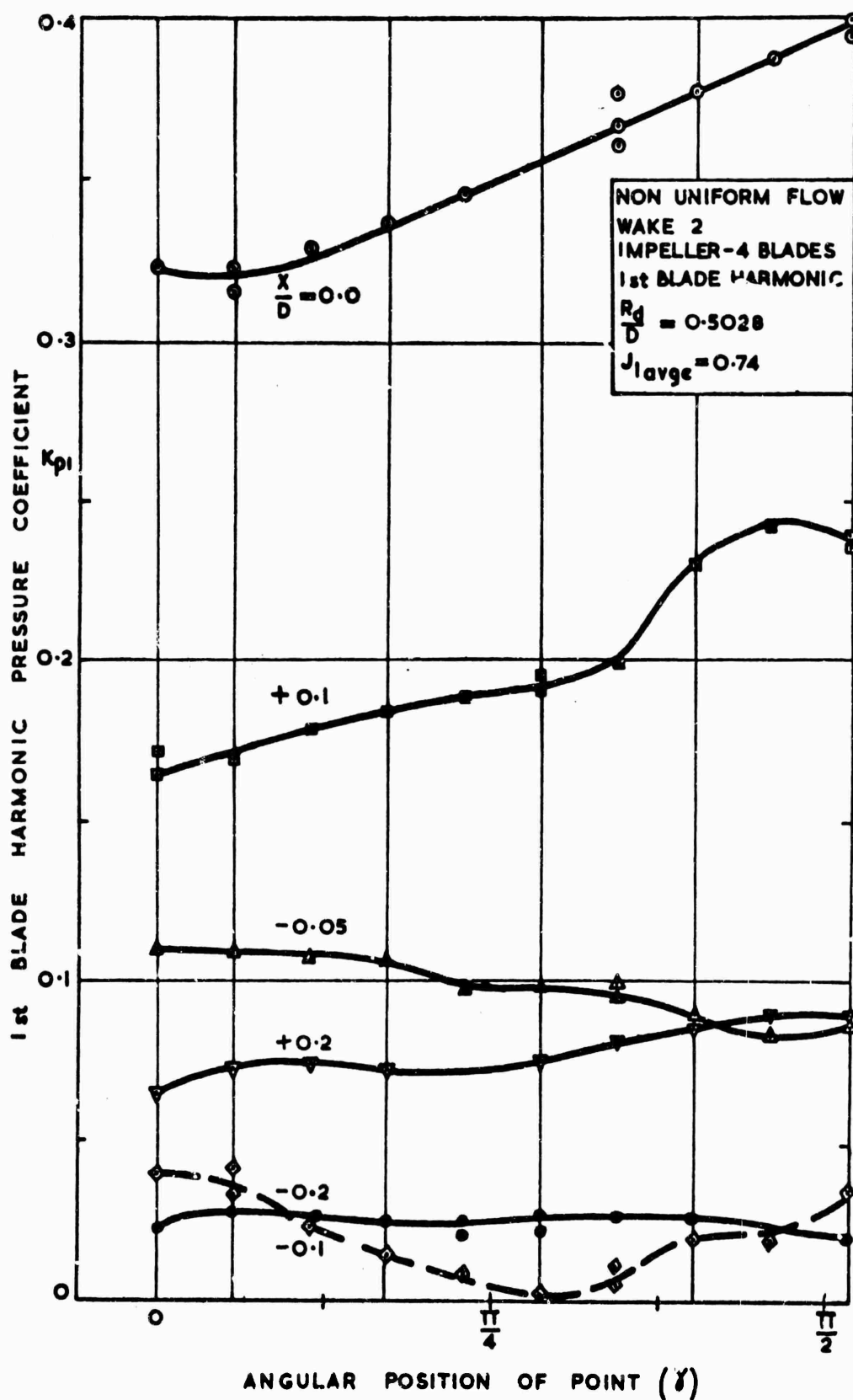
Fig. 5.20 — Pressure Coefficient for the 1st Blade Frequency
Harmonic with Wake-2.

Fig. 5.21
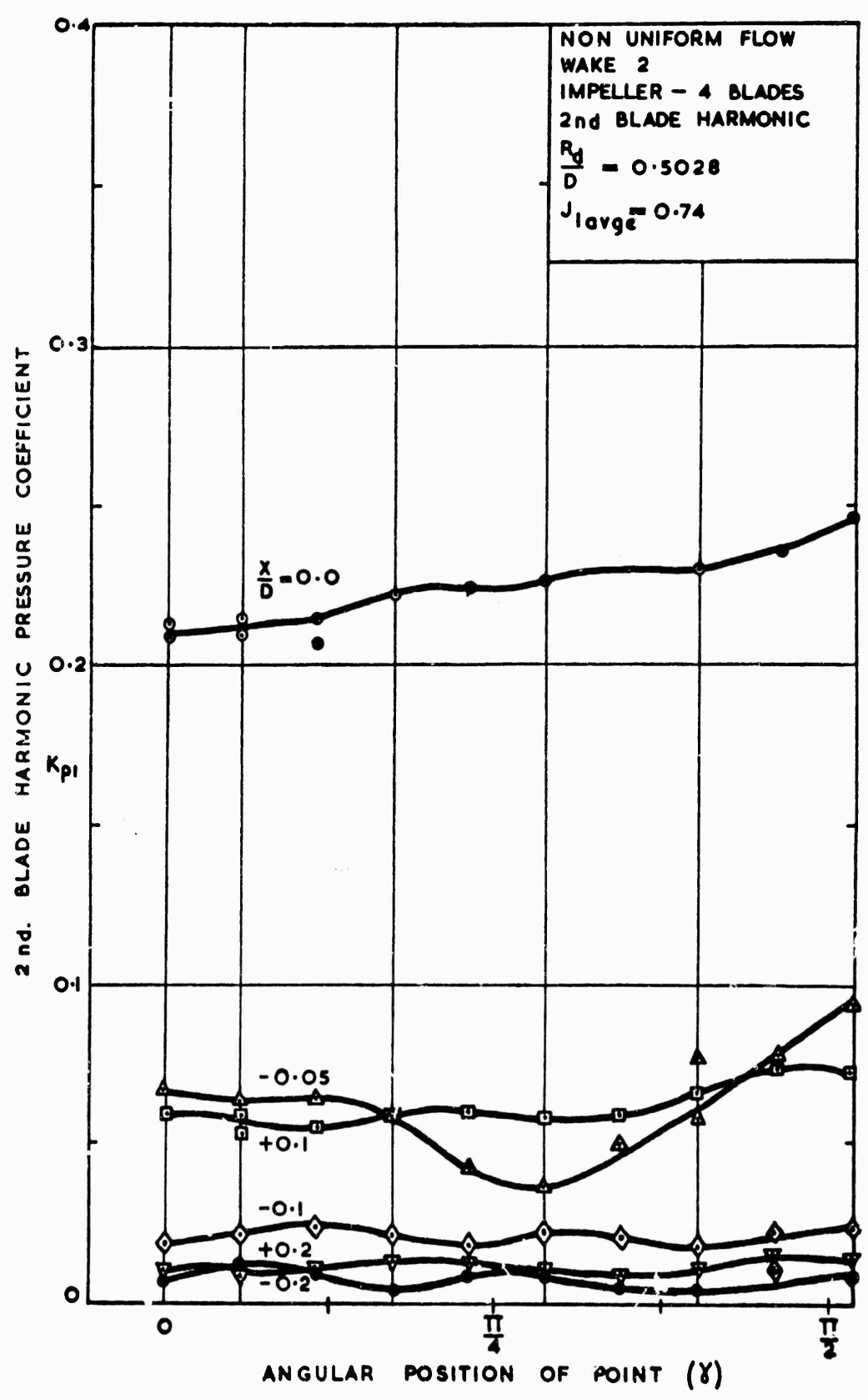
Fig. 5.21 - Pressure coefficient for the 2rd Frequency
Harmonic with Wake-2.

Fig. 5.22
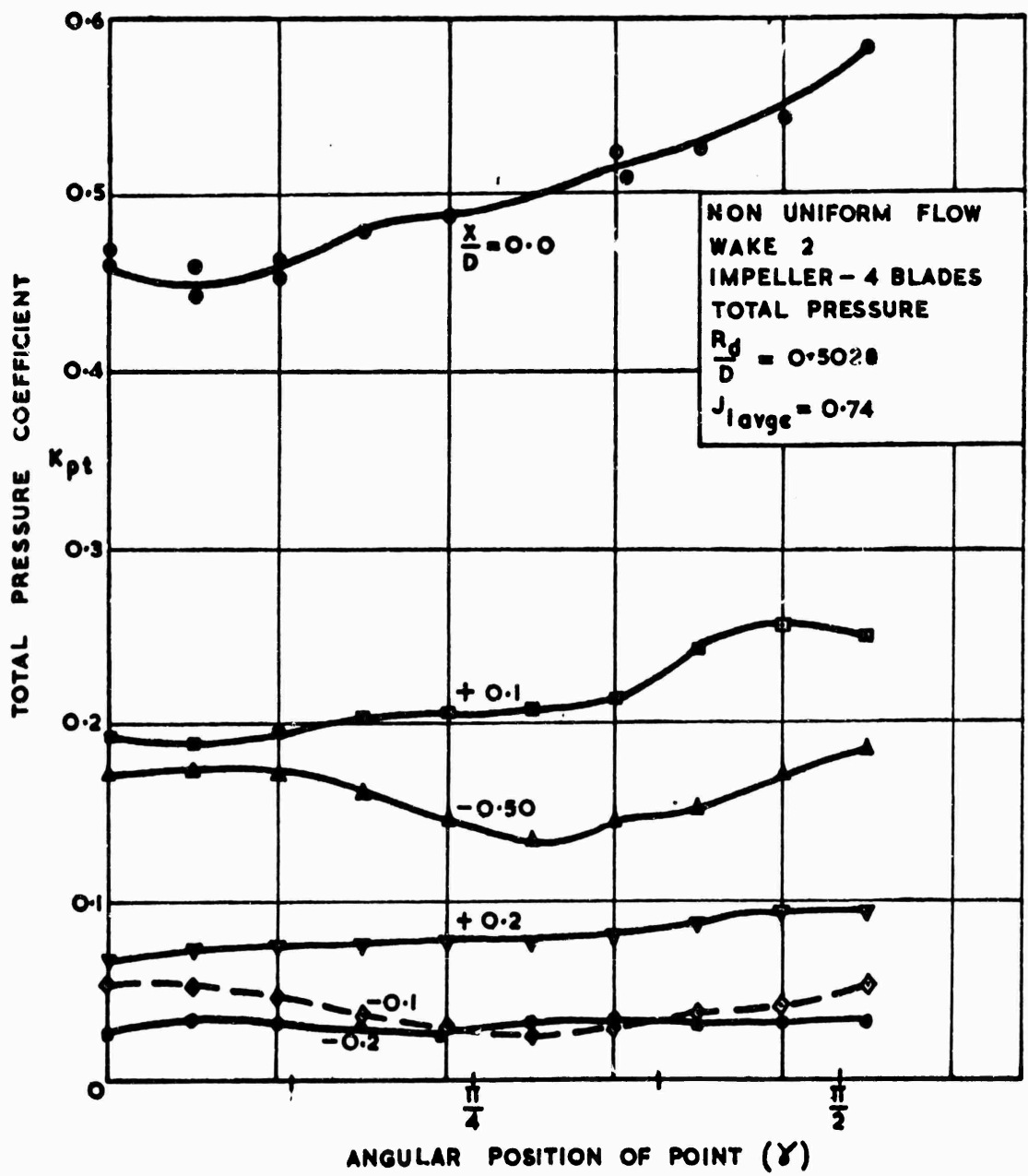
Fig. 5.22 - Pressure Coefficient of the Total Pressure with Wake-2.

Fig. 5.23
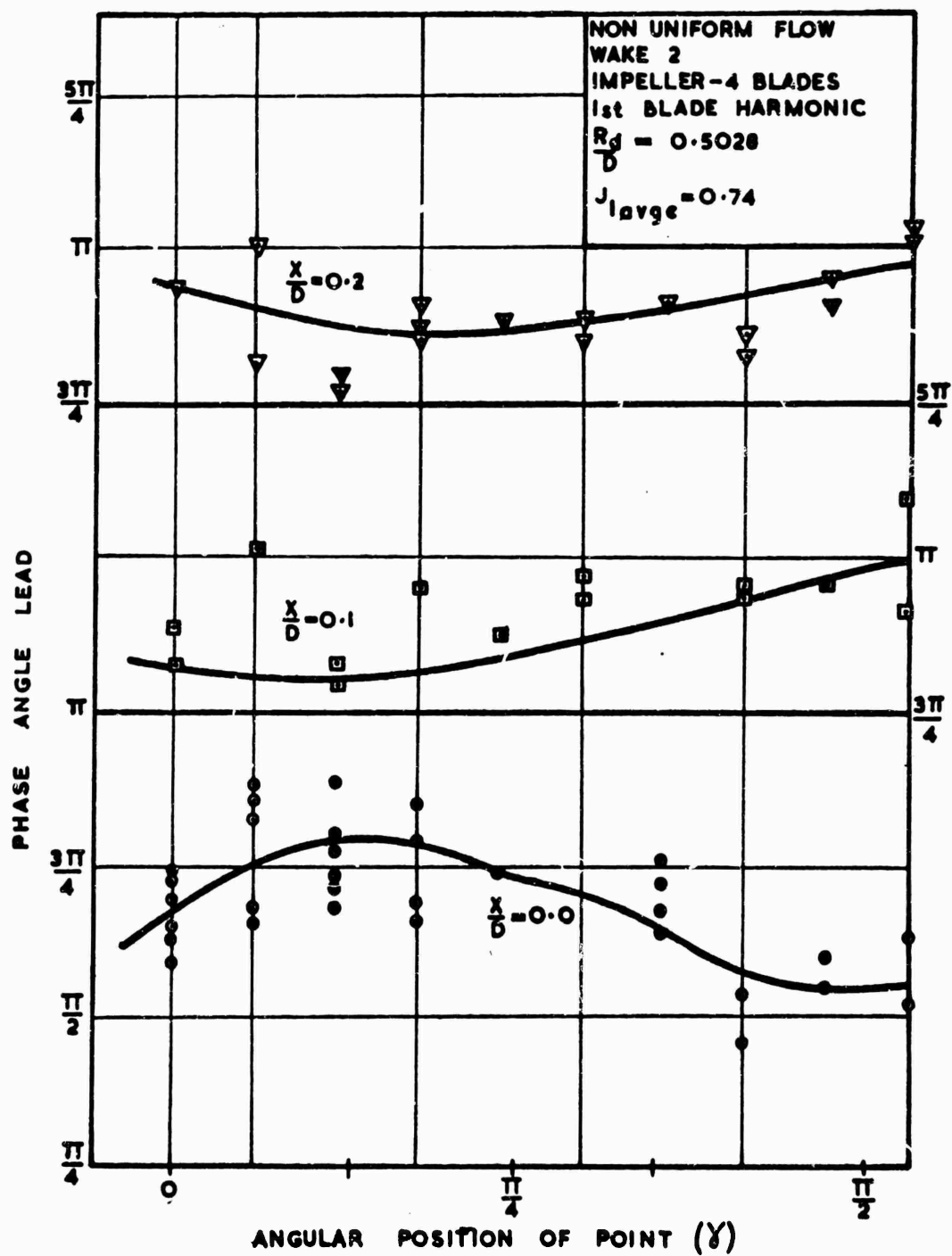
Fig. 5.23 - Phase Angle (Lead) for the 1st Blade Frequency
Harmonic with Wake-2.

Fig. 5.24
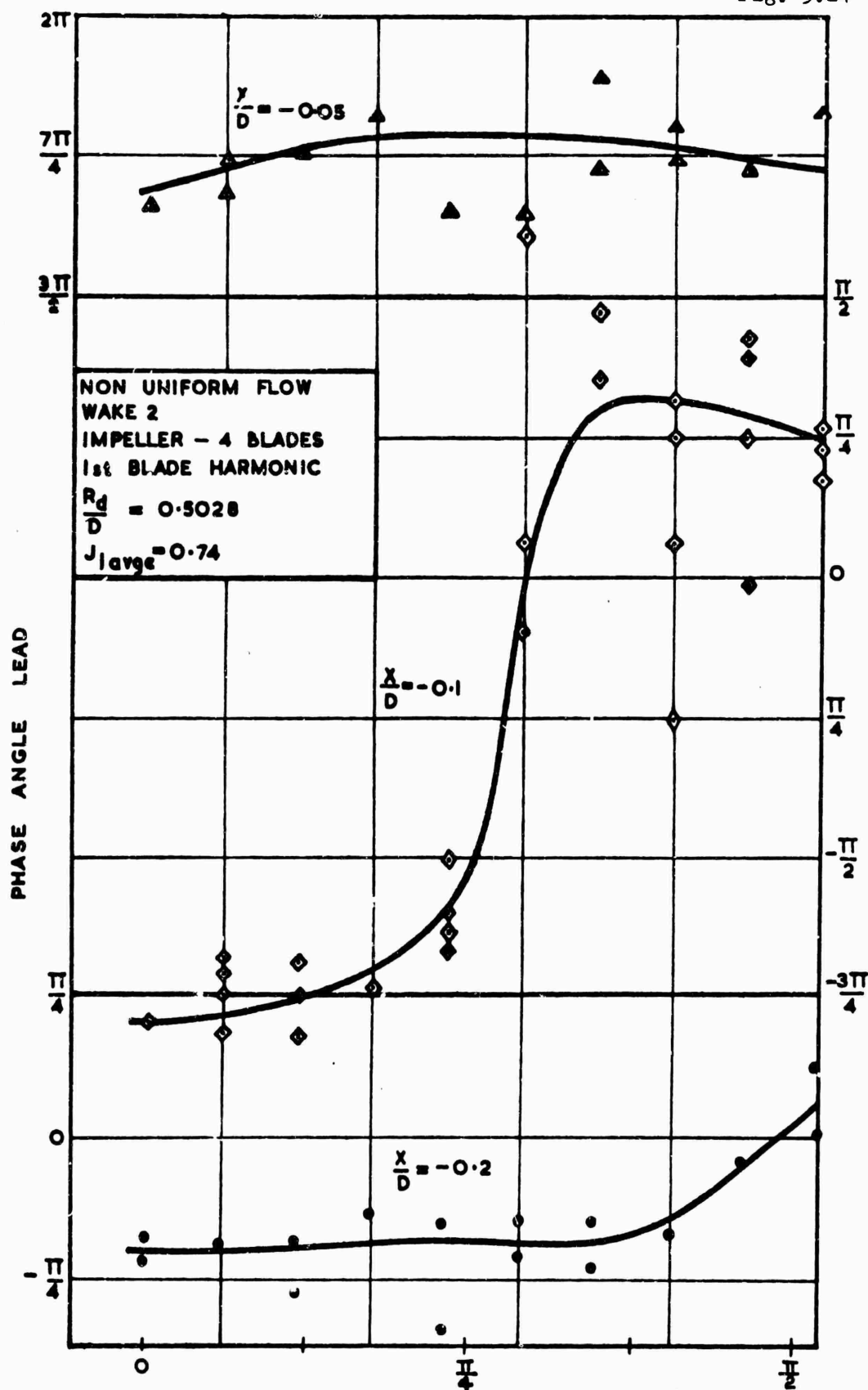
Fig. 5.24 - Phase Angle (Lead) for the 1st (γ) Blade Frequency Harmonic with Wake-2.

Fig. 5.25
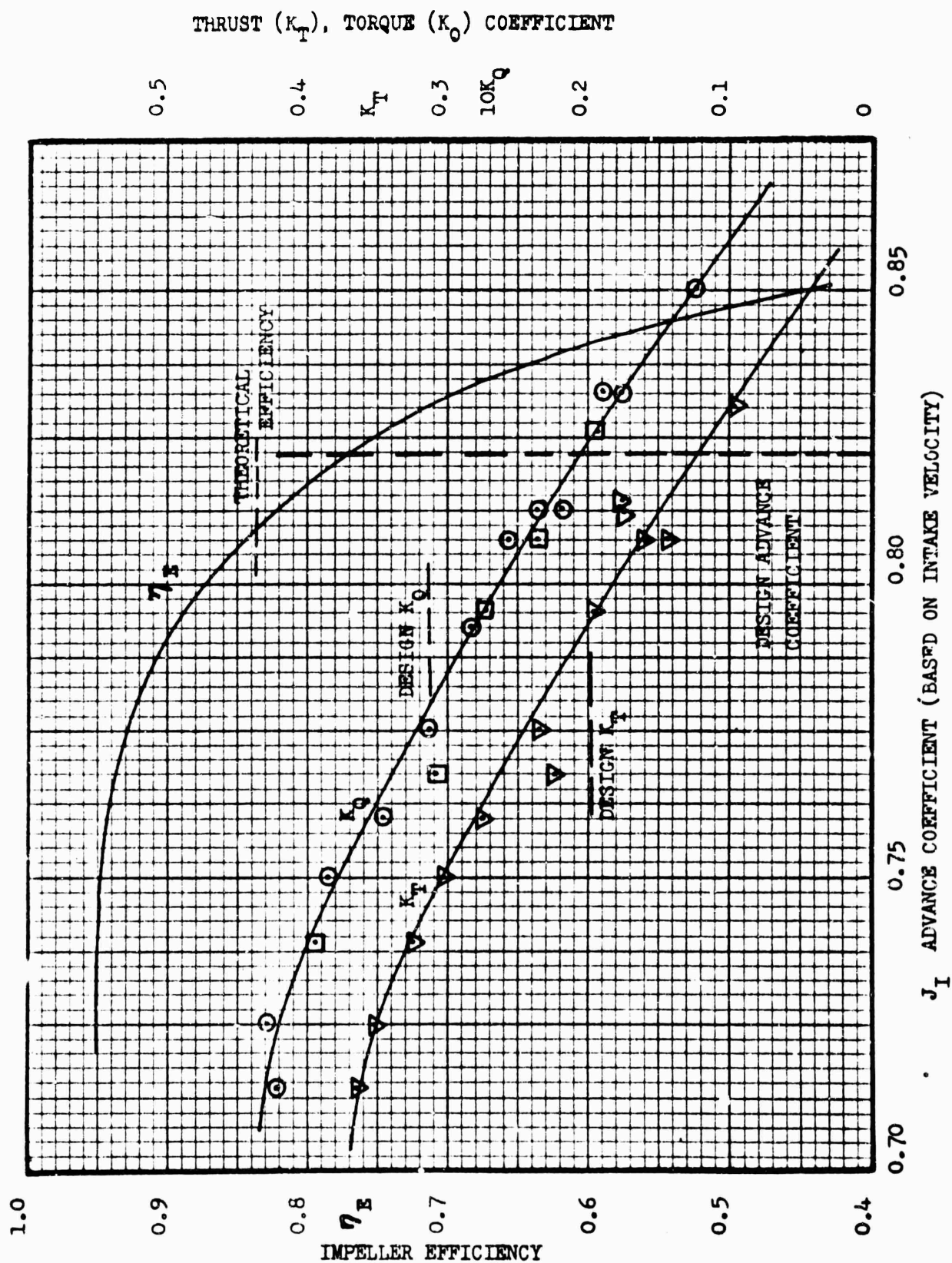
Fig. 5. 25 -   Impeller Performance Characteristics
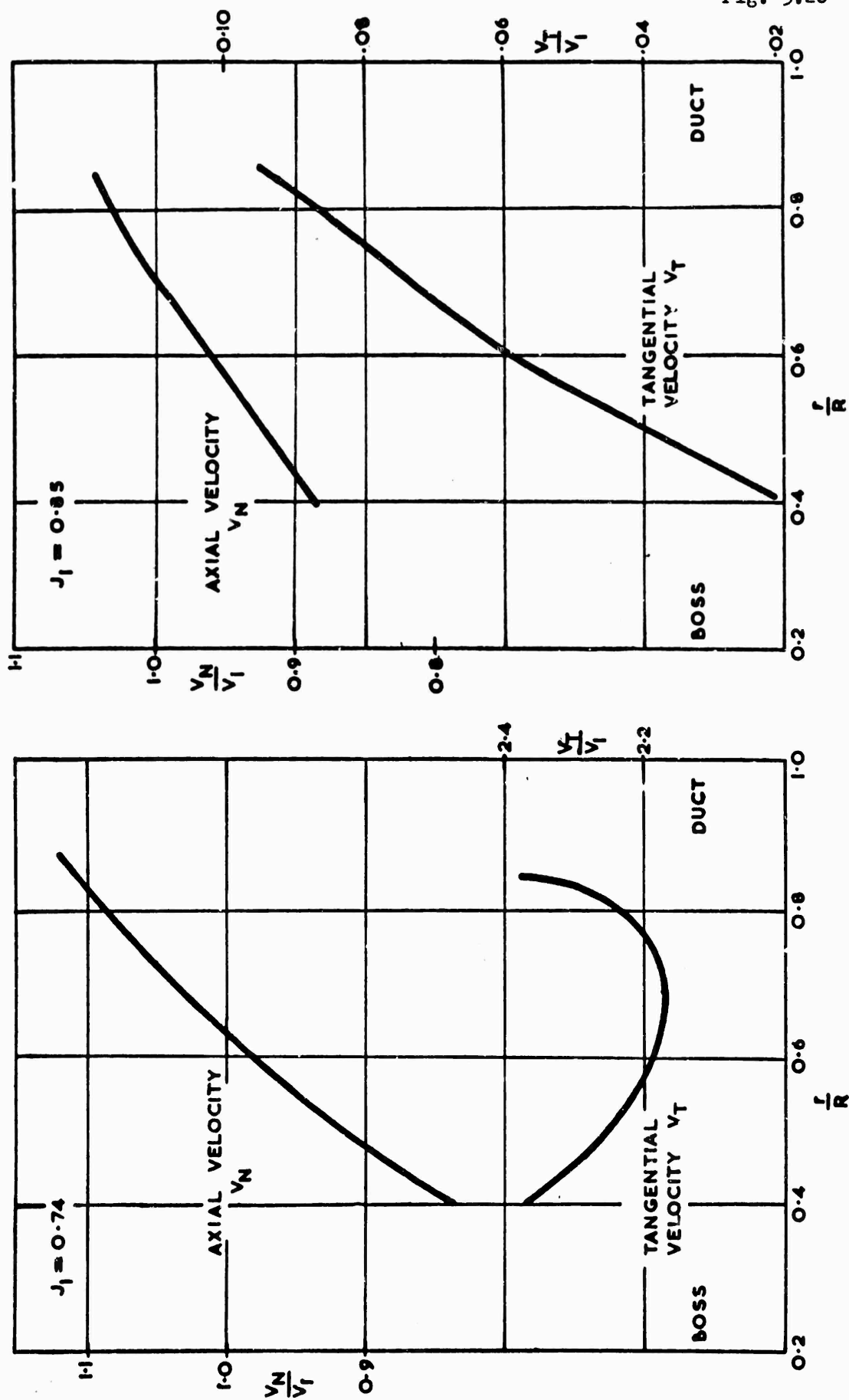
Fig. 5.26 - Induced Velocities behind the Impeller at $\frac{X}{D}$ = -0.49.

APPENDIX A1

THE DESIGN OF DUCTED

IMPELLERS USING A VORTEX LINE

ANALYSIS

and

AN OPTIMIZING COMPUTER TECHNIQUE

by

M.R.Hale

UNIVERSITY OF ADELAIDE

DEPARTMENT OF MECHANICAL ENGINEERING

Report Mech. Eng. R65/2

March, 1965.

APPENDIX   A2

COMPUTATION OF

RECTANGULAR MACHINING CO-ORDINATES

for

AN ARBITRARY IMPELLER DESIGN

by

M.R. Hale

UNIVERSITY OF ADELAIDE

DEPARTMENT OF MECHANICAL ENGINEERING

Report Mech. Eng. R65/3.

March, 1965.

APPENDIX A3

MACHINING PROCEDURE FOR THE MODEL IMPELLER.

APPENDIX A3

MACHINING PROCEDURE FOR THE MODEL IMPELLER.

1. The master templates were cast with free cutting alluminium alloy (6% Si, 0.2% Cu, 0% Fe).

2. After rough machining the base of the templates and heat treating them, the surfaces were accurately machined and hand-scraped.

3. To accurately position the templates on the table of a milling machine, it was necessary to machine two surfaces normal to each other and normal to the base of the templates.   It was arranged that these surfaces were parallel to the axes which were used to describe the geometry of the impeller blade.

4. A datum jig (Fig. 2.6) was constructed and fixed relative to the above three surfaces to locate the origin from which the machining coordinates were computed.   (details in Appendix A2)

5. After having positioned the milling cutter directly over the datum jig, the milling machine positioning dials were pre-set to zero.

6. The surface as defined by the points, was then machined (Fig.2.6).

7. A small amount of hand filing and scraping was necessary to remove the excess material from between the accurately machined points.

8. The inner and outer cylindrical surfaces of the templates were machined and a dummy hub fitted to the inner surface .

9. The model impeller material was rough machined, heat treated, and bored to final size.

10.   A precision indexing table was mounted on the pantograph copying machine to support the model impeller(Fig. 2.7). Care was taken to align the master templates and the model material in the correct position relative to the follower and cutter of the copying machine.

11.   The model impeller was then roughly machined all over to within 0.040 of an inch (Fig. 2.8).

12.   One surface of all the blades was then finished.

13.   Before machining the second side of the blades, the blades were supported from behind with plastic putty to increase the stiffness of the material and reduce deflections when machining (Fig. 2.7).

14.   Finally the accuracy and balance of the model was checked (Fig. 2.9).

APPENDIX   A4

PROPULSIVE EFFICIENCY OF DUCTED

PROPULSION SYSTEM.

APPENDIX A 4

PROPULSIVE EFFICIENCY OF A DUCTED PROPULSION SYSTEM.

Assuming all the losses in the ducting can be expressed as a fraction (ξ) of the total kinetic energy of the fluid at the intake to the duct.

$$\text{duct loss /unit mass flow} = \xi \frac{V_I^2}{2} \qquad \text{... A4.1}$$

Then the total head across the impeller is, referring to figure below.
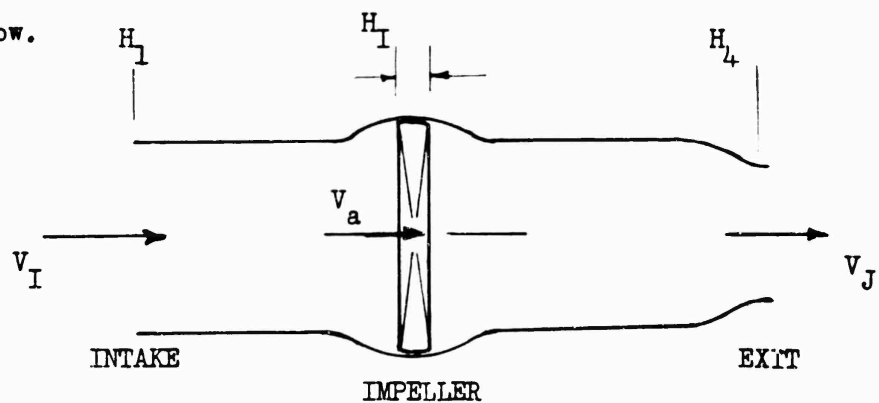
$$H_I = H_4 - H_1 + h \qquad \text{... A4.2}$$

$$= \frac{V_J^2}{2g} - \frac{V_I^2}{2g} + \xi \frac{V_I^2}{2g} \qquad \text{... A4.3}$$

$$= \frac{1}{2g}[V_J^2 - V_I^2(1 - \xi)] \qquad \text{... A4.4}$$

The power supplied to an impeller which has an efficiency η_E

$$P = \frac{1}{\eta_E} g M H_I \qquad \text{... A4.5}$$

where M = mass of fluid flowing per second.

Assuming the intake and jet velocities are uniform, then the thrust developed by unit is equal to rate of change of momentum.

$$T \quad = \quad M \, (V_J - V_I) \qquad \qquad \text{... A4.6}$$

To estimate the expended horse power delivered by the impeller a hull efficiency factor must be included because the resistance of the ship does not usually equal the thrust of the propulsion unit and the ship's velocity differs from the intake velocity to the propulsion system.

Defining the hull efficiency η_H in the normal way as

$$\eta_H \quad = \quad \frac{(1 - t)}{(1 - w)} \qquad \qquad \text{... A4.7}$$

where t = thrust deduction factor

and w = wake factor

Hence the expended horse power is

$$\text{E.H.P.} \quad = \quad \eta_H \, (V_J - V_I) \, M \, V_I \qquad \qquad \text{... A4.8}$$

and the propulsive efficiency η_P of the unit is

$$\eta_P \quad = \quad \frac{\text{E.H.P.}}{\text{Power input}} \quad = \quad \eta_E \, \eta_H \, \frac{2 \, V_I \, (V_J - V_I)}{[V_J^2 - V_I^2 (1 - \zeta)]} \qquad \qquad \text{... A4.9}$$

$$= \quad \eta_E \, \eta_H \, \frac{2\mu \, (1 - \mu)}{[1 - \mu^2 (1 - \zeta)]} \qquad \qquad \text{... A4.10}$$

where $\mu = \dfrac{V_I}{V_J}$

The maximum efficiency for a given ζ is

$$\eta_{P\ opt} = \eta_E\ \eta_H\ \frac{1}{[1 + \sqrt{\zeta}]} \qquad \ldots A4.11$$

and occurs where $\mu_{opt} = \dfrac{1}{1 + \sqrt{\zeta}}$

The propulsive efficiency can also be expressed in terms of the thrust load coefficient (C_{TL}) of the impeller.

$$\eta_{P\ opt} = \eta_E\ \eta_H\ \frac{4\ (C_{TL}\ K_A)}{[\ (C_{TL}\ K_A)^2 + 4\ (C_{TL}\ K_A) + 4\ \zeta\ ]} \qquad \ldots A4.12$$

where $C_{TL} = \dfrac{T}{\frac{1}{2}\ \rho\ Va^2\ A_o}$

$$= 2\ K_A\ [\ \frac{1}{\mu} - 1\ ]$$

where Va = axial velocity at the impeller plane

A_o = area of impeller annulus

K_A = ratio of impeller annulus area to area of duct at intake.

The optimum propulsive efficiency for a given ζ corresponds to a unique value of thrust load coefficient where ,

$$\eta_{P\ opt} = 2\ \eta_E\ \eta_H\ \frac{1}{[C_{TLopt}\ K_A + 2\ ]} \qquad \ldots A4.13$$

where $C_{TLopt} = \dfrac{2\ \sqrt{\zeta}}{K_A}$

APPENDIX A5

HYDRO-JET PROPULSION REDUCES VIBRATION

by

M.R. Hale and D.H. Norrie

<u>APPENDIX A6</u>

THE ANALYSIS AND CALIBRATION OF THE

FIVE-HOLE SPHERICAL PITOT

by

M.R. Hale and D.H. Norrie

APPENDIX   A7 and A8

MOVADAS   -   DATA ACQUISITION SYSTEM

and

COMPUTING PROCEDURE

by

M.R. HALE

DOCUMENT CONTROL DATA - R & D

Security classification of title, body of abstract and indexing annotation must be entered when the overall report is classified)

1. ORIGINATING ACTIVITY (Corporate author)	2a. REPORT SECURITY CLASSIFICATION
Department of Mechanical Engineering University of Adelaide Adelaide, South Australia	Unclassified
	2b. GROUP

3. REPORT TITLE

Hydrojet Ducted Propulsion System; Impeller Induced Vibratory Pressures and

Performance Characteristics

4. DESCRIPTIVE NOTES (Type of report and inclusive dates)

Final Report (September 1, 1964 – November 30, 1966)

5. AUTHOR(S) (First name, middle initial, last name)

Malcolm R. Hale and Douglas H. Norrie

6. REPORT DATE	7a. TOTAL NO. OF PAGES	7b. NO. OF REFS
November 1966	158	37

8a. CONTRACT OR GRANT NO	9a. ORIGINATOR'S REPORT NUMBER(S)
NONR-4738(00)(X)	
b. PROJECT NO.	Mech. Eng. R66/3
SR 009 01 01	
c.	9b. OTHER REPORT NO(S) (Any other numbers that may be assigned this report)
d.	

10. DISTRIBUTION STATEMENT

Distribution of this document is unlimited.

11. SUPPLEMENTARY NOTES	12. SPONSORING MILITARY ACTIVITY
	David Taylor Model Basin Washington, D.C. 20007

13. ABSTRACT

A vortex-line theory developed for an impeller in a long duct was used to optimize the design of a Hydrojet impeller. A model Hydrojet with this impeller was instrumented for pressure field and impeller performance measurements. Fluctuating pressures were high near impeller but attenuate to <10% at 0.4D. 1st/2nd/3rd blade frequency harmonics were approximately in ratio of 1.0/0.6/0.25. 0.85 - 0.90 impeller efficiency appears possible.

14 KEY WORDS	LINK A		LINK B		LINK C	
	ROLE	WT	ROLE	WT	ROLE	WT
Hydrojet						
Ducted Propulsion						
Propulsion						
Vibration						
Propulsion Vibration						
Impellers						
Ducted Propellers						